Chapter 4
Results and Discussion

"A positive attitude causes a chain reaction of positive thoughts, events and outcomes. It is a catalyst and it sparks extraordinary results".
-Wade Boggs

4.1. Utilization of local plants of selected Mimosoids

The knowledge of medicinal plants in India has been accumulated in course of many centuries based on several ancient medicinal systems, including ayurveda, unani and siddha (Lone and Bhardwaj, 2013). According to the survey report of World Health Organization (WHO, 2002), 80% people of the developing world use plant remedies for several therapeutic purposes. India, one of the richest floristic regions of the world has diverse socioeconomic, ethnic, linguistic and cultural areas. Therefore, the indigenous knowledge of medicinal plants and their use in treating several ailments might reasonably be expected in this country. Chandel *et al*. (1996) have reported that nearly about 70% of tribal and rural inhabitants of India are to a large extent depended on medicinal plants for their primary healthcare management due to either insufficient or inaccessible or less availability of modern healthcare system.

Despite of having different indigenous races and their own inherited knowledge of practices, not much attention was paid to explore the ethno-botanical information lies in Malda and Uttar Dinajpur districts. Hence, an initiative was undertaken to obtain those unrevealed information of medicinal practices by means of semi-questionnaire process, direct and group discussion with local people, practitioners and traditional healers. It was observed that the local people use those polyherbal formulations pleasantly rather than taking standardized drug. A total of 337 medicinal plants were identified (Saha *et al*., 2014a, 2014b, 2014c; De Sarker *et al*., 2015) to be used to treat different ailments in those two districts during survey (data is not presented here). Since the focus of the present endeavor was on the utilization of Mimosaceae, only local ethno-botanical knowledge of Mimosoids was represented here. A total of six species of Mimosaceae (Mimosoideae) were found to have different ethnopharmacological activities combating various types of ailments in the present study (Fig. 4.1). Of these, the root

decoction of *Mimosa pudica* was reported to heal leucorrhoea while leaf decoction is effectively used in the management of breast cancer or tumor (Saha *et al*., 2014c). *M. invisa* root juice was also administrated to treat leucorrhoea by the aboriginal tribe of Malda districts. Further, tender leaves of *Acacia nilotica* were found to be used to treat diabetes (Saha *et al*., 2014c). The bark of *A. catechu* along with other ingredients was reported to be effective against bone crack, ankle sprain and leucorrhea (Saha *et al*., 2014a). Consequently, the leaf and fruits infusion of *Acacia concinna* are mixed together and applied externally on head to promote hair growth (De Sarker *et al.*, 2015) while root is used as anti-dysenteric. Furthermore, the bark of *Albizia lebbeck* is used as anthelmintic and in case of eczema, leucoderma and other skin disorders. Apart from these, one taxa from Mimosaceae i.e. *A. catechu* was identified to be used as ethno-veterinarian purposes (Saha *et al*, 2014b).

4.2. *In-vitro* antioxidant activities

The endogenous free radical forming pathway demonstrates a cascade of diverse free radicals originating from molecular oxygen. Therapeutic benefits of medicinal plants are usually attributed to their antioxidant properties preventing the deleterious effects of oxidative stress by scavenging free radicals (Gandhi and Abramov, 2012). Hence, the present study was intended to investigate the free radical scavenging and reducing capabilities of selected plant species. The plants were chosen on the basis of preliminary screening of DPPH scavenging activity of all the extracts (Table 4.1). Results showing more than 80% of free radical inhibitory activity at 100 µg/ml concentrations through DPPH were only selected for further comprehensive analysis. Herein, four plant species, namely *Acacia catechu* (ACL), *A. nilotica* (ANL), *Mimosa pudica* (MPD) and *M. invisa* (MIN) were responded to this test, thereby rest were discarded.

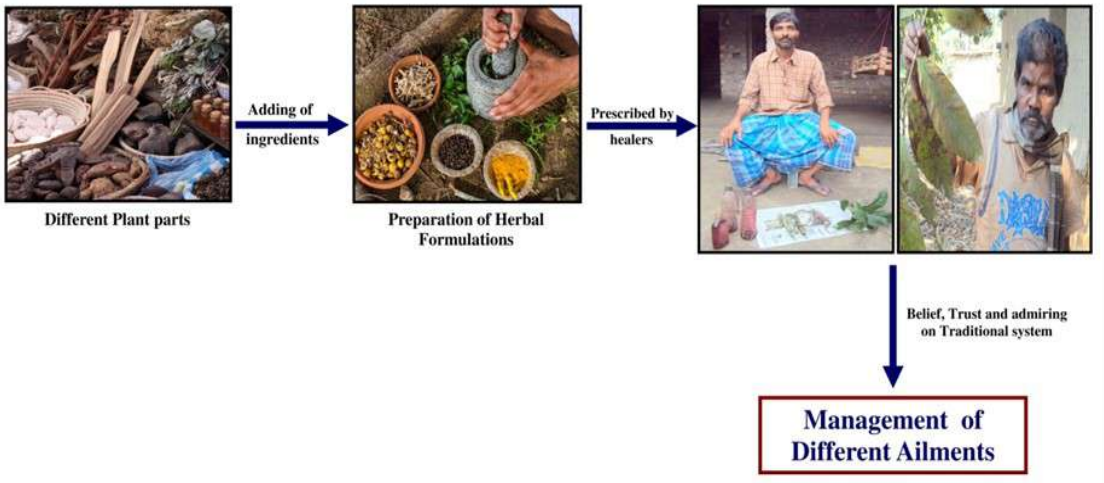

Fig. 4.1. Preparation of herbal-formulations by traditional healers.

The *in-vitro* DPPH free radical scavenging analysis of all four extracts revealed significant antioxidant potential compared to standard ascorbic acid. ACL extract exhibited higher quenching activity of than the ANL, MPD, MIN as well as standard at a dose of 100µg/ml (Fig. 4.2.A; Table 4.2).

ACL revealed 86.30±0.18% of inhibition while ANL, MPD and MIN showed 83.79±0.92%, 82.29±0.85% and 80.63±1.25% of inhibition at 100µg/ml respectively with greater inhibitory effect than the standard (28.32±1.39% at 100µg/ml). Actually, a decrease in the absorbance of the reaction mixture signifies decent free radical scavenging activity of the compound (Krishnaiah *et al.*, 2011). In fact, all the extracts exhibited higher DPPH scavenging activity compared to many other studied medicinal and aromatic plants, reported so far (Miliauskas *et al.*, 2004). This may be due to elevated levels of the active phytocompounds together with the polyphenolics in the extracts which scavenged DPPH radicals and thus attributed to their higher antioxidant activity (Cheung *et al.*, 2003). In hydroxyl radical ($OH^{\bullet}$) quenching activity, ANL extract was found to be much higher inhibitory activity in all studied doses (94.98±0.39% at 200µg/ml) than the others.

Though, at 200µg/ml, ACL, MPD and MINV were found to display lower hydroxyl radical quenching activity of 54.90±1.75%, 54.04±1.09% and 52.25±0.95% respectively (Fig. 4.2.B), they are strong enough to establish their prominent role as a potent source of antioxidants as evident from other studies (Miliauskas *et al*., 2004). Superoxide anion ($O_2^{\bullet-}$) is a weak oxidant but it gives rise to highly reactive cell-damaging free radicals and oxidizing agents namely, $OH^{\bullet}$ and singlet oxygen ($^1O_2$), both of which in turn

Table 4.1. DPPH scavenging activity of all 9 Mimosoids

Name of the plant	Percentage of inhibition			
	10 µg/ml	**20 µg/ml**	**80 µg/ml**	**100 µg/ml**
Mimosa pudica	22.56±1.93	42.36±1.93	67.88±0.98	**82.29±0.85**
Mimosa invisa	19.68±3.34	34.18±0.63	62.15±0.47	**80.63±1.25**
Acacia nilotica	33.72±2.12	43.13±1.38	78.91±0.63	**83.79±0.92**
Acacia nilotica var. indica	21.02±0.62	30.95±2.73	69.40±0.84	74.85±0.61
Acacia catechu	38.28±2.22	48.54±3.63	81.68±0.66	**86.30±0.18**
Acacia concinna	23.10±0.82	33.00±1.48	72.93±0.53	76.07±0.66
Albizia lebbeck	20.19±1.23	33.63±1.74	66.96±0.88	72.27±0.61
Albizia chinensis	18.38±0.51	31.74±0.72	64.29±0.88	70.23±1.16
Samanea saman	20.99±2.71	30.09±1.65	62.57±0.30	68.77±1.07

cause oxidative stress in biological systems. In fact, $^1O_2$ induces hyper-oxidation and oxygen cytotxicity and decreases antioxidative activity in cells (Halliwell and Gutteridge, 2015). ANL extract was found to possess better superoxide anion scavenging activity (40.97±0.34% at 100µg/ml) in dose dependent manner followed by ACL, MPD and MIN with lower IC_{50} value (121.07±2.24µg/ml) compared to others (Fig. 4.2.C; Table 4.2).

Decent amount of singlet oxygen ($^1O_2$) scavenging activity was observed in the following order MIN> ACL> MPD > ANL (Table 4.2) as given in Figure 4.2.D. The results were much lower than the inhibitory activity of standard lipoic acid, nevertheless, they have still great importance as therapeutic agents in preventing or lowering the progress of free radical like, $^1O_2$. Hence, the result indicated presence of certain active metabolites which reacted with singlet oxygen revealing potent scavenging activity. On the other hand, H_2O_2 has the capacity to inactivate several enzymes by means of oxidation of essential thiol groups. In addition, $O_2^{\bullet-}$ converts into H_2O_2 by the action of superoxide dismutase (SOD) as well as reacts with Fe^{2+} or Cu^{2+} ions inside the cells which leads to the generation of $OH^{\bullet}$ causing DNA damage and lipid peroxidation (Halliwell and Gutteridge, 1999).

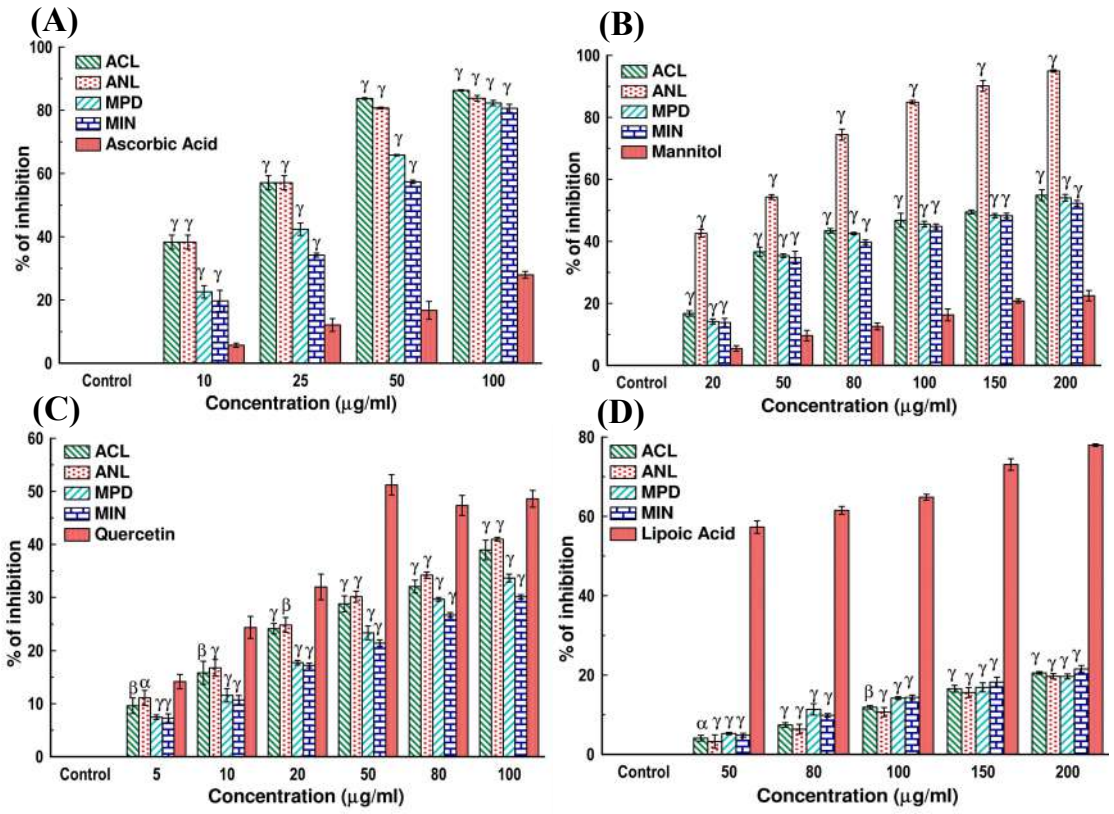

Fig. 4.2. Free radical scavenging activity through **(A)** DPPH, **(B)** Hydroxyl radical, **(C)** Superoxide anion and **(D)** Singlet oxygen scavenging activity of 4 different Mimosoids and their respective standards. [Each value represents mean ±SD (n=6); Where, γ= *P*<0.001, β= *P*<0.01 and α= *P*<0.05 Vs standard (µg/ml)].

Table 4.2. Percentage of inhibition of all four plant species.

Parameters	ACL (%)	ANL (%)	MPD (%)	MIN (%)	Standard (%)
DPPH (at 100 µg/ml)	86.30±0.18	83.79±0.92	82.29±0.85	80.63±1.25	27.93±1.10 (Ascorbic Acid)
Hydroxyl Radical (at 200 µg/ml)	54.90±1.75	94.98±0.39	54.04±1.09	52.25±0.95	22.48±1.68 (Mannitol)
Hydrogen Peroxide (at 2 mg/ml)	11.57±1.49	21.99±0.99	15.12±0.63	11.88±1.45	54.43±4.72 (Sodium Pyruvate)
Nitric Oxide (at 100 µg/ml)	63.04±0.36	60.55±0.84	57.91±0.30	60.72±0.44	55.08±1.93 (Curcumin)
Superoxide Anion (at 100 µg/ml)	38.94±1.86	40.97±0.34	33.64±0.73	30.13±0.38	48.59±1.58 (Quercetin)
Hypochlorous Acid (at 100 µg/ml)	41.37±2.56	44.17±1.06	39.27±1.11	37.91±1.04	36.10±2.80 (Ascorbic Acid)
Total Antioxidant Activity (at 200 µg/ml)	92.66±0.05	94.82±0.07	92.58±0.03	91.12±0.12	68.95±0.50 (Ascorbic Acid)
Peroxynitrite (at 200 µg/ml)	17.52±0.56	20.12±1.04	19.05±0.42	16.80±0.35	16.72±0.91 (Gallic Acid)
Singlet Oxygen (at 200 µg/ml)	20.56±0.35	16.69±0.68	19.67±0.68	21.53±0.88	77.97±0.30 (Lipoic Acid)
Lipid Peroxidation (at 25 µg/ml)	50.28±0.51	45.15±2.30	37.09±0.51	33.46±0.34	77.58±1.03 (Trolox)
Iron chelation (at 200 µg/ml)	35.14±0.55	33.67±1.54	33.25±1.07	32.52±0.79	99.57±0.15 (6 µg/ml) (EDTA)

Total Phenol and Flavonoid Content :

ACL	Total phenol content was recorded as 89.59 ± 2.71 mg gallic acid equivalent per 100 mg of plant extract while total flavonoid content was observed as 13.92 ± 1.60 mg quercetin equivalent per 100 mg of plant extract.
ANL	Total phenol content was 83.21 ± 1.32 mg gallic acid equivalent per 100 mg of plant extract and total flavonoid content was noted as 16.56 ± 2.36 mg quercetin equivalent per 100 mg of plant extract.
MPD	Total phenol content was 76.6±0.02 mg gallic acid equivalent per 100 mg of plant extract and total flavonoid content was found as 35.2±0.5 mg quercetin equivalent per 100 mg of plant extract.
MIN	Total phenol content was 61.9±0.5 mg gallic acid equivalent per 100 mg of plant extract and total flavonoid content was recorded as 30.4±0.2 mg quercetin equivalent per 100 mg of plant extract.

It was observed that all the extracts significantly scavenged H_2O_2 (Fig. 4.3.A), which might be attributed to the presence of phenolic groups that could donate electrons to H_2O_2 thereby, neutralizing it into water. Amongst four extracts, ANL showed better H_2O_2 inhibitory potentiality (P <0.001) than the others as evident from Table 4.2. Further, iron chelating capacity assay was employed to evaluate the ability of extracts to disrupt the formation of the ferrozine-complexes (reaction between ferrous ion and ferrozine). The iron chelating activity of ACL was observed to be of 35.14±0.55% at 200µg/ml followed by ANL> MPD> MIN (Fig. 4.3.C) showing the inhibition percentage of 33.67±1.54%, 33.24±1.07% and 32.51±0.79% respectively at 200µg/ml (Table 4.2) which reflected their decent chelating activity.

Accordingly, nitric oxide (NO) is a potent mediator of pro-inflammatory cellular activation causing subsequent inflammatory cellular injury. Moreover, spontaneous coupling of NO with superoxide radicals give rise to highly reactive peroxynitrite ($ONOO^-$), which is responsible for causing inflammation in cognitive disorders (Gimenez-Garzo *et al.*, 2015). Besides, hypochlorous acid (HOCl) is produced at the sites of inflammation due to oxidation of Cl^- ions by the neutrophil enzyme, myeloperoxidase and induces target cell lysis (Aruoma *et al.*, 1989). Result exhibited that ACL, ANL, MPD and MIN extracts not only possess higher inhibitory capacities with lower IC_{50} value (Table 4.3) to scavenge NO, $ONOO^-$ and HOCl, the quenching activities (Table 4.2) are also better (Fig. 4.3.B; 4.4.A and 4.4.B) than the respective standards such as curcumin, gallic acid and ascorbic acid respectively indicating potent antioxidant agents.

Therefore, it may be inferred that the extracts might be regarded as a potent antioxidative agents that probably reacted with reactive nitrogen species (RNS) preventing NO-mediated tissue damage or inflammation. Lipid peroxidation is another complex chain process that involves a variety of free radicals especially $^1O_2$, H_2O_2 and $OH^\bullet$, where in

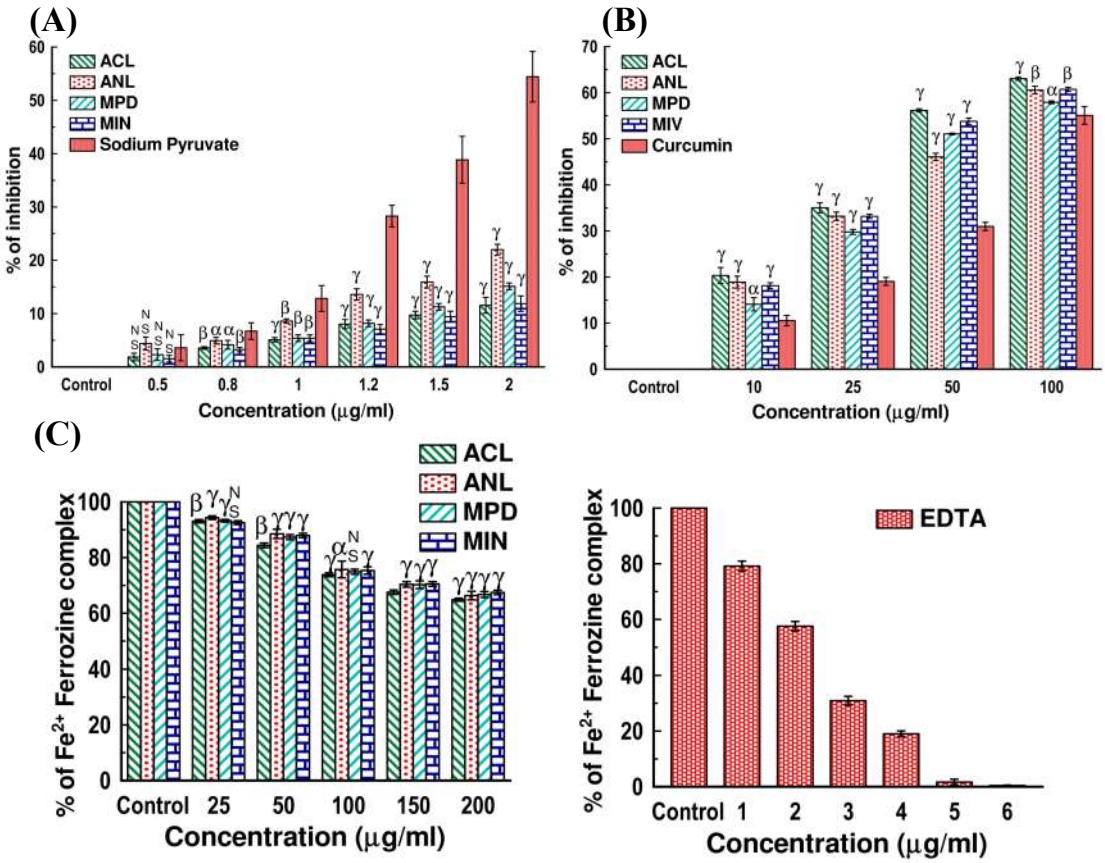

Fig. 4.3. (A) H_2O_2, **(B)** NO quenching activity and **(C)** Iron chelating properties of different Mimosoids and positive control. [Each value represents mean ±SD (n=6); Where, γ= *P*<0.001, β= *P*<0.01 and α= *P*<0.05 Vs standard (µg/ml)].

presence of antioxidants, lipid peroxidation becomes minimal. Figure 4.4.C exhibited significant lipid peroxidation inhibitory activity of each extracts with lower IC_{50} value (Table 4.2 and Table 4.3) revealing their adequate potency against alleged free radicals.

Such observation seems well justified by the possibility that the extracts may possess some bioactive compounds or anti-oxidative agents which react with the free radicals reducing lipid oxidation.

Results (Fig. 4.4.D) obtained from total antioxidant activity, clearly specified that the leaf extracts of *Acacia nilotica*, displayed a higher reduction potential (reduction of Mo(VI) to Mo(V) by electron donation) than ACL> MPD> MIN extracts and standard ascorbic acid thus, emphasizing its strong antioxidant nature. Eventually, the total phenolic content of ACL extract was found to be highest (89.59 ± 2.71 mg gallic acid equivalent per 100 mg of plant extract) than the other extracts while MPD extracts exhibited highest (Table 4.2) flavonoid content (35.2±0.5 mg quercetin equivalent per 100 mg of plant extract) suggesting their probable role as a chief contributors for such antioxidant activities.

4.3. Principal component analysis (PCA) and hierarchical cluster analysis (HCA)

4.3.1. PCA and HCA analysis of *A. catechu* (ACL) extract among the

Table 4.3. IC_{50} values of each extract with their respective standard used in the present study.

Name of the assays	IC_{50} values[$] (µg/ml)				
	ACL	ANL	MPD	MIN	Standard
DPPH	15.5 ±0.4$^{\beta}$	15.5±0.5$^{\beta}$	29.6±0.7$^{\beta}$	38.5±1.0$^{\beta}$	Ascorbic acid (240.1±28.3)
Hydroxyl Radical	121.2 ±1.2$^{\beta}$	6.9±0.2$^{\beta}$	128.4±1.6$^{\beta}$	135.4±5.2$^{\beta}$	Mannitol (589.0±46.5)
Hydrogen Peroxide	15604.9±613.8$^{\alpha}$	8.3±0.2$^{\gamma}$	12984.6±340.6$^{\gamma}$	16027.2± 1013.2$^{\beta}$	Sodium Pyruvate (3176.4±140.2)
Hypochlorous	130.6±4.7$^{\alpha}$	117.5±3.8$^{\alpha}$	140.2±2.7$^{\delta}$	156.9±2.1$^{\delta}$	Ascorbic acid (165.9±16.3)
Iron Chelation	320.6 ± 10.8$^{\gamma}$	363.9±30.4$^{\beta}$	356.7±3.5$^{\beta}$	364.8±3.1$^{\gamma}$	EDTA (1.4±0.01)
Lipid Peroxidation	32.1 ± 0.9$^{\gamma}$	210.6±37.3$^{\alpha}$	60.4±0.4$^{\gamma}$	57.5±2.0$^{\gamma}$	Trolox (11.1±0.2)
Nitric Oxide	45.5±1.3$^{\beta}$	56.4±2.1$^{\beta}$	58.7±0.6$^{\beta}$	50.5±0.2$^{\beta}$	Curcumin (96.8±5.0)
Peroxynitrite	854.0±59.9$^{\alpha}$	747.5±53.0$^{\delta}$	772.8±23.0$^{\beta}$	918.8±16.3$^{\beta}$	Gallic acid (734.8±28.3)
Singlet Oxygen	1103.7±24.6$^{\gamma}$	866.0±8.7$^{\gamma}$	735.0±41.3$^{\beta}$	698.4±23.1$^{\gamma}$	Lipoic acid (48.4±2.0)
Superoxide Radical	131.9±4.4$^{\gamma}$	121.0±2.2$^{\gamma}$	170.8±4.2$^{\gamma}$	197.2±0.7$^{\gamma}$	Quercetin (63.9±4.1)
Total Antioxidant	9.3±0.0$^{\beta}$	5.6±0.10$^{\beta}$	10.1±0.4$^{\gamma}$	9.9±0.1$^{\beta}$	Ascorbic acid (93.1±4.9)

[$] Data are expressed as mean ± S.D; $^{\alpha}p < 0.05$, $^{\beta}p < 0.01$, $^{\gamma}p < 0.001$ and $^{\delta}p>0.05$ vs Standard.

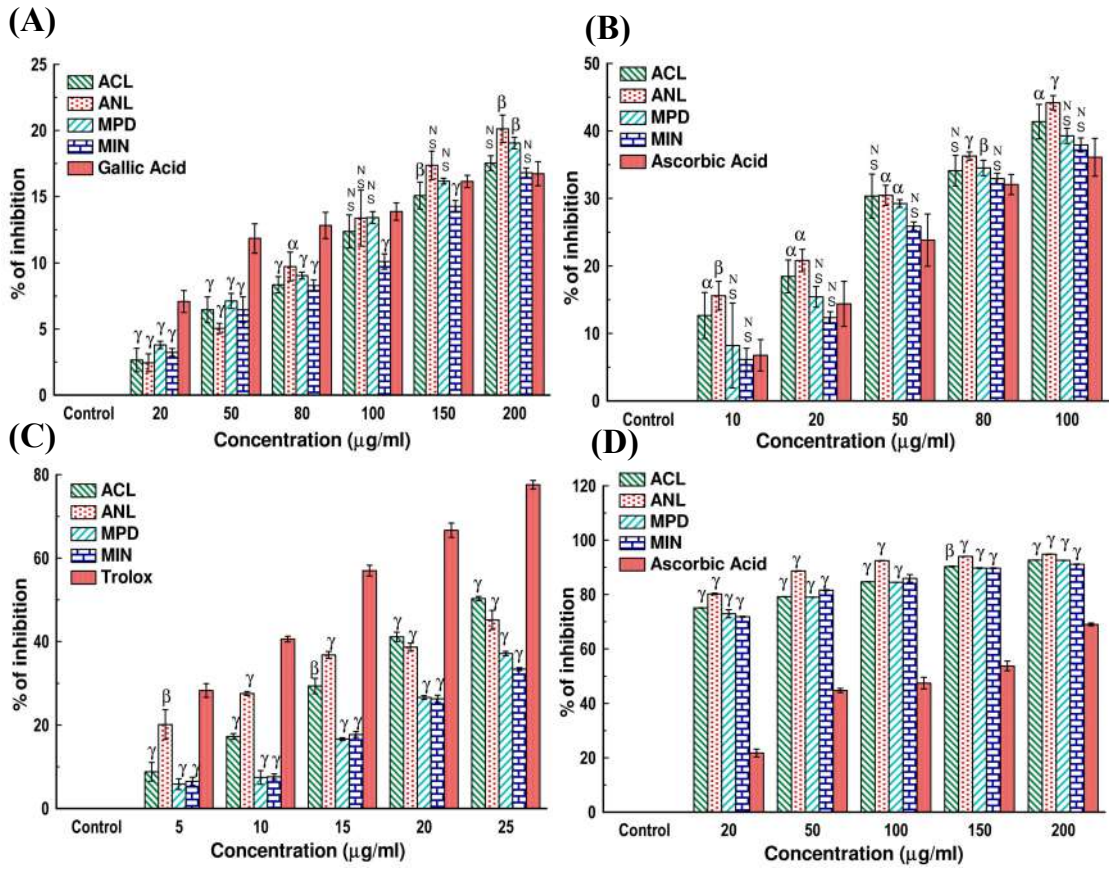

Fig. 4.4. Antioxidant properties of 4 Mimosoids by means of **(A)** Peroxynitrite, **(B)** HOCl, **(C)** Lipid peroxidation and **(D)** Total antioxidant activity assay. [Each value represents mean ±SD (n=6); Where, γ= *P*<0.001, β= *P*<0.01 and α= *P*<0.05 Vs standard (µg/ml)].

selected antioxidant traits

In the present study, principal component analysis (PCA) of *A. catechu* was performed to determine how the seven parameters namely DPPH, Hydroxyl radical, NO, iron chelation, lipid peroxidation, phenol and flavonoid content correlate with each other under univariate analysis. The first and second principal component (PC1 and PC2) accounted for 57.38% and 34.42% of the variance, respectively. The loading plot revealed that hydroxyl radical and DPPH were firmly located positively on the PC1 with cosine value of 0.945 and 0.962 respectively while lipid peroxidation was firmly located positively on the PC2 with cosine value of 0.967. The correlation matrix (Table 4.4) generated from PCA loading plot revealed highest positive correlation between hydroxyl radical and DPPH activity (0.843) while highest negative correlation had been observed between flavonoid with and hydroxyl radical (-0.990) followed by iron chelation and hydroxyl radical scavenging activity (-0.934).

A dendrogram was prepared through hierarchical cluster analysis (HCA) grouping the antioxidant capacities of ACL into statistically significant clusters (Fig. 4.5). The data of HCA virtually corroborated with the results of PCA. The

present dendrogram revealed a broad cluster between lipid peroxidation, NO, hydroxyl radical, DPPH and phenolic content which were located positively on PC1. The iron chelation was found to be closely associated with flavonoid content whereas the hydroxyl radical and flavonoid content were merged at highest distance (proximity matrix value of 19.90) among all the variables. Interestingly, there was no cluster formation between flavonoid and phenolic content which are said to be chiefly responsible for antioxidant activities. Therefore, the bioactivity of EKH may be due to the presence of other class of phytochemicals apart from phenolics and flavonoids.

4.3.2. PCA and HCA analysis of *M. pudica* and *M. invisa* extract among the selected antioxidant traits

The results obtained from antioxidant and free-radical scavenging assays were further analyzed based on their dose-dependent activities, to interpret the underlying inter-correlation patterns in MPD and MIN. The results revealed that the overall bioactivities of both extracts are highly comparable, demonstrating similarly in both the distribution of variables in the component plot (Fig. 4.6) as well as dose-dependent percentage of inhibition in all the assay. The extent of similarity was reflected by the closeness of traits in the component plot. For instance, optimum correlation was found between DPPH with both inhibition of lipid peroxidation and NO (0.998) whereas, lowest correlation resided between H_2O_2 and TAA (-0.623) in *M. pudica* (Fig. 4.6.B). Concurrently, in case of *M. invisa*, maximum correlation was observed between DPPH and lipid peroxidation (0.999) whereas, lowest correlation was found between superoxide and TAA (-0.642). This finding was further supported by the data obtained from hierarchical clustering (Fig. 4.6.E). Interestingly, the most prominent difference between MPD and MINV was the divergence of superoxide radical scavenging activity, representing its independent allocation in the component plot (Fig. 4.6.A and 4.6.D). The

Table 4.4. Correlation Matrix of different antioxidant assays in ACL extract.

	DPPH	Hydroxyl	NO	Iron	Lipid	Phenol	Flavonoid
DPPH	1.000						
Hydroxyl	0.843	1.000					
NO	0.540	0.339	1.000				
Iron	-0.595	-0.934	-0.147	1.000			
Lipid	0.765	0.300	0.553	0.062	1.000		
Phenol	-0.294	0.266	-0.366	-0.593	-0.840	1.000	
Flavonoid	-0.910	-0.990	-0.402	0.875	-0.430	-0.129	1.000

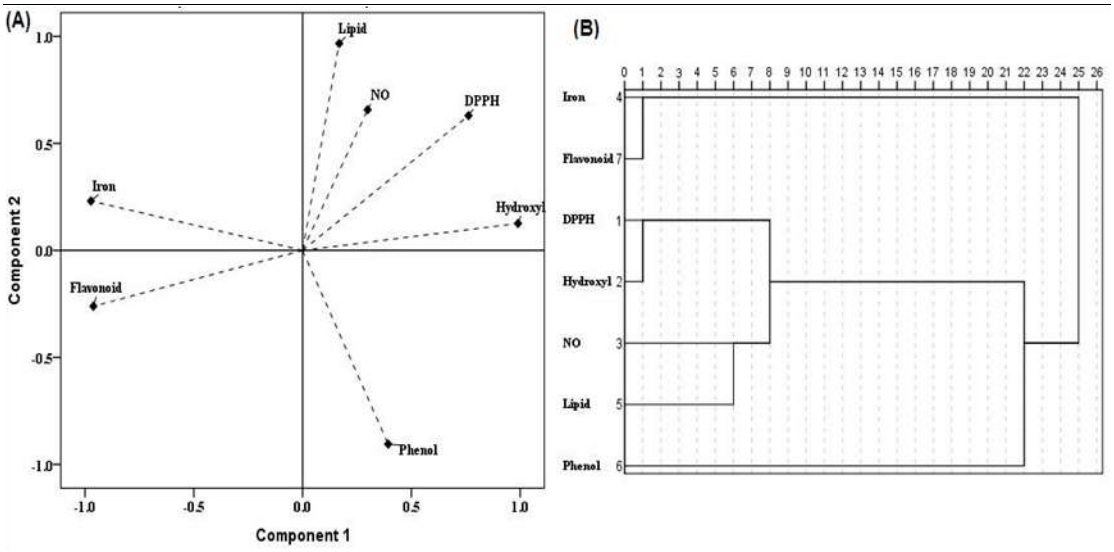

Fig. 4.5. PCA **(A)** and HCA **(B)** analysis of ACL extract among selected antioxidant traits.

component plot reveals that the highly reactive hydroxyl radical is probably generated from H_2O_2 under the presence of transition metal such as iron. Clustering pattern in HCA reveals that there is no intervening effect of iron chelation on the hydroxyl radical scavenging activities and the activity is marginally influenced by inhibition of H_2O_2. The individual proximity scores has been depicted through heat map, where red to green represents high to low proximity scores (Fig. 4.6.C and 4.6.F). The details of correlation matrix, proximity scores and screet plots of MPD and MINV are provided in Table 4.5 and 4.6 respectively.

4.4. Evaluation of cytotoxicity

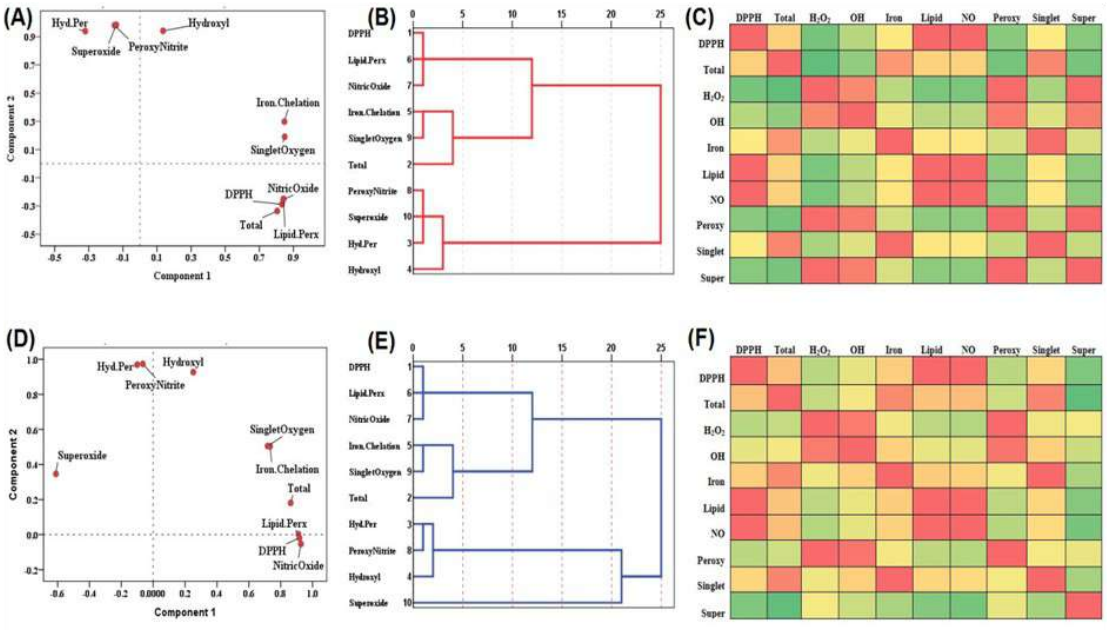

Fig. 4.6. PCA, HCA and heat map analysis different antioxidant traits used in MPD and MIN extracts. PCA **(A)**, HCA **(B)** and Heat Map **(C)** of MPD extract; PCA **(D)**, HCA **(E)** and Heat Map **(F)** of MIN extract.

In order to investigate probable cytotoxic and detrimental effects of ACL, ANL, MPD and MINV extracts on normal body cells upon consumption, haemolytic activity, erythrocyte membrane stabilizing activity and MTT assay on splenocyte and macrophage cells were further considered.

4.4.1. Assessment of haemolytic activity

The haemolytic activity of plant extracts or any compounds is an indication towards the cytotoxicity of normal healthy cells (Da Silva *et al.*, 2004). The hemolysis process is actually related to the concentration and potency of extract. Plant derived metabolites showed haemolytic activity by altering changes in the erythrocyte membrane by means of destruction of red blood cells. Hence, *in-vitro* haemolytic assay by spectroscopic method represents a simple and effectual method for the quantitative measurement of hemolysis. Figure 4.7.A exhibited that all of four samples possess very low haemolytic effect towards human erythrocytes. A dose dependant increase of inhibition was observed; for instance, MIN was found to be showed 8.79±0.29%, MPD revealed 8.20±0.84% while ACL and ANL displayed 7.79±0.55% and 6.74±0.43% of inhibition respectively at 100µg/ml of each concentration which is virtually a negligible one. Therefore, these data suggested the non-toxic effect of the extracts making it suitable for the preparation of drugs involved in the treatment of various diseases.

4.4.2. Erythrocyte membrane stabilizing activity (EMSA)

EMSA indirectly evaluates the antioxidant capacity of test sample against the superoxide radical mediated destruction of the erythrocyte membrane. Actually, erythrocytes are filled with haemoglobin and their membranes are composed of highly unsaturated fatty acids. The auto-oxidation of riboflavin takes place in

Table 4.5. Correlation matrix of different antioxidant assays in MPD extract.

	DPPH	Total	Hydro Perx.	Hydroxyl	Iron Chelation	Lipid Perx.	Nitric Oxide	Peroxy Nitrite	Singlet Oxy	Super-oxide
DPPH	1.00									
Total	0.53^{NS}	1.00								
Hydro Perx.	-0.48^{NS}	-0.62^{NS}	1.00							
Hydroxyl	-0.06^{NS}	-0.30^{NS}	0.84^{**}	1.00						
Iron Chelation	0.41^{NS}	0.78^{**}	-0.03^{NS}	0.28^{NS}	1.00					
Lipid Perx.	0.99^{***}	0.52^{NS}	-0.45^{NS}	-0.02^{NS}	0.43^{NS}	1.00				
Nitric Oxide	0.99^{***}	0.52^{NS}	-0.46^{NS}	-0.02^{NS}	0.43^{NS}	0.99^{***}	1.00			
Peroxy Nitrite	-0.36^{NS}	-0.49^{NS}	0.98^{***}	0.90^{**}	0.13^{NS}	-0.32^{NS}	-0.33^{NS}	1.00		
Singlet Oxy	0.41^{NS}	0.86^{**}	-0.14^{NS}	0.20^{NS}	0.97^{***}	0.43^{NS}	0.43^{NS}	0.01^{NS}	1.00	
Superoxide	-0.37^{NS}	-0.47^{NS}	0.97^{***}	0.90^{**}	0.16^{NS}	-0.33^{NS}	-0.33^{NS}	0.99^{***}	0.03^{***}	1.00

The matrix is based on the PCA performed by SPSS statistics. NS= Non-significant (1-tailed), ***p<0.001; **p<0.01 (1-tailed).

Table 4.6. Correlation matrix of different antioxidant assays in MIN extract.

	DPPH	Total	Hydro Perx.	Hy-droxyl	Iron Chelation	Lipid Perx.	Nitric Oxide	Peroxy Nitrite	Singlet Oxy	Superox-ide
DPPH	1.00									
Total	0.60^{NS}	1.00								
Hydro Perx.	-0.04^{NS}	0.02^{NS}	1.00							
Hydroxyl	0.25^{NS}	0.33^{NS}	0.91^{**}	1.00						
Iron Chelation	0.54^{NS}	0.84^{**}	0.32^{NS}	0.53^{NS}	1.00					
Lipid Perx.	0.99^{***}	0.59^{NS}	-0.03^{NS}	0.27^{NS}	0.55^{NS}	1.00				
Nitric Oxide	0.99^{***}	0.62^{NS}	-0.08^{NS}	0.24^{NS}	0.53^{NS}	0.98^{***}	1.00			
Peroxy Nitrite	-0.04^{NS}	0.09^{NS}	0.99^{***}	0.93^{***}	0.35^{NS}	-0.02^{NS}	-0.07^{NS}	1.00		
Singlet Oxy	0.50^{NS}	0.86^{**}	0.31^{NS}	0.53^{NS}	0.99^{***}	0.51^{NS}	0.49^{NS}	0.35^{NS}	1.00	
Superoxide	-0.43^{NS}	-0.64^{NS}	0.35^{NS}	0.06^{NS}	-0.15^{NS}	-0.41^{NS}	-0.49^{NS}	0.27^{NS}	-0.18^{NS}	1.00

The matrix is based on the PCA performed by SPSS statistics. NS= Non-significant (1-tailed), ***p<0.001; **p<0.01 (1-tailed).

presence of light, generating superoxide radicals which induce the haemolysis of RBC (Dey *et al.*, 2013). In the present study, Fig. 4.7.B revealed significant (P <0.001) percentage of erythrocyte membrane protection in all the doses indicating ANL (66.21 ± 1.34% at 200µg/ml) as a potent natural dietary supplement than the others whereas MIN extract was also found to be exhibited 63.51±2.69% of inhibition at the same concentration (200µg/ml) followed by ACL > MPD which suggest all the extracts might be treated as effective antioxidants to stabilize the erythrocyte membrane.

4.4.3. MTT cell viability assay

To investigate further probable cytotoxic and detrimental effects of ACL, ANL, MPD and MINV on normal body cells upon consumption, we further considered routine MTT assay on murine splenocyte and peritoneal macrophage. Result (Fig. 4.7.C and 4.7.D) demonstrated no cytotoxic effect on either of splenocyte or macrophage cells as no drastic change in metabolic activity of cells was observed up to the highest dose. The effect of extracts on the cell viability was found to be non-significant ($P > 0.05$) compared to the control. Hence, both extracts could well be treated as consumable bio-safety stuff.

Hence, from the above experiments it could be inferred that all the extracts revealed negligible cytotoxic activity up to certain consumable doses, and therefore, can be safely used as bio-safety nutrient supplement for future purposes.

4.5. Neurotherapeutic effects of plant extract

4.5.1. AChE inhibitory activity of ACL, ANL, MPD and MIN extracts (*in-vitro*)

Despite of having potent antioxidative function of extracts claiming their indirect

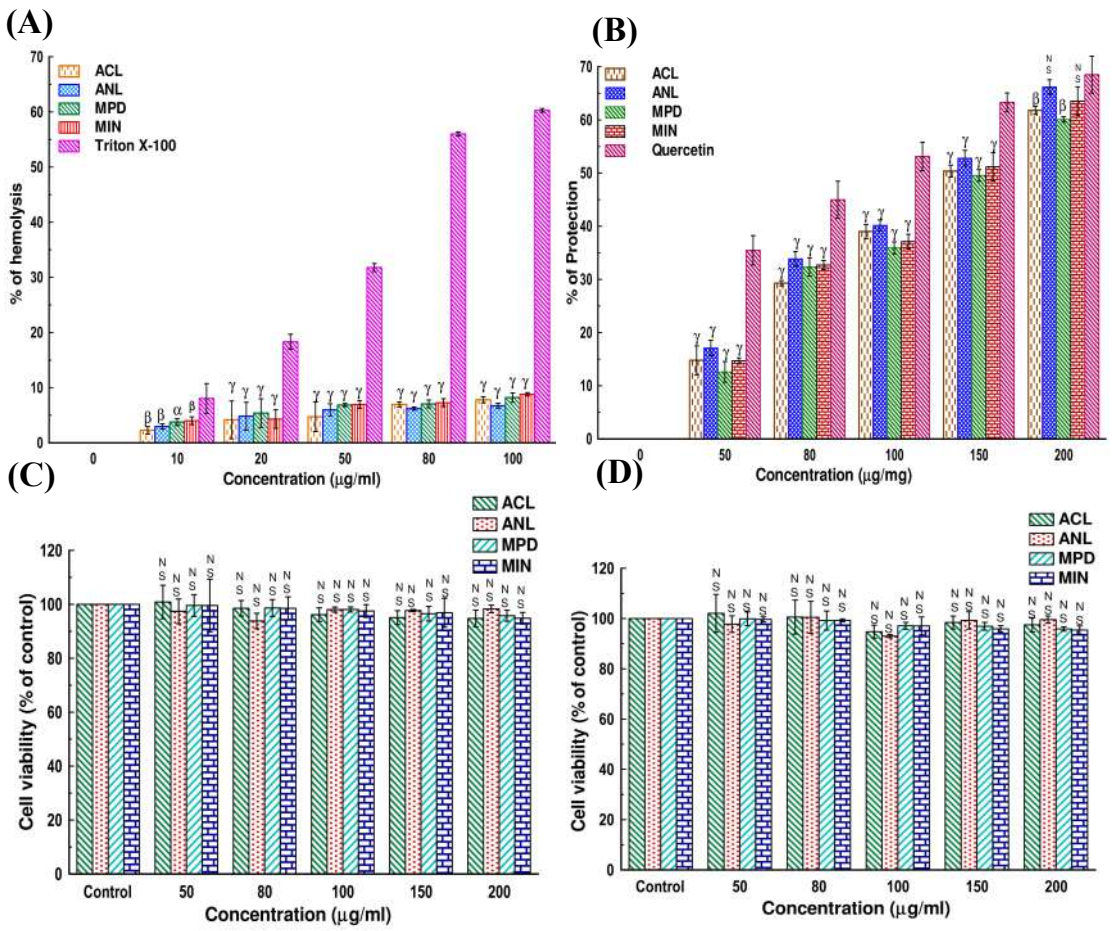

Fig. 4.7. Haemolytic activity of selected Mimosoids and standard Triton X-100 **(A);** Erythrocyte membrane stabilizing activity **(B);** MTT cell viability activity of splenocyte **(C)** and macrophage **(D)** [Each value represents mean ±SD (n=6); Where, γ= *P*<0.001, β= *P*<0.01 and α= *P*<0.05 Vs standard (µg/ml)]

role against neurodegenerative disorders or NDs (Barnham *et al.*, 2004), it was further intended to assess the AChE inhibitory activity of ACL, MPD and MIN over NDs for the first time. The experiment was undertaken considering the complexities of several age-related disorders (e.g., dementia, AD and PD) occurring due to oxidative stress which lowers the function of acetylcholine (ACh) and dopamine in brain (Chattipakorn *et al.*, 2007). Synthesis of ACh by AChE is the most crucial pathway for the pathophysiology of AD. Therefore, use of acetylcholinesterase inhibitor (AChEI) to suppress the degradation of ACh seems to be a rational approach which would maintain the balance of ACh in synaptic cleft (Birks, 2006). In essence, acetylcholinesterase enzyme hydrolyses the substrate (acetylthiocholine iodide) and produces thiocholine which in turn reacts with Ellamn's reagent (5, 5'-dithiobis-2-nitrobenzoic acid) and a yellow color compound, 5-thio-2-nitrobenzoic acid is thus produced (Chattipakorn *et al.*, 2007). The inhibition of cholinesterase enzyme activity is evident by fading of yellow color of the compound. In the present study, the AChE inhibitory activity of

ACL was found to be 73.47±0.303% at 200µg/ml with lower IC_{50} value of 75.91 ±2.28µg/ml. ANL yields 68.21±0.47% of inhibitory activity at 200µg/ml and the IC_{50} value was found to be 86.27±1.32 µg/ml whereas MPD revealed 74.40±0.52% of inhibition at 200µg/ml with IC_{50} value of 109.41±2.46µg/ml and MIN showed quite similar inhibitory activity of 75.24±0.85% at 200µg/ml with the IC_{50} value of 107.25±1.46µg/ml. However, the IC_{50} values of ACL, MPD and MIN were found to be relatively higher than standard eserine (0.023±0.0005µg/ml). Even although, the results reflected better AChE inhibitory activities than other reported medicinal plants (Mathew and Subramanian, 2015; Mukherjee *et al.*, 2007), thereby suggesting the potent role of ACL, MPD and MIN as cholinesterase inhibitors (AChEI) and might be useful as anti-cholinesterase drug against AD and PD.

4.5.2. Effects of MPD and MIN extracts on scopolamine-induced memory impairment in mice

Since enhanced result was observed from *in-vitro* AChE inhibitory assay, it was intended to perceive whether MPD and MIN extracts have any memory improvement or retention activity on scopolamine-induced rodent model. In essence, scopolamine causes oxidative stress by means of interference with acetylcholine in brain leading to cognitive impairment as well as increases the levels of AChE (Rahnama *et al.*, 2015). The oxidative stress contributes to pathogenesis and histological changes in patients with NDs (Gilgun-Sherki *et al.*, 2001). In this context, MPD and MIN had already been exposed to be potent anti-oxidative agents in the present study. Therefore, the neurotherapeutic effect of MPD and MIN on memory deficits in a mouse model of amnesia (passive avoidance test) induced by scopolamine was evaluated. As a result, passive avoidance test, a fear-motivated avoidance test, was employed to describe the way in which the animal learns to avoid an aversive stimulus (electric foot-shock) as a part of long-term memory. Table 4.7 revealed that the initial latency time to enter the dark chamber was significantly longer in the mice given only scopolamine as compared to the control group suggesting amnesic effect of mice. The treatment with MPD and MIN extracts significantly (P<0.001) attenuated the scopolamine-induced memory deficit in mice to a great extent and also associated with the short-term memory (STL) improvement (Table 4.7) suggesting anti-amnesic effect of extracts in the scopolamine-induced rodent model. While considering brain AChE-inhibitory activity, MPD and MIN were also recorded to be reversed the scopolamine-induced memory impairment in mice by increasing cholinergic activity through the inhibition of AChE (Fig. 4.8.A). Hence, it can be inferred that MPD and MIN could

Table 4.7. Effect of MPD and MIN extracts on scopolamine-induced memory impairment in the passive avoidance test.

Groups	IL (Sec.)	STL (Sec.)
Group I (Control)	20.33±2.25	141.33±8.16
Group II (SCP)	103.16 ± 5.03^{a}	83.16 ± 9.45^{a}
Group III (SCP + Donepezil)	$28.33\pm2.33^{a\,\alpha}$	$178.16\pm9.86^{a\,\alpha}$
Group IV (SCP + MPD-low)	$67.83\pm4.62^{a\,\alpha\,A}$	$136.33\pm10.48^{d\,\alpha\,A}$
Group V (SCP + MPD-high)	$34.33\pm4.17^{a\,\alpha\,C}$	$167.83\pm9.62^{a\,\alpha\,D}$
Group VI (SCP + MIN-low)	$73.16\pm4.11^{a\,\alpha\,A}$	$131.50\pm11.97^{d\,\alpha\,A}$
Group VII (SCP + MIN-high)	$39.66\pm3.20^{a\,\alpha\,A}$	$160.83\pm4.95^{a\,\alpha\,B}$

IL- Initial latency; STL- Step Through Latency; SCP- Scopolamine; $^{a}p<0.001$; $^{b}p<0.01$; $^{c}p< 0.05$; ^{d}p=non-significant (p>0.05) vs control group; $^{\alpha}p<0.001$; $^{\beta}p<0.01$; $^{\gamma}p< 0.0$; $^{\Psi}p$=non-significant (p>0.05) vs Scopolamine group; $^{A}p<0.001$; $^{B}p<0.01$; $^{C}p< 0.05$; ^{D}p=non-significant (p>0.05) vs SCP+Donepezil group [Data represented as mean ± SD]

be a potent AChE-inhibitors by hindering the destruction of ACh (McGleenon *et al.*, 1999), thereby confirm the results as found in *in-vitro* tests. This result also supports the ideas which might be due to a decrease in gene transcription, translation and enhance cholinergic activity thereby improving cognitive function (Shahidi *et al.*, 2008).

It has been well-speculated that every cellular organism sustains its own antioxidant stability to protect tissues from oxidative damage at a certain stage. SOD, catalase, GSH etc. are the fundamental antioxidant enzymes that protect tissues from highly reactive hydroxyl radicals and superoxide anions, linked with NDs (Gilgun-Sherki *et al*., 2001). In the present study, scopolamine treatment significantly (P<0.001) depleted antioxidant capacity of SOD, catalase and GSH system in brain tissues (Fig. 4.8.B-D). At the same time, these alterations were further ameliorated significantly by the administration of MPD and MIN extracts. High dose of MPD was found to be more protective one in all cases than others; for instance, 85.48±5.35% of control was observed in catalase, 81.80±3.77% in SOD and 75.11±4.39% in GSH activity. However, MIN showed lower percentage of control in every case than MPD, it is defensive enough combating oxidative stress prompted by scopolamine. Hence, the results suggest antioxidative prospective of MPD and MIN that contributed to effective neuronal plasticity and memory function. Thus, most importantly, we provide first evidence for a potent neurotherapeutic role of MPD and MIN in the protection from ROS-mediated neuronal damage as well as we identified some of the responsible target phytocompounds that could be treated as future CNS drug.

4.6. Anti-diabetic activity of *Acacia nilotica* (ANL) extract

Diabetes is progressively affecting a large number of populations and fatally reducing their quality of life. The use of conventional medicines in diabetes

management is quite expensive, thus, unreasonable to most of patients. Furthermore, most of these conventional drugs exert adverse side-effects. Inclusion of herbal remedy into conventional healthcare system may considerably improve the overall healthcare system. The advantage of herbal remedy over modern medicines is that most of the herbal medicines are plant-based and comparatively cheaper, possess fewer side-effects owing easy acceptability.

In the present study, anti-diabetic appraisal of ANL extract was investigated. Initially, no mortality has been observed upon oral administration of 2000 mg/kg BW ANL extract. Hence, ANL extract may be safe for consumption.

Alloxan, a β-cytotoxin, induces diabetes in a wide variety of animal species by

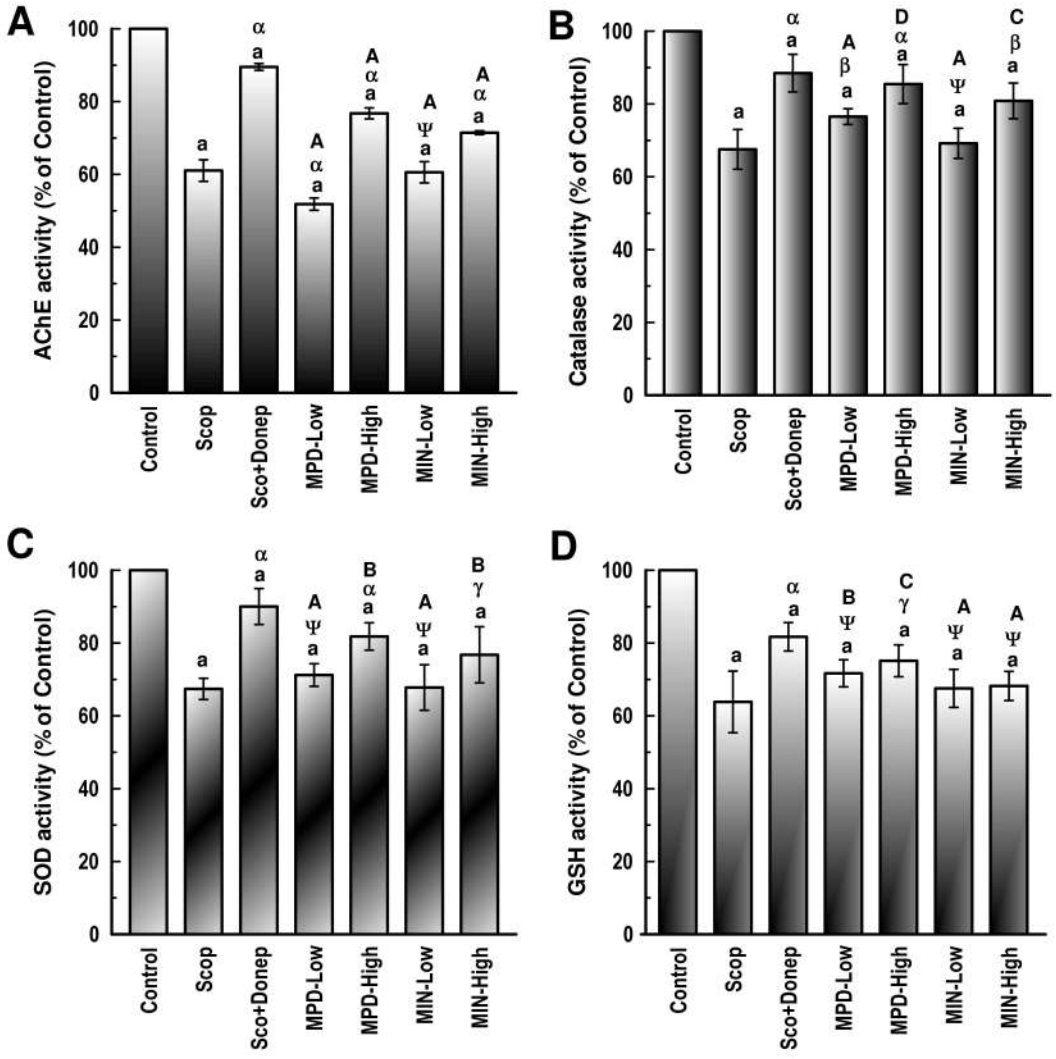

Fig. 4.8. Effect of MPD and MIN extracts on scopolamine-induced memory impairment in the passive avoidance test. **(A)** AChE, **(B)** Catalase, **(C)** SOD and **(D)** GSH activity of MPD and MIN extracts. Scop= Scopolamine, Donep= Donepezil. $^{a}p<0.001$; $^{b}p<0.01$; $^{c}p< 0.05$; ^{d}p=non-significant ($p>0.05$) vs control group; $^{\alpha}p<0.001$; $^{\beta}p<0.01$; $^{\gamma}p< 0.0$; $^{\Psi}p$=non-significant ($p>0.05$) vs Scopolamine group; $^{A}p<0.001$; $^{B}p<0.01$; $^{C}p< 0.05$; ^{D}p=non-significant ($p>0.05$) vs Sco+Donep group [Data represented as mean ± SD]

damaging the insulin secreting pancreatic β-cells via formation of reactive oxygen species like nitric oxide leading to a reduction of endogenous insulin release and increase blood glucose level in tissues (Szkudelski, 2001). This hyperglycemic condition was found to be lowered significantly (P <0.001) after 20 consecutive days of high-dose (200mg/kg BW) ANL treatment (Fig. 4.9.A). It was observed that the glucose level was lowered from 237.2±9.23mg/dl on day 1 to 74±14.37mg/dl on day 20 in HD-ANL group with a decrease of 68.80%. In fact, this anti-hyperglycaemic activity of HD-ANL was quite similar to standard drug, glibenclamide (78.8±12.51mg/dl) after 20 days of administration indicating a significant anti-diabetic activity of ANL in mice. It might be due to increasing glycogenesis, inhibiting gluconeogenesis in the liver or inhibiting the absorption of glucose from the intestine. In another study, reduced blood glucose level was also observed in alloxan-treated rabbits after administration of *A. nilotica* pod extracts at 400mg/kg BW dose (Ahmad *et al.*, 2008). Vats *et al.* (2002) also showed a significant reduction in the levels of blood glucose after the treatment of *Trigonella foenum-graecum*, *Ocimum sanctum* and *Pterocarpus marsupium* extract in normal and alloxanized diabetic rats. Subsequently, decline in body weight is often found to be coupled with diabetic conditions. Therefore, body weight of each group was also measured during dose administration to find out whether any alterations occurred or not. Result (Table 4.8) exhibited that the body weight of diabetic group was decreased after 20 days of alloxan administration while LD-ANL and HD-ANL group exhibited almost at per body weight with standard glibenclamide group. Hence, it may be inferred that ANL extract is help in maintaining the body weight after affected by diabetes.

Besides, insulin plays a major role in glucose homeostasis along the side of a counter regulatory hormone, glucagon, which elevates serum glucose. The reduced level of insulin (64%) in the diabetic group leads to the pathogenesis of diabetes and its several complications thereby enhancing glucose level in blood. Even though the insulin level was not restored upto normal level, it was significantly (P<0.01) improved 85% by high ANL treatment. Thus, present study revealed a distinct hypoglycaemic action through the stimulation of surviving β-cells of islets of langerhans to release more insulin. Treatment with ANL extract and glibenclamide probably increased the insulin secretion (Fig. 4.9.B), which in turn, activated the glucokinase, thereby increasing utilization of glucose and thus, the increased utilization leads to decreased blood sugar level.

On the other hand, it is well-known that glycogen is the major intracellular storable

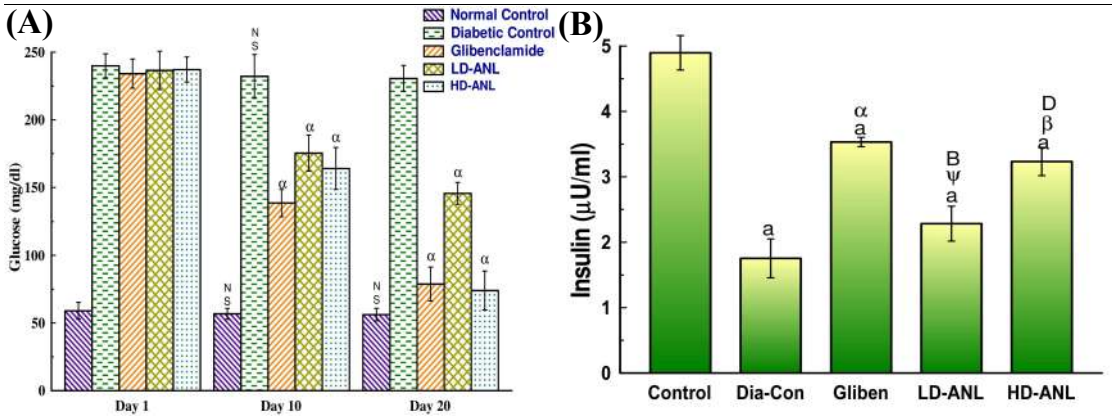

Fig. 4.9. (A) Effect of different groups on blood glucose (mg/dl) level in alloxan-induced diabetic mice on 20 days of treatment [$^{NS}P > 0.05$, $^{\alpha}P < 0.001$ vs day 1 of corresponding group]. **(B)** Insulin level of different groups after 20 days of ANL treatment. Dia-Con= Diabetic control, Gliben= Glibenclamide group. Here, $^{a}p<0.001$; $^{b}p<0.01$; $^{c}p< 0.05$; ^{d}p=non-significant (p>0.05) vs control group; $^{\alpha}p<0.001$; $^{\beta}p<0.01$; $^{\gamma}p< 0.0$; $^{\psi}p$=non-significant (p>0.05) vs diabetic control group; $^{A}p<0.001$; $^{B}p<0.01$; $^{C}p< 0.05$; ^{D}p=non-significant (p>0.05) vs Glibenclamide group [Data represented as mean ± SD]

Table 4.8. Role of ANL extract on body weight (gm) of diabetic mice.

	Control gr.	Diabetic gr.	Glibenclamide gr.	LD-ANL gr.	HD-ANL gr.
1st Day	27.16±0.53	30.35±0.75	26.18±0.85	25.89±1.28	26.25±1.61
10th Day	27.24±1.13$^{N.S.}$	25.57±0.63$^{N.S.}$	26.58±1.07$^{N.S.}$	25.21±1.06$^{N.S.}$	26.09±1.29$^{N.S.}$
20th Day	29.60±1.12$^{N.S.}$	22.34±1.31$^{N.S.}$	27.27±0.83$^{N.S.}$	25.68±1.24$^{N.S.}$	27.56±0.59$^{N.S.}$

Here, $^{N.S.}P > 0.05$ vs day 1 of corresponding group

form of glucose in various body tissues and its level in such tissues, especially liver is a direct reflection of insulin activity (Sharma *et al.*, 1993). Actually, insulin enhances glycogen deposition by means of regulating glycogen synthase and by inhibiting glycogen phosphorylase. It was observed that the hepatic glycogen level in diabetic group was dramatically deceased by 56% comparison to control group which was significantly ($P < 0.001$) improved by 45%, 15% and 30% in glibenclamide, low and high ANL group respectively (Fig. 4.10.A). The possible mechanism underlying restored glycogen content involves the activation of glycogen synthase system and inhibition of glycogen phosphorylase by the extract (Bansal *et al.*, 1981).

During diabetes, the excess amount of glucose present in the blood reacts with haemoglobin reducing its amount to form glycosylated haemoglobin or HbA1c (Koenig *et al.*, 1976) which is monitored as a reliable index of glycemic control in diabetes. In fact, HbA1c was found to increase in patients and/or animals with the onset of diabetes and this increasing ratio was directly proportional to the fasting blood glucose levels (Sheela and Augusti,

1992). Administration of ANL extract for 20 consecutive days to diabetic mice reduced the glycosylation of haemoglobin and thus decreased the levels of HbA1c was observed in diabetic animals (Fig. 4.10.B). In the present study, the diabetic control group revealed higher levels of glycosylated haemoglobin compared to control mice which was further decreased in LD-ANL and HD-ANL group indicating their potent anti-hyperglycaemic effect.

An imbalance between oxidants and antioxidants arise during diabetes mellitus initiating several diabetes-induced complications (Smirnoff, 2001). Higher levels of reactive oxygen species (ROS) or free radicals in diabetic subject are capable of chemically altering all major types of biomolecules including lipids, proteins and nucleic acids, by changing their structure and functions, thus leading to cell damage (Sinclair, 1993). Malondialdehyde (MDA), a marker of lipid peroxidation, results due to the peroxidation of polyunsaturated fatty acids (PUPA) in the cell membrane. Presence of elevated MDA in the serum signifies the onset of diabetes mellitus caused by oxidative stress (Ceriello, 2000). Fig. 4.11.A revealed increased level of MDA in diabetic control group while it was normalized upon administration of ANL extract. It may be inferred that certain phytochemicals present in the extract which reacted with free radicals, thus avoided lipid peroxidation as well as the risk of cordiovascular diseases (Pari and Umamaheswari, 2000).

In addition, catalase (CAT) and peroxidase (PX) are two significant indices of oxidative stress. Autoxidation of alloxan-induced diabetes generates more ROS like superoxide radical ($O_2^{\bullet-}$), H_2O_2 and hydroxyl radical ($OH^{\bullet-}$) that accumulate

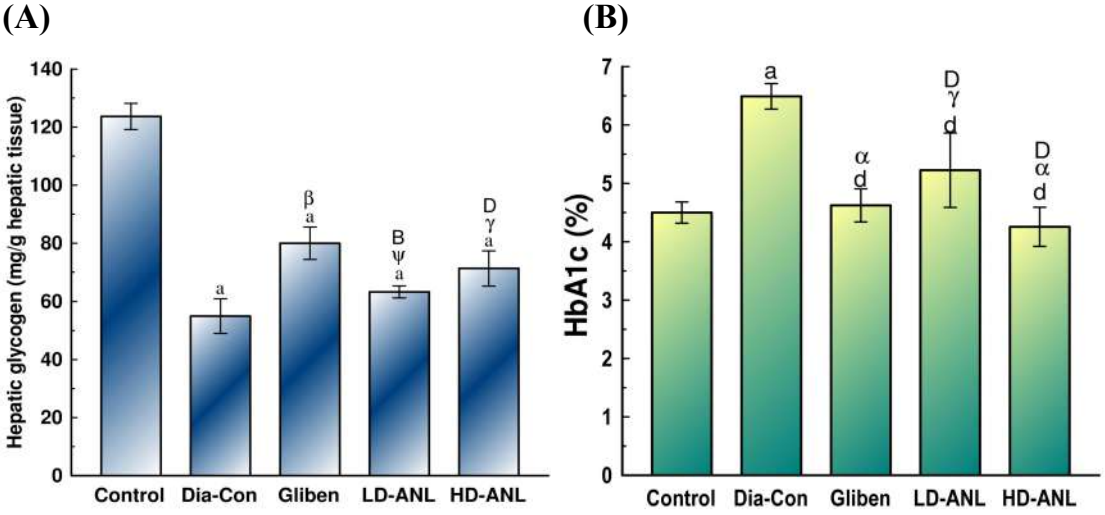

Fig. 4.10. (A) Hepatic glycogen level and **(B)** HbA1c level of different groups after 20 days of ANL treatment. [Dia-Con= Diabetic control, Gliben= Glibenclamide group. Here, ^{a}p<0.001; ^{b}p<0.01; ^{c}p< 0.05; ^{d}p=non-significant (p>0.05) vs control group; $^{\alpha}p$<0.001; $^{\beta}p$<0.01; $^{\gamma}p$< 0.0; $^{\Psi}p$=non-significant (p>0.05) vs diabetic control group; ^{A}p<0.001; ^{B}p<0.01; ^{C}p< 0.05; ^{D}p=non-significant (p>0.05) vs Glibenclamide group; Data represented as mean ± SD]

over time in liver, kidney and skeletal muscle, thereby contribute cell injury and development of human diseases (Sinclair, 1993). Present findings exhibited that treatment with ANL extract upregulated the activity of CAT (Fig. 4.11.B) and PX (Fig. 4.11.C) enzymes compared to diabetic mice and thus may help to counteract the damage by the ROS generated during diabetes. In fact, a significant decrease (P <0.01-0.001) in CAT and PX activities were seen in liver, kidney and skeletal muscle, which were subsequently normalized due to glibenclamide and ANL treatment. A 34%, 30% and 38% lowered PX activity and 48%, 44% and 57% lowered CAT activity was measured in liver, kidney and skeletal muscle. When treated with high ANL, highest increase (51%, P <0.001) of peroxidase and catalase activities were (123%, P <0.001) was seen in case of skeletal muscle. Similar type of activity of these enzymes in diabetic group was also documented by several investigators (Montefusco-Pereira *et al.*, 2013; Sekeroglu *et al.*, 2000) suggesting ANL could be beneficial for correcting the

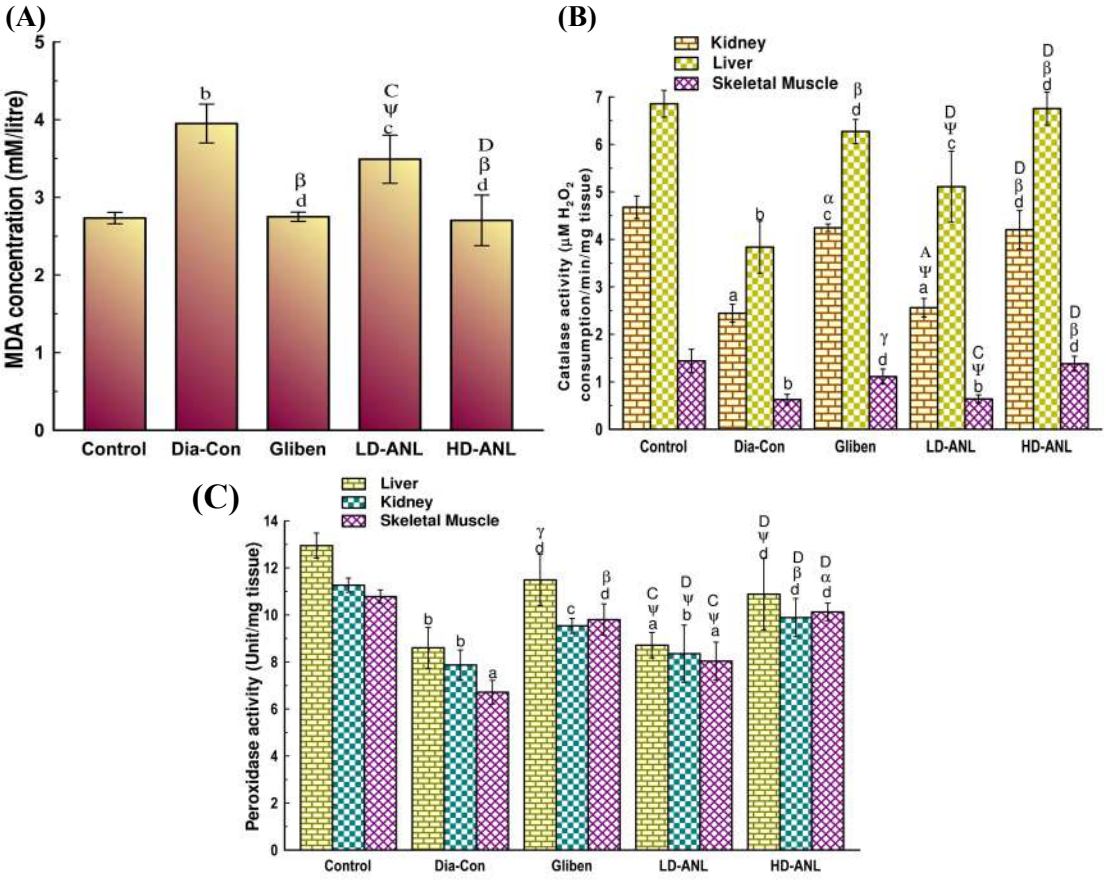

Fig. 4.11. (A) MDA concentration level, **(B)** Catalase activity and **(C)** Peroxidase activity in liver, kidney and skeletal muscle of different groups after 20 days of ANL administration. Dia-Con= Diabetic control, Gliben= Glibenclamide group. Here, ^{a}p<0.001; ^{b}p<0.01; ^{c}p< 0.05; ^{d}p=non-significant (p>0.05) vs control group; $^{\alpha}p$<0.001; $^{\beta}p$<0.01; $^{\gamma}p$< 0.0; $^{\Psi}p$=non-significant (p>0.05) vs diabetic control group; ^{A}p<0.001; ^{B}p<0.01; ^{C}p< 0.05; ^{D}p=non-significant (p>0.05) vs Glibenclamide group [Data represented as mean ± SD]

hyperglycemia and it may prevent diabetic complications due to lipid peroxidation and free radical oxidation.

In a further attempt to gain an insight into the underlying biochemical mechanisms involved in anti-diabetogenic activities of plant extract, several renal parameters were investigated associated with diabetes. Kidneys are such major organs of the body that remove metabolic wastes such as urea, uric acid, creatinine and thereby optimum chemical composition of body fluids is maintained. The elevation in the levels of blood urea, uric acid and creatinine is considered as significant markers of renal or kidney dysfunction associated with diabetes. During diabetic condition, continuous catabolism of amino acid results high quantity of urea from urea cycle and eventually produces uric acid in the blood (Landin *et al.*, 1991). Creatinine, the metabolite of muscle creatine, is easily excreted by the kidneys and its elevated level in the serum signifies kidney impairment (Landin *et al*, 1991). Administration of ANL extract, however, produced a significant reduction in the levels of these three metabolites (Table 4.9), thereby indicating protection against impairment of kidneys due to diabetes. Simultaneously, high concentration of cholesterol and triglycerides in the blood becomes a risk factor for coronary heart disease occurring due to the increase in the mobilization of free fatty acids from the peripheral depots, since insulin inhibits the hormone-sensitive lipase (Al-Shamaony *et al.*, 1994). Table 4.9 clearly reflected that the treatment with ANL to diabetic animals significantly reduced the plasma cholesterol level to near normalcy and thus minimized the risk of cardiovascular disease (Rhoads *et al.*, 1976). Correspondingly, ANL was also able to bring down the levels of triglycerides in diabetic animals to an appreciable extent (Table 4.9) when compared to the untreated diabetic group.

Furthermore, acid phosphatase (ACP) and alkaline phosphatase (ALP) are two liver marker enzymes often employed to evaluate the integrity of plasma membrane and endoplasmic reticulum (Akanji *et al.*, 1993). In essence, elevation level of these two enzymes in the serum reflects obliteration of structural integrity of the liver during diabetes. In addition, transaminases i.e. aspartate aminotransferase (AST) and alanine aminotransferase (ALT) are two recognized enzymes used as biomarkers to assess possible toxicity to the liver (Rahman *et al.*, 2001). An increase level of AST and ALT in the serum may chiefly be due to the leakage of these enzymes from the liver cytosol into the blood stream providing an indication of liver damage as well. Present study has documented that ACP, ALP, AST and ALT levels were significantly elevated in the diabetic control animals and subsequently reduced (Table 4.9) in diabetic groups after the

Table 4.9. Different enzymatic and biochemical parameters of the serum of different five experimental groups.

Parameters (units)	Control	Diabetic control	Glibenclamide	LD-ANL	HD-ANL
ACP (K.A.)	3.19±0.11	7.19±0.14^{b}	5.7±0.57$^{c\ \psi}$	6.95±0.10$^{a\ \psi\ C}$	5.93±0.27$^{b\ \gamma\ D}$
ALP (K.A.)	11.0±1.01	21.23±1.42^{a}	12.34±0.42 $^{d\ \alpha}$	16.02±1.51$^{b\ \gamma\ C}$	13.53±1.74$^{d\ \beta\ D}$
AST (U/ml)	66.58±0.86	99.64±3.78^{a}	75.62±1.01$^{a\ \alpha}$	86.61±1.19$^{a\ \beta\ A}$	76.97±3.89$^{c\ \beta\ D}$
ALT (U/ml)	42.19±1.48	87.46±2.45^{a}	53.82±2.66$^{b\ \alpha}$	74.87±2.02$^{a\ \beta\ A}$	72.19±13.95$^{c\ \psi\ D}$
Creatinine (mg/dl)	0.19±0.005	0.35±0.01^{a}	0.19±0.004$^{d\ \alpha}$	0.25±0.03$^{c\ \gamma\ C}$	0.17±0.01$^{d\ \alpha\ D}$
Triglyceride (mg/dl)	90.36±6.45	137.83±6.93^{a}	89.07±7.73$^{d\ \beta}$	117.45±17.79$^{d\ \psi\ D}$	112.89±25.74$^{d\ \psi\ D}$
HDL Cholesterol (mg/dl)	82.17±8.02	129.87±3.50^{a}	83.30±15.80$^{d\ \beta}$	133.14±44.61$^{d\ \psi\ D}$	93.29±10.91$^{d\ \beta\ D}$
Urea (mg/dl)	21.24±0.05	26.10±1.2^{b}	22.72±2.52$^{d\ \psi}$	24.32±1.00$^{d\ \gamma\ D}$	22.52±1.35$^{b\ \psi\ D}$
Urea N_2 (mg/dl)	9.92±0.23	22.37±1.85^{a}	10.61±1.17$^{d\ \alpha}$	10.52±0.63$^{d\ \alpha\ D}$	11.36±0.47$^{b\ \alpha\ D}$
Uric acid (mg/dl)	1.57±0.14	2.26±0.12^{b}	1.90±0.14$^{d\ \gamma}$	2.70±0.10$^{a\ \beta\ B}$	2.03±0.11$^{c\ \psi\ D}$

^{a}p<0.001; ^{b}p<0.01; ^{c}p< 0.05; ^{d}p=non-significant (p>0.05) vs control group; $^{\alpha}p$<0.001; $^{\beta}p$<0.01; $^{\gamma}p$< 0.0; $^{\psi}p$=non-significant (p>0.05) vs diabetic control; ^{A}p<0.001; ^{B}p<0.01; ^{C}p< 0.05; ^{D}p=non-significant (p>0.05) vs Glibenclamide group [Data represented as mean ± SD]

administration of ANL leading towards the alleviation of liver injury (El-Demerdash *et al.*, 2005).

In conclusion, present study is significant as it covers different biochemical and metabolic aspects responsible for the progression of diabetes. What's more, ANL extract exhibited significant increase in ameliorating varied diabetic complications and blood glucose control compared to glibenclamide. However, at this stage it is difficult to predict whether any phytochemical compound acted independently or in synergetic manner because active principles or biomolecules are always responsible for their antidiabetogenic effect (Bhat *et al.*, 2011; Coman *et al.*, 2012). Hence, it may be inferred that ANL extract possibly helped in islets regeneration/protection and insulin production (Kanter *et al.*, 2003) which indirectly modulated all other biochemical parameters, thus ANL holds a hope towards the discovery of new anti-diabetic drug.

4.7. Chemical Characterizations of selected plant extracts

Since the extracts exhibited potent antioxidant, anti-neurodegenerative and anti-diabetic activity, it would be an amicable one to identify the active phytocompounds responsible for those activities present in the extracts. In this regard, FTIR, GC-MS and NMR analysis have been considered.

4.7.1. FT-IR analysis

Fourier transform infrared spectroscopy (FT-IR) analysis, one of the most widely

accepted methods, is utilized preliminary to characterize the functional groups based on the peak value in the region of infrared radiation. Besides, it is a required process to identify medicines in Pharmacopoeia (Liu *et al.*, 2006). In the present study, FTIR analysis of ACL and ANL extracts were employed. Figure 4.12 and 4.13 revealed that the major peaks indicated the presence of phenols, alkanes, aldehydes, aromatics, amides, alkenyls etc (Table 4.10). Hence, it may be inferred that *A. catechu* (ACL) and *A. nilotica* (ANL) extracts may be the potent source of many natural flavonoids and sterols including quercetin, iso-quercetrin, kaempferol, myricetin, isorhamnetin, stigmasterol, campesterol etc. inhibiting or suppressing the formation of free radicals by binding to the metal ions or quenching singlet oxygen.

4.7.2. GC-MS analysis

4.7.2.1. GC-MS analysis of A. catechu (ACL) extract

GC-MS analysis (Fig. 4.14) of ACL extract was performed to identify the presence of various bioactive metabolites and neurotransmitters, if any. A total of 41 different bioactive compounds (Table 4.11) have been identified by GC-MS analysis. Of the 41 compounds, 5 compounds have already been proven as potent antioxidants including gallic acid, D -mannitol, catechin, epicatechin and isoquercitrin (Fig. 4.15).

Amongst these phytometabolites, catechin, D-mannitol, epicatechin and isoquercitrin

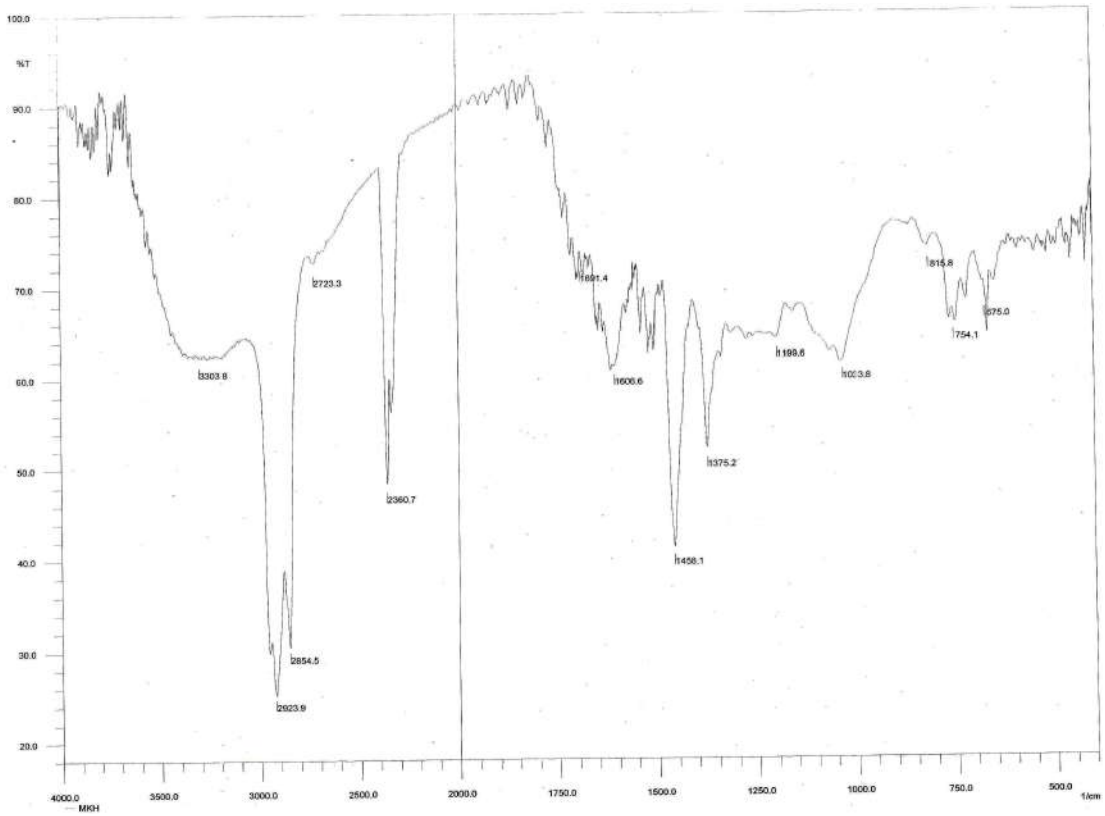

Fig. 4.12. FT-IR spectroscopic analysis of ACL.

Table 4.10. FTIR absorption values and functional groups of ACL and ANL extracts.

Plant Sample	Wave number (cm^{-1})	Types of Bond	Functional groups	Absorption intensity
ACL	3303.8	C≡C-H stretch	Alkynes	Strong
		O-H stretch, H-bonded	Alcohols	Strong
	2923.9	C-H stretch	Alkanes	Strong
	2854.5	C-H stretch	Alkanes	Strong
	2723.3	O=C-H stretch	Aldehydes	Weak
	2360.7	Unknown	Unknown	Unknown
	1691.4	C=O Stretch	Aldehydes	Strong
	1606.6	C=O Stretch	Amides	Weak
	1458.1	C-H Stretch	Alkanes	Strong
	1375.2	C-H Stretch	Alkanes	Strong
	1199.6	C=C Stretch	Alkenyl	Medium
	1033.8	C-O Stretch	Primary alcohol	Medium
	815.8	C-H Stretch	Alkanes	Strong
	754.1	Unknown	Unknown	Unknown
	675.0	C–H "oop"	Aromatics	Medium
ANL	3296.1	O-H stretch	Alcohols	Strong
	2922.0	C-H stretch	Alkanes	Strong
	2852.5	C-H stretch	Alkanes	Strong
	2723.3	O=C-H stretch	Aldehydes	Weak
	2358.8	Unknown	Unknown	Unknown
	1687.6	C=O Stretch	Aldehydes	Strong
	1614.3	C=C Stretch	Alkenes	Medium
	1454.2	C-H Stretch	Alkanes	Strong
	1317.3	C=C Stretch	Alkenyls	Medium
	1203.5	C=C Stretch	Alkenyls	Medium
	1134.1	C=O Stretch	Ketones	Strong
	1033.8	C-O Stretch	Primary alcohol	Medium
	864.0	Unknown	Unknown	Unknown
	815.8	C-H Stretch	Alkanes	Strong
	721.3	Unknown	Unknown	Unknown
	669.3	C–H "oop"	Aromatics	Medium

are known to be effective scavengers of hydroxyl, peroxyl, superoxide and DPPH radicals with significant anti-cancerous activity (Desesso *et al.*, 1994; Valcic *et al.*, 2000; Vellosa *et al.*, 2011) while gallic acid is known as strong antioxidative agent (Yen *et al.*, 2002). In addition, catechin and epicatechin reveal monosamine

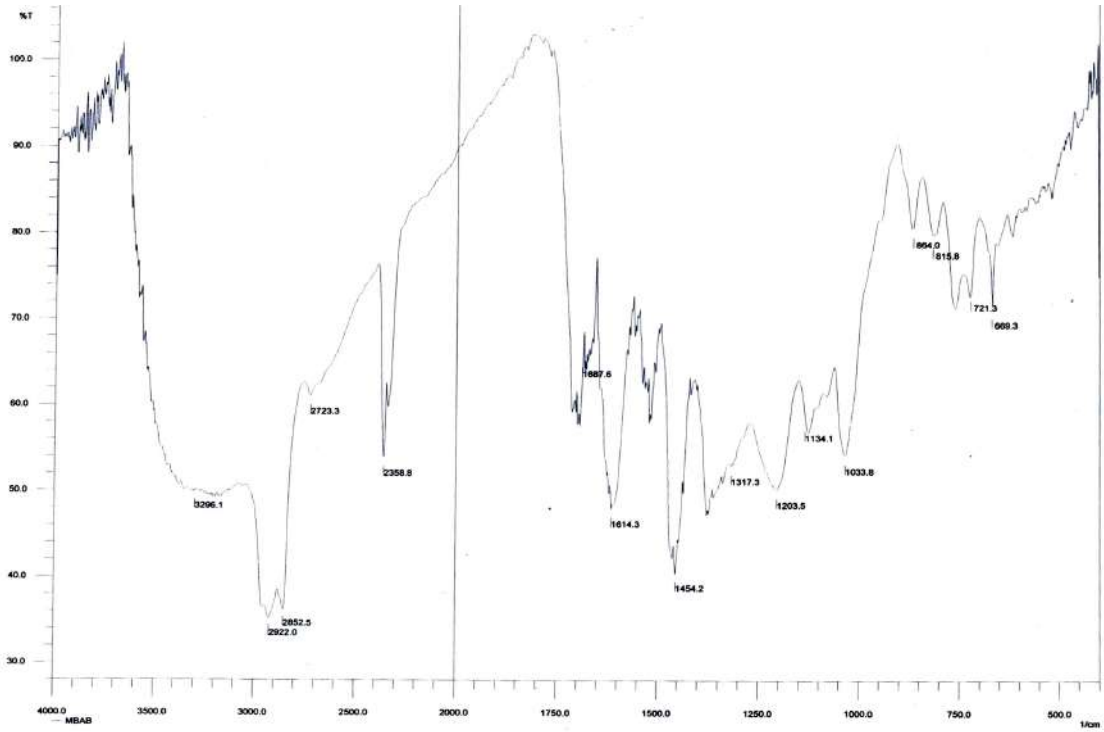

Fig. 4.13. FT-IR spectroscopic analysis of ANL.

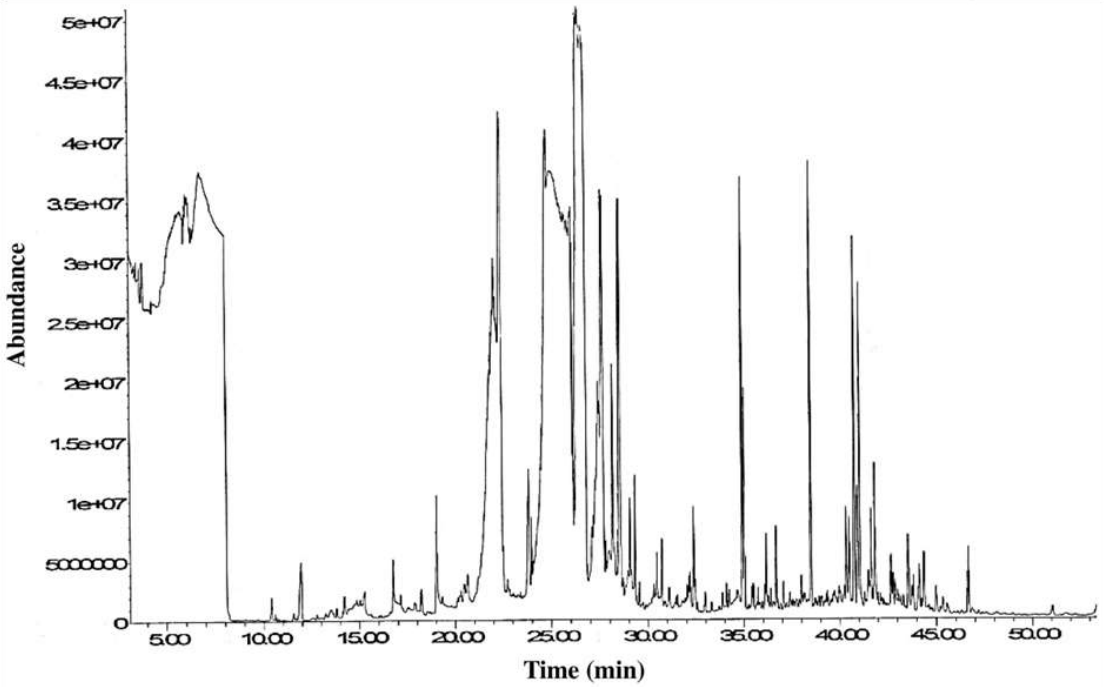

Fig . 4.14. Gas chromatogram-Mass spectroscopy of *A. catechu* leaf extract.

oxidase inhibitory activity responsible partly for Parkinson's disease (PD), Alzheimer's disease (AD) and others cognitive disorders (CDs).

Concurrently, a few other bioactive compounds namely, phenylalanine, tyramine, dopamine, and serotonin have been identified which have either anti-neurodegenerative properties or are known as the precursor of compounds which are

Table 4.11. List of metabolites detected in *A. catechu* leaf extract by GC-MS analysis.

Name of the Metabolites	Log of RRR*	
	Average	SD
L-(+) lactic acid	1.07	0.32
L- alanine	0.55	0.19
L- valine	0.94	0.12
Urea	0.23	0.33
Pipecolic acid	1.28	0.42
Glycerol	2.32	0.02
Phosphoric acid	1.30	0.02
L-threonine	1.10	0.17
Glycine	0.56	0.09
Succinic acid	0.77	0.19
Glyceric acid	1.22	0.09
Beta-alanine	0.90	0.10
D- malic acid	1.53	0.03
O-acetylsalisylic acid	0.40	0.21
L- glutamic acid 3 (dehydrated)	1.64	0.13
4-guanidinobutyric acid	1.57	0.25
Phenylalanine	0.59	0.17
Phenylethylamine	1.09	0.08
Meleamic acid	0.48	0.17
L-glutamic acid	0.16	0.05
Lauric acid	1.33	0.50
L- asparagine	1.77	0.05
Xylitol	2.14	0.25
Arabitol	0.79	0.05
Putrescine	1.04	0.09
Methyl-beta-D-galactopyranoside	1.25	0.05
Quinic acid	1.41	0.48
Allantoin	1.69	0.06
Tyramine	3.22	0.11
D-sorbitol	1.19	0.07
D-mannitol	1.13	0.09
Gallic acid	3.19	0.02
Palmitic acid	1.80	0.08
Dopamine (hydroxytyramine)	1.02	0.07
L-tryptophan	1.52	0.02
Stearic acid	1.10	0.22
Serotonin	1.01	0.04
Sucrose	2.28	0.00
(-)- epicatechin	2.14	0.02
Catechin	2.05	0.07
Isoquercitrin	1.69	0.03

*RRR: Relative Response Ratio; SD: Standard Deviation.

anti-CDs. Out of these bioactive compounds, dopamine along with nor-epinephrine (noradrenaline) are collectively called catecholamines which are synthesized following the two equally active routes (Kulma and Szopa, 2007). In one of the routes, phenylalanine transfers into tyrosine by means of amino acid hydroxylase. Afterward, tyrosine decarboxylated to tyramine through the action of tyrosine decarboxylase and subsequently generates dopamine and norepinephrine (noradrenaline) catalysed by enzyme monophenol hydroxylase and dopamine beta- hydroxylase respectively. Therefore, it might be suggested that the synthesis of catecholamines in ACL probably follows the described route (Fig. 4.16). Previous studies (Basu and Dasgupta, 2000; Chinta and Andersen, 2005; Kulma and Szopa, 2007) exhibited that catecholamines and other neurotransmitters have distinct function to combat against neurodegeneration or cognitive disorders like AD, PD and dementia.

Hence from the above illustration, it might be inferred that *A. catechu* or ACL extract could be regarded as a potent future antioxidative stuff as well anti-psychiatric drug especially for Alzheimer's and Parkinson's disease.

4.7.2.2. GC-MS analysis of A. nilotica (ANL) extract

GC-MS data of ANL (Fig. 4.17) revealed

the exploration of a total of 29 phyocompounds (Table 4.12). Amongest this catechol, pyrogallol, γ-tocopherol, α-tocopherol, stigmasterol, β-sitosterol were reported to be as potent antioxidant (Avase *et al.*, 2015; Dillard *et al.*, 1983; Gupta *et al.*, 2011; Huang *et al.*, 1994; Justino *et al.*, 2006). Apart from it, result also yieleds that γ-tocopherol, α-tocopherol, β-sitosterol, stimasterol hold effectual anti-diabetic activity (Jamaluddin *et al.*, 1994). As evidenced from anti-diabetic appraisal

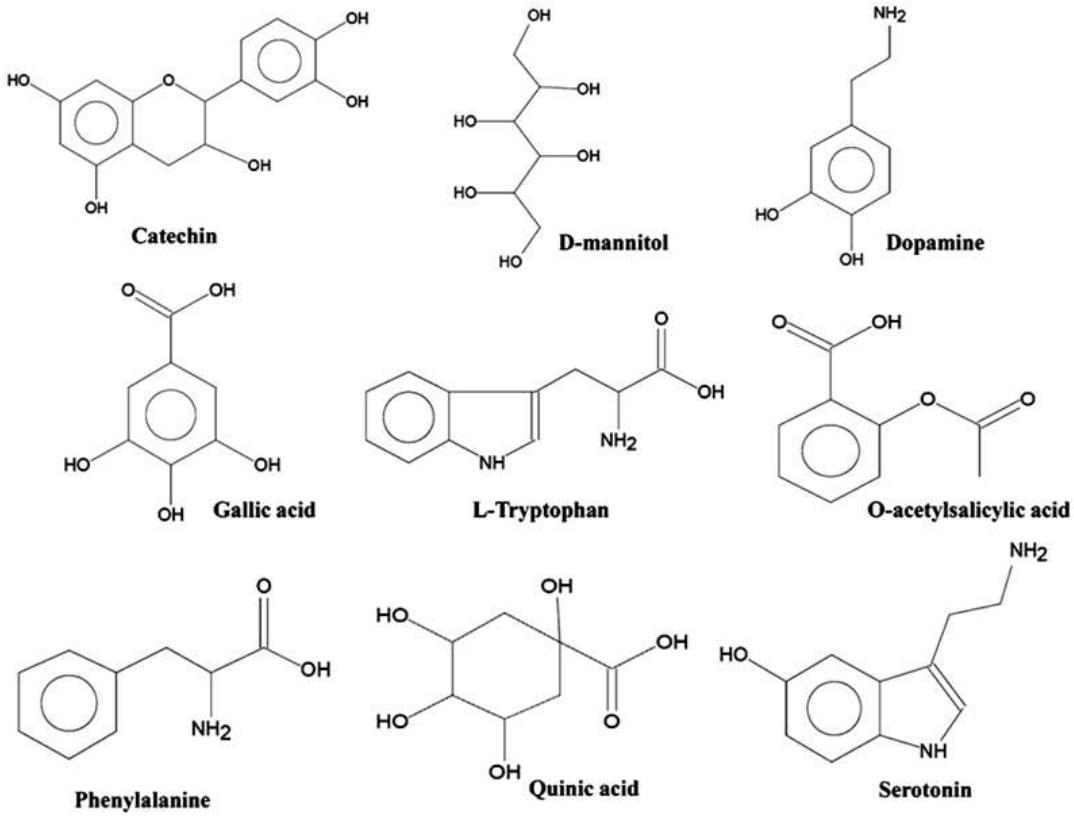

Fig. 4.15. Chemical structures of some essential bioactive metabolites identified in ACL extract by GC-MS.

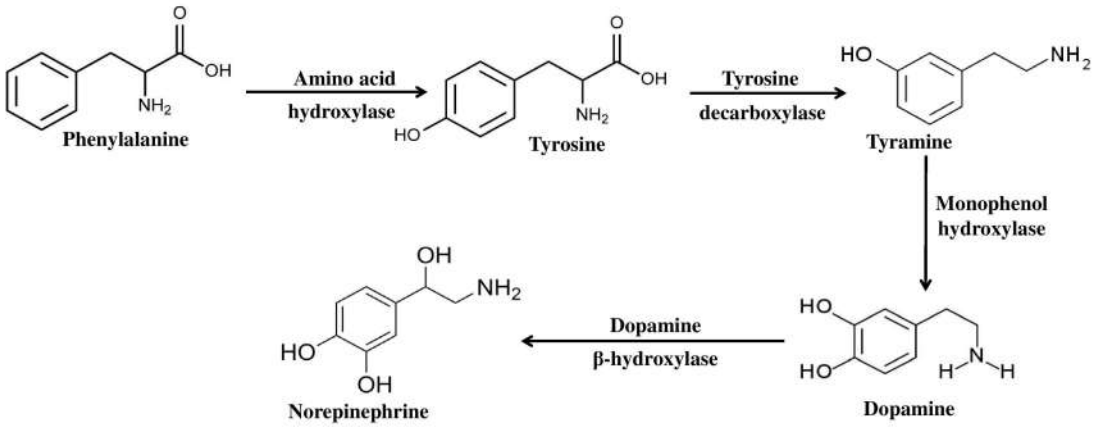

Fig. 4.16. Schematic representation of possible biosynthetic pathway of catecholamines identified in ACL extract.

of ANL, it may be presumed that these compounds might play significant role in ameliorating diabetes and its complications in mice model.

4.7.2.3. *GC-MS analysis of M. pudica (MPD) and M. invisa (MIN) extracts*

During GC-MS analysis, MPD and MIN extracts were first derived through Silylation method, which revealed the presence of several bioactive phytochemicals with known physiological implications in diverse pathological conditions. Silylation primarily substitutes the active hydrogen present in different functional groups (-OH, -COOH, -NH, -NH2, and -SH) in a molecule and introduces a silyl group in the form of dimethylsilyl [$SiH(CH_3)_2$], t-butyldimethylsilyl [$Si(CH_3)_2C(CH_3)_3$] and chloromethyldimethylsilyl [$SiCH_2Cl(CH_3)_2$] (Orata, 2012). This substitution of terminal hydrogen by silyl group in the sample lowers the hydrogen bonding and thus, reduces polarity of the sample, resulting in a comparatively more volatile sample, easy to detect in GC. The bioactive phytocompounds identified in MPD and MIN (Fig. 4.18 and Fig. 4.19) corresponding to GC chromatogram have been enlisted in Table 4.13 and Table 4.14 respectively.

A total of 34 bioactive metabolites were identified in MPD extract by GC-MS whereas MIN extract exhibited a total of 40 bioactive compounds (Fig. 4.20). Most of the compounds were identified in their TMS (C_3H_9Si) derivated form, resulting in

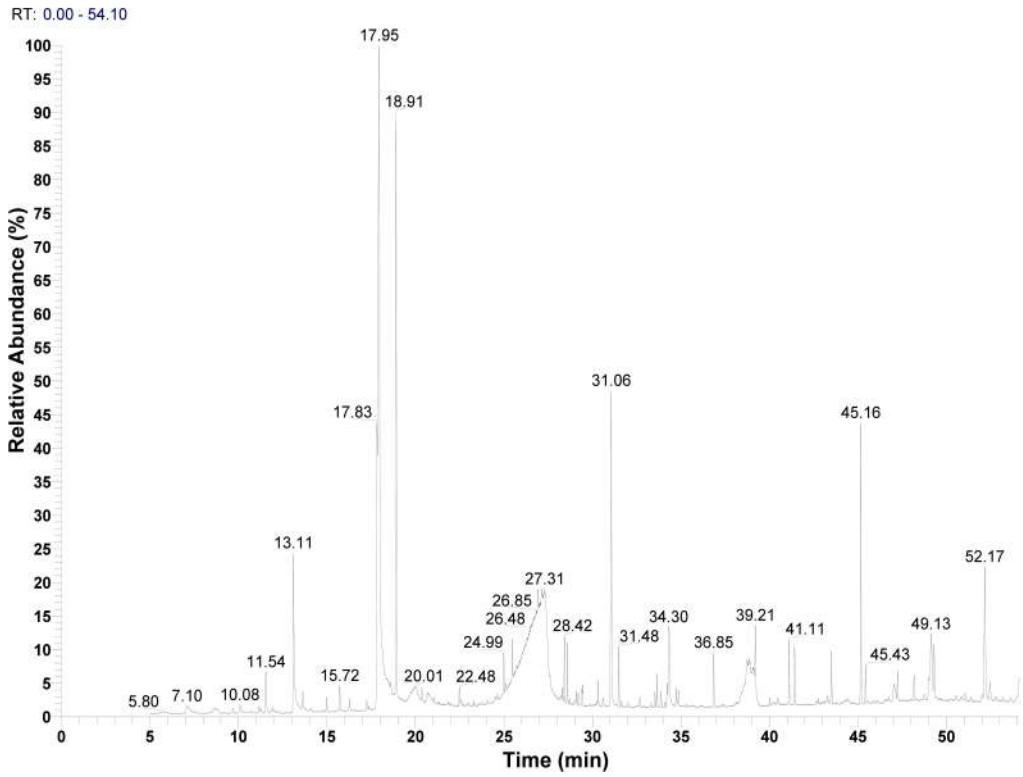

Fig. 4.17. GC-MS chromatogram of ANL extract.

Table 4.12. List of metabolites detected in *A. nilotica* leaf extract by GC-MS analysis.

Identified Compounds	MW	RT (min)	Formula
2-Propanone, 1,1-diethoxy-	146	7.10	$C_7H_{14}O_3$
Epomediol	186	10.08	$C_{10}H_{18}O_3$
Pyranone	144	11.54	$C_6H_8O_4$
Catechol	110	13.11	$C_6H_6O_2$
Phenol, 4-ethenyl-, acetate	162	13.63	$C_{10}H_{10}O_2$
5H-1-Pyrindine	117	15.72	C_8H_7N
p-Vinylguaiacol	150	16.27	$C_9H_{10}O_2$
Pyrogallol 1,3-dimethyl ether	154	17.25	$C_8H_{10}O_3$
Resorcinol	110	17.83	$C_6H_6O_2$
Pyrogallol	126	17.95	$C_6H_6O_3$
Bisphenol C	256	18.91	$C_{17}H_{20}O_2$
Dodecanoic acid	200	22.48	$C_{12}H_{24}O_2$
Hexadecanoic acid, methyl ester	270	30.32	$C_{17}H_{34}O_2$
9-Hexadecenoic acid	254	30.59	$C_{16}H_{30}O_2$
Estradiol, 3-deoxy-	256	32.01	$C_{18}H_{24}O$
Hexadecanoic acid	256	32.68	$C_{16}H_{32}O_2$
2-Hexadecanol	242	33.32	$C_{16}H_{34}O$
7,10-Octadecadienoic acid, methyl ester	294	33.53	$C_{19}H_{34}O_2$
Linolenic acid, methyl ester	292	33.65	$C_{19}H_{32}O_2$
Phytol	296	33.88	$C_{20}H_{40}O$
9,12-Octadecadienoic acid (Z,Z)-	280	34.22	$C_{18}H_{32}O_2$
Oleic Acid	282	34.73	$C_{18}H_{34}O_2$
8,11,14-Eicosatrienoic acid, (Z,Z,Z)-	306	34.86	$C_{20}H_{34}O_2$
Squalene	410	45.16	$C_{30}H_{50}$
γ-Tocopherol	416	48.16	$C_{28}H_{48}O_2$
Pregnan-18-oic acid, 20-hydroxy-, γ-lactone, (5α)-	316	49.13	$C_{21}H_{32}O_2$
dl-α-Tocopherol	430	49.30	$C_{29}H_{50}O_2$
Stigmasterol	412	52.17	$C_{29}H_{48}O$
β-Sitosterol	414	52.46	$C_{29}H_{50}O$

MW= Molecular weight; RT=Retention time.

an increase of m/z 73. Almost similar kinds of compounds were identified in both of cases belonging to the same genus of *Mimosa*.

Wide arrays of organic acids were identified in both MPD and MIN extracts namely, lactic acid, succinic acid, glutaric acid, malic acid, lauric acid, etc. Out of other bioactive metabolites characterized, azelaic acid have already been reported as an approved therapeutic agent for the skin condition rosacea (Jones, 2009) while salicylic acid, another identified metabolite, plays an important role in cytoprotection (De La Cruz *et al.*, 2004). Among the other indentified compounds gallic acid, squalene, α-tocopherol, campesterol, β-sitosterol and stigmasterol have also been established to display strong antioxidative features and protective properties against several disorders like cardiovascular disorders, cancer and NDs (Badhani *et al.*, 2015; Yoshida and Niki, 2003). Amongst these, gallic acid, a well-known polyphenolic constituent, was reported to scavenge ROS and RNS remarkably and inhibit lipid peroxidation and metal chelation (Badhani *et al*., 2015). Squalene and α-tocopherol are also excellent natural scavengers of free radicals found in vegetative oils. On the other hand campesterol, β-sitosterol and stigmasterol, collectively known as phytosterols (PS), have immense antioxidant activities (Li *et al.*, 2007; Yoshida and Niki, 2003). Moreover, they

Table 4.13. List of bioactive metabolites detected in MPD leaf extract by GC-MS analysis.

Compound Name	Formula	MW	Mass fragments (m/z)	RT(min)	RA(%)
Lactic acid, (2TMS)	$C_9H_{22}O_3Si_2$	234	147 ($C_5H_{11}O_3Si$), 117 ($C_5H_{13}OSi$), 73* (C_3H_9Si)	9.41	3.64 ± 0.86
2-acetoxyacetate (TMS)	$C_7H_{14}O_4Si$	190	133 (C_4H_9O3Si), 117 ($C_4H_5O_4$), 73* (C_3H_9Si)	12.74	5.71 ± 0.57
Propylene glycol, di-TMS	$C_9H_{24}O_2Si_2$	220	147 ($C_6H_{15}O_2Si$), 117* ($C_5H_{13}OSi$), 73 (C_3H_9Si)	13.19	0.48 ± 0.04
Glycerol, tris-TMS	$C_{12}H_{32}O_3Si_3$	308	205 ($C_8H_{21}O_2Si_2$), 147 ($C_6H_{15}O_2Si$), 73* (C_3H_9Si)	15.58	7.85 ± 0.53
3-Butenoic acid, 3-(trimethylsiloxy)-, TMS ester	$C_{10}H_{22}O_3Si_2$	246	231 ($C_9H_{19}O_3Si_2$), 147 ($C_7H_{15}O_3$), 73* (C_3H_9Si)	15.83	0.43 ± 0.10
Succinic acid (2TMS)	$C_{10}H_{22}O_4Si_2$	262	147 ($C_7H_{19}OSi$), 129 ($C_5H_9O_2Si$), 73* (C_3H_9Si)	16.43	3.25 ± 0.48
Glyceric acid, (3TMS)	$C_{12}H_{30}O_4Si_3$	322	189 ($C_7H_{17}O_2Si_2$), 147 ($C_5H_{10}O_3Si$), 73* (C_3H_9Si)	17.10	0.76 ± 0.22
Glutaric acid, bis-TMS	$C_{11}H_{24}O_4Si_2$	276	158 ($C_7H_{14}O_2Si$), 147* ($C_8H_{19}O_2$)	18.80	0.49 ± 0.07
Malic acid (3TMS)	$C_{13}H_{30}O_5Si_3$	350	233 ($C_9H_{31}O_3Si2$), 147 ($C_7H_{15}O_3$), 73 (C_3H_9Si)	21.15	3.56 ± 0.18
Adipic acid (TMS)	$C_{12}H_{26}O_4Si_2$	290	147 (C_7H_9OSi), 111 ($C_6H_{19}O_2Si$), 73* (C_3H_9Si)	21.34	0.83 ± 0.24
Salicylic acid, bis-TMS	$C_{13}H_{22}O_3Si_2$	282	267 ($C_{12}H_{19}O_3Si_2$), 149 (C_8H_9OSi), 73* (C_3H_9Si)	21.47	0.86 ± 0.18
Erythronic acid, (4TMS) deriv.	$C_{16}H_{40}O_5Si_4$	424	292 ($C_{11}H_{28}O_3Si_3$), 205 ($C_7H_{17}O_3Si_2$), 73* (C_3H_9Si)	23.09	0.34 ± 0.04
Pimelic acid (2TMS)	$C_{13}H_{28}O_4Si_2$	304	155 ($C_8H_{15}OSi$), 125 ($C_7H_9O_2$),73* (C_3H_9Si)	23.64	0.51 ± 0.11
Lauric acid (TMS)	$C_{15}H_{32}O_2Si$	272	257 ($C_{14}H_{29}O_2Si$), 117*	24.63	0.75 ± 0.32
Suberic acid (2TMS)	$C_{14}H_{30}O_4Si_2$	318	169 ($C_9H_{17}OSi$), 73* (C_3H_9Si)	25.77	0.93 ± 0.06
Nonadecane	$C_{19}H_40$	268	85 (C_6H_3), 71 (C_5H_{11}), 57 (C_4H_9)	27.75	0.26 ± 0.04
Azelaic acid, bis-TMS	$C_{15}H_{32}O_4Si_2$	332	201 ($C_{10}H_{21}O_2Si$), 73* (C_3H_9Si)	27.87	2.09 ± 0.25
Myristic acid, TMS ester	$C_{17}H_{36}O_2Si$	300	117 ($C_4H_9O_2Si$), 73* (C_3H_9Si), 55 (C_4H_7)	28.83	1.14 ± 0.14
Tridecanoic acid, 4,8,12-trimethyl-, methyl ester	$C_{17}H_{34}O_2$	270	197 ($C_{14}H_{29}$), 87* ($C_4H_7O_2$)	30.31	1.52 ± 0.06
n-Pentanoic acid, TMS ester	$C_{18}H_{38}O_2Si$	314	299 ($C_{17}H_{35}O_2Si$), 117* ($C_{18}H_9O_2Si$)	30.80	0.94 ± 0.33
Gallic acid, tetraTMS	$C_{19}H_{38}O_5Si_4$	458	280 ($C_{13}H_{21}O_3Si_2$), 73* (C_3H_9Si)	31.39	0.47 ± 0.52
Palmitic acid, TMS	$C_{19}H_{40}O_2Si$	328	313 ($C_{18}H_{37}O_2Si$), 117* ($C_{18}H_9O_2Si$)	32.69	61.26 ± 1.08
Linolenic acid, methyl ester	$C_{19}H_{32}O_2$	292	236 ($C_{15}H_{24}O_2$), 79 (C_6H_7)	33.64	1.48 ± 0.04
Margaric acid, TMS ester	$C_{20}H_{42}O_2Si$	342	327 ($C_{19}H_{39}O_2Si$), 117 ($C_4H_9O_2Si$), 73* (C_3H_9Si)	34.47	0.82 ± 0.26
1-Trimethylsiloxy-3,7,11,15-tetramethyl-2-hexadecene	$C_{23}H_{48}OSi$	368	143* ($C_7H_{15}OSi$), 123 (C_9H_{15}),	35.08	11.25 ± 0.78
Linoleic acid, TMS	$C_{21}H_{40}O_2Si$	352	337 ($C_{20}H_{37}O_2Si$), 73* (C_3H_9Si)	35.66	28.74 ±2.06
α-Linolenic acid, TMS	$C_{21}H_{38}O_2Si$	350	335 ($C_{20}H_{35}O_2Si$), 129 ($C_5H_9O_2Si$), 73 (C_3H_9Si)	35.80	99.08 ± 1.34
Octadecanoic acid, TMS	$C_{21}H_{44}O_2Si$	356	341 ($C_{20}H_{41}O_2Si$), 117 ($C_4H_9O_2Si$)	36.21	24.35 ± 2.58
Behenic acid, TMS ester	$C_{25}H_{52}O_2Si$	412	145 ($C_6H_{13}O_2Si$), 117* ($C_4H_9O_2Si$), 55 (C_4H_7)	42.47	0.53 ± 0.21
Squalene	$C_{30}H_{50}$	410	95 (C_7H_{11}), 81 (C_6H_9), 69* (C_5H_9)	45.15	9.79 ± 0.68
(+)-α-Tocopherol, O-TMS	$C_{32}H_{58}O_2Si$	502	277 ($C_{16}H_{25}O_2Si$), 237 ($C_{17}H_{33}$)	49.52	5.38 ± 0.74
Campesterol, TMS ether	$C_{31}H_{56}OSi$	472	382 ($C_{26}H_{42}Si$), 343 ($C_{25}H_{43}$), 129* ($C_6H_{13}OSi$)	51.43	2.46 ± 0.46
Stigmasterol, TMS	$C_{32}H_{56}OSi$	484	255 ($C_{19}H_{27}$), 129 ($C_6H_{13}OSi$), 83* (C_6H_{11})	51.99	5.26 ± 0.51
β-Sitosterol TMS	$C_{32}H_{58}OSi$	486	396* ($C_{29}H_{48}$), 357 ($C_{26}H_{45}$), 129* ($C_6H_{13}OSi$)	53.11	5.58 ± 0.88

MW= Mol. Wt.; RT= Retention Time; RA= Relative Abundance

accumulate in the brain by crossing the blood-brain barrier (BBB) which is one of the crucial factors for becoming a novel drug and thus, they might facilitate with cell signaling, membrane protein trafficking and neurotransmission (Burg *et*

Table 4.14. List of bioactive metabolites detected in MIN leaf extract by GC-MS analysis.

Compound Name	Formula	MW	Identifying MS (m/z)	RT	RA (%)
Lactic acid, (2TMS)	$C_9H_{22}O_3Si_2$	234	147 ($C_5H_{11}O_3Si$), 117 ($C_5H_{13}OSi$), 73* (C_3H_9Si)	9.41	5.22 ± 0.41
L-Valine, TMS ester	$C_8H_{19}NO_2Si$	189	146 ($C_5H_{12}NO_2Si$), 72* (C4H10N)	10.01	2.07 ± 0.26
l-Proline, TMS ester	$C_8H_{17}NO_2Si$	187	103 ($C_3H_7O_2Si$), 70* (C4H8N)	12.47	2.14 ± 0.51
2-Hydroxyisocaproic acid, TMS ester	$C_9H_{20}O_3Si$	204	117 ($C_5H_9O_3$), 73* (C_3H_9Si)	13.81	1.16 ± 0.25
2-Propanone, bis(trimethylsilyloxy)-	$C_9H_{22}O_3Si_2$	234	147 ($C_5H_{11}O_3Si$), 103 ($C_4H_{11}OSi$), 73* (C_3H_9Si)	13.95	1.56 ± 0.08
L-Serine, O-(TMS)-, TMS este	$C_9H_{23}NO_3Si_2$	249	147 ($C_5H_{13}NO_2Si$), 116 ($C_4H_{10}NOSi$), 73 (C_3H_9Si)	14.93	0.97± 0.12
Glycerol, tris-TMS	$C_{12}H_{32}O_3Si_3$	308	205 ($C_8H_{21}O_2Si_2$), 147 ($C_6H_{15}O_2Si$), 73* (C_3H_9Si)	15.58	28.21 ± 0.98
L-Threonine, O-(TMS)-, TMS ester	$C_{10}H_{25}NO_3Si_2$	263	147 ($C_5H_{13}NO_2Si$), 130 ($C_5H_{12}NOSi$), 73* (C_3H_9Si)	15.97	0.79 ± 0.04
Succinic acid, bis-TMS	$C_{10}H_{22}O_4Si_2$	262	147 ($C_7H_{19}OSi$), 129 (C5H9O2Si),	16.43	2.38 ± 0.63
Glyceric acid, (3TMS)	$C_{12}H_{30}O_4Si_3$	322	189 ($C_7H_{17}O_2Si_2$), 147 ($C_5H_{10}O_3Si$), 73* (C_3H_9Si)	17.10	0.58 ± 0.05
Glutaric acid, bis-TMS	$C_{11}H_{24}O_4Si_2$	276	158 ($C_7H_{14}O_2Si$), 147*	18.80	0.72 ± 0.12
Dodecane, 2,6,11-trimethyl-	$C_{15}H_{32}$	212	85 (C_6H_{13}), 71 (C_5H_{11}), 57*	20.91	4.05 ± 0.86
Malic acid (3TMS)	$C_{13}H_{30}O_5Si_3$	350	233 ($C_9H_{31}O_3Si_2$), 147	21.15	2.62 ± 0.45
Adipic acid, (2TMS)	$C_{12}H_{26}O_4Si_2$	290	147 (C_7H_9OSi), 111	21.33	2.18 ± 0.38
Pyroglutamic acid, di(TMS)-	$C_{11}H_{23}NO_3Si_2$	273	156 ($C_7H_{14}NOSi$), 147 ($C_7H_{17}NO_2$), 73* (C_3H_9Si)	21.77	4.42 ± 0.72
DL-Phenylalanine, TMS ester	$C_{12}H_{19}NO_2Si$	237	146 (C_9H_8NO), 120 (C8H10N)	22.20	1.41 ± 0.06
Hexadecane	$C_{16}H_{34}$	226	71 (C_5H_{11}), 57 (C_4H_9)	23.36	2.19 ± 0.31
Glycerol, tris-TMS ether	$C_{12}H_{32}O_3Si_3$	308	205 ($C_8H_{21}O_2Si_2$), 147 (C6H15O2Si), 73* (C3H9Si)	23.68	12.13 ± 0.68
Lauric acid (TMS)	$C_{15}H_{32}O_2Si$	272	257 ($C_{14}H_{29}O_2Si$), 117*	24.64	1.04 ± 0.24
Suberic acid (2TMS)	$C_{14}H_{30}O_4Si_2$	318	169 (C9H17OSi), 73* (C3H9Si)	25.77	3.25 ± 0.68
Azelaic acid, bis-TMS	$C_{15}H_{32}O_4Si_2$	332	201 ($C_{10}H_{21}O_2Si$), 73* (C3H9Si)	27.88	5.96 ± 0.46
Tetradecanoic acid, TMS	$C_{17}H_{36}O_2Si$	300	285* ($C_{16}H_{33}O_2Si$), 129	28.84	4.08 ± 0.69
2,5-Dihydroxyacetophenone, bis(TMS) ether	$C_{14}H_{24}O_3Si_2$	296	281* ($C_{13}H_{21}O_3Si_2$), 73 (C_3H_9Si)	30.04	32.55 ± 1.31
Gallic acid, tetraTMS	$C_{19}H_{38}O_5Si_4$	458	280 ($C_{13}H_{21}O_3Si_2$), 73* (C3H9Si)	31.40	11.13 ± 0.58
Hexadecanoic acid, TMS	$C_{19}H_{40}O_2Si$	328	132 ($C_5H_{12}O_2Si$), 117	32.72	75.64 ± 2.06
Linoleic acid, TMS	$C_{21}H_{40}O_2Si$	352	337 ($C_{20}H_{37}O_2Si$), 73* (C3H9Si)	35.68	23.81 ± 1.64
α-Linolenic acid, TMS	$C_{21}H_{38}O_2Si$	350	335 ($C_{20}H_{35}O_2Si$), 129 ($C_5H_9O_2Si$), 73 (C_3H_9Si)	35.84	98.52 ± 1.32
Stearic acid, TMS ester	$C_{21}H_{44}O_2Si$	356	341 ($C_{20}H_{41}O_2Si$), 117 ($C_4H_9O_2Si$), 73* (C_3H_9Si)	36.23	43.52 ± 0.83
Arachidic acid, TMS ester	$C_{23}H_{48}O_2Si$	384	132 ($C_5H_{12}O_2Si$), 117 ($C_4H_9O_2Si$), 73 (C_3H_9Si), 55 (C4H7)	39.46	2.31 ± 0.41
1-Monopalmitin TMS ether	$C_{25}H_{54}O_4Si_2$	474	371 ($C_{21}H_{43}O_3Si$), 147 ($C_6H_{15}O_2Si$), 73* (C_3H_9Si)	41.92	3.85 ± 0.22
Behenic acid, TMS ester	$C_{25}H_{52}O_2Si$	412	145 ($C_6H_{13}O_2Si$), 117*	42.48	1.68 ± 0.45
9-Octadecenoic acid, 1,3-bis-(OTMS)-2-propyl ester	$C_{27}H_{56}O_4Si_2$	500	203 ($C_8H_{19}O_2Si_2$), 129 ($C_6H_{13}OSi$), 73* (C_3H_9Si), 67	44.45	12.59 ± 0.98
Squalene	$C_{30}H_{50}$	410	95 (C_7H_{11}), 81 (C_6H_9), 69* (C5H9)	45.17	18.37 ± 1.05
tert-Hexadecanethiol	$C_{16}H_{34}S$	258	187 ($C_{11}H_{23}S$), 57* (C_4H_9)	46.71	0.94 ± 0.35
Heptacosane	$C_{27}H_{56}$	380	85 (C_6H_{13}), 71 (C_5H_{11}), 57 (C4H9)	48.69	0.78 ± 0.12
(+)-α-Tocopherol, O-TMS-	$C_{32}H_{58}O_2Si$	502	277 ($C_{16}H_{25}O_2Si$), 237 (C17H33)	49.54	14.52 ± 0.59
Campesterol, TMS ether	$C_{31}H_{56}OSi$	472	382 ($C_{26}H_{42}Si$), 343 ($C_{25}H_{43}$), 129* ($C_6H_{13}OSi$)	51.55	2.17 ± 0.46
Stigmasterol, TMS	$C_{32}H_{56}OSi$	484	255 ($C_{19}H_{27}$), 129 (C6H13OSi),	52.01	8.22 ± 0.63
Triacontyl TMS ether	$C_{33}H_{70}OSi$	510	495* ($C_{32}H_{67}OSi$)	52.77	34.62± 0.80
β-Sitosterol TMS	$C_{32}H_{58}OSi$	486	396* ($C_{29}H_{48}$), 357 ($C_{26}H_{45}$), 129*	53.16	15.45 ± 0.62

MW= Mol. Wt.; MS= Mass fragment; RT= Retention Time (Min.); RA= Relative Abundance

al., 2013).

Therefore, it may be conclude that the present study has made a significant contribution in making MPD and MIN as powerful candidates against neuro-degenerative activities.

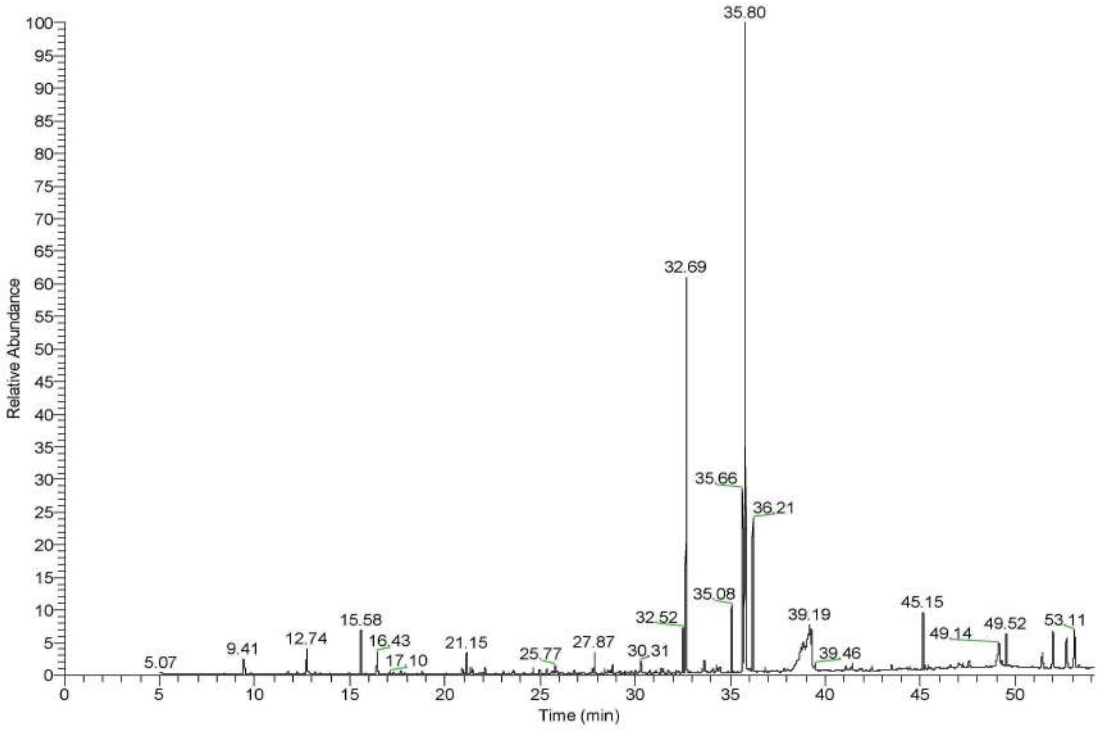

Fig. 4.18. Gas chromatogram-Mass spectroscopy of *M. pudica* leaf extract.

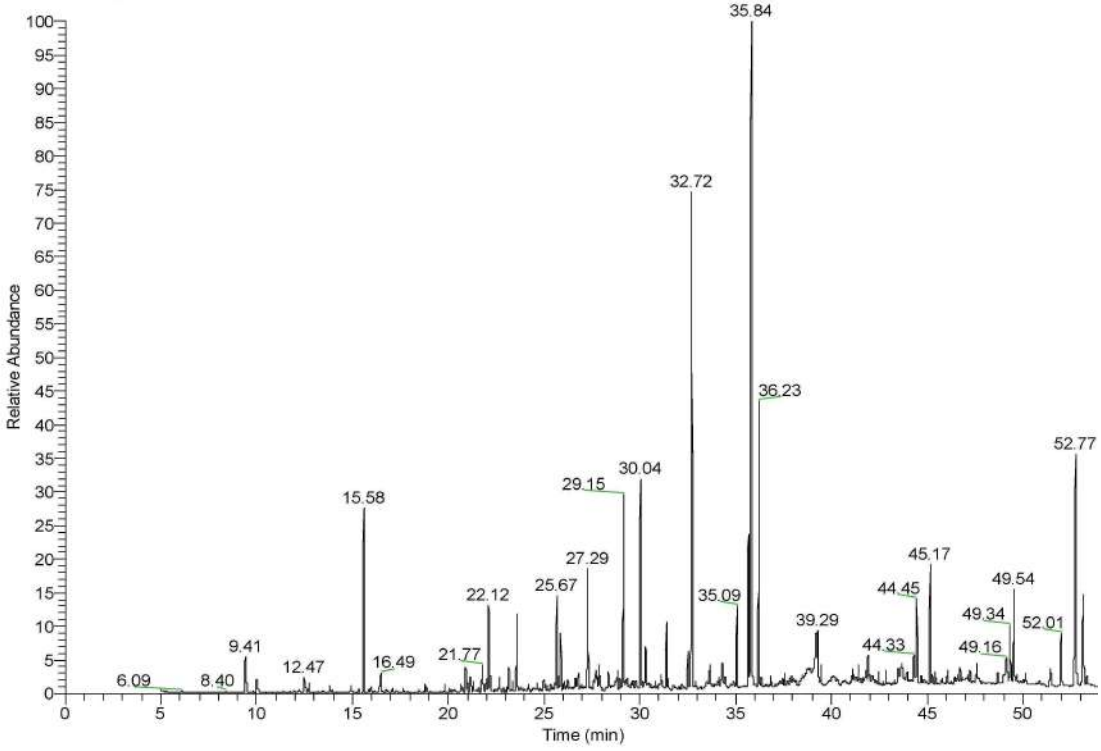

Fig. 4.19. Gas chromatogram-Mass spectroscopy of *M. invisa* leaf extract.

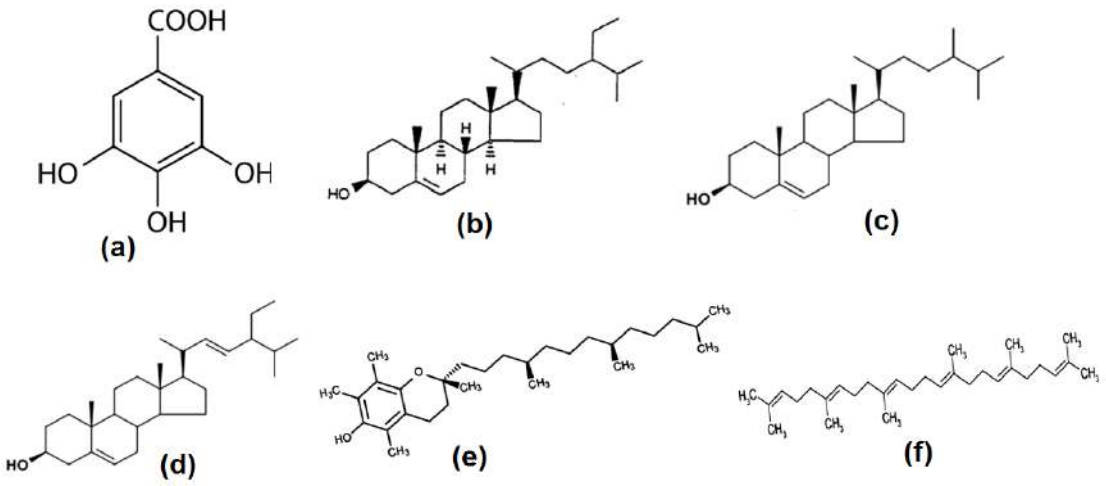

Fig. 4.20. Chemical structures of few active metabolites identified in *M. pudica* and *M. invisa* extracts by GC-MS: gallic acid (a); β-sitosterol (b); campesterol (c); sigmasterol (d); α-tocopherol (e); squalene (f).

4.7.3. NMR analysis

4.7.3.1. NMR analysis of ACL extract

^{13}C NMR spectra of ACL extract (Fig. 4.21.A) revealed several peaks in the aliphatic (δ=19.0–84.2) and aromatic region (δ=115.8–156.6) confirming the presence of both aliphatic and aromatic carbons (Silverstein *et al*., 2006). Likewise, ^{1}H NMR spectra (Fig. 4.21.B) exhibited peaks related to aliphatic, aromatic and olefinic protons. Besides, a hump near δ=8.75 indicates the presence of amine functional group supporting the result found in GC-MS analysis of ACL extract which might be responsible for the bioactive properties of the extract.

4.7.3.2. NMR analysis of MPD and *MIN extracts*

NMR spectra of MPD extract (Fig. 4.22) clearly indicated the peaks of squalene, a natural antioxidative agent, while MIN extract exhibited the structure (Fig. 4.23) of gallic acid, another strong antioxidant having potent lipid peroxidation property. The NMR spectral analysis of squalene is as follows: ^{1}H NMR (300 MHz, $CDCl_3$) δ5.14 (m, internal vinylic protons), δ2.0 (m, methylene protons), δ1.68 (s, methyl protons), δ1.60 (s, methyl protons); ^{13}C NMR (75 MHz, $CDCl_3$) δ16.0–25.6 (eight methyl carbon), δ26.7–39.7 (ten methylene carbon), δ124.3–135.2 (twelve double bonded carbon). In case of gallic acid, the NMR spectral analysis is as follows: ^{1}H NMR (300 MHz, DMSO-d_6) δ6.94 (s, 2H); ^{13}C NMR (75 MHz, $CDCl_3$) δ173.0 (C-7), δ146.2 (C-3 and C-5), δ139.2 (C-4), δ128.4 (C-1), δ116.5 (C-2 and C-6).

4.8. *In-silico* drug targeting and Pharmacokinetic study

Since the phytochemicals, identified in the present study, were found to be effective as potent free radical scavengers or antioxidants, anti-neurodegenerative stuffs, and anti-diabetic agents, it further prompted towards the discovery of new drugs through *in-silico* computational

approach opening a new door for pharmaceutical industry.

4.8.1. In-silico drugability prediction and ROS (Reactive Oxygen Species)

Interestingly, it has been observed that FAS Ligand protein (FasL; ID- 4MSV), Toll like receptors (TLR; ID- 5AWA) and NADPH oxidase (NOX; ID- 1OEY) have a crucial role on ROS generation causing most of ROS-induced diseases and/or disorders in human body. Therefore, suppressing or avoiding of these proteins could be a rational pathway to combat against ROS. Phytochemicals like stigmasterol, β-sitosterol, and campesetrol

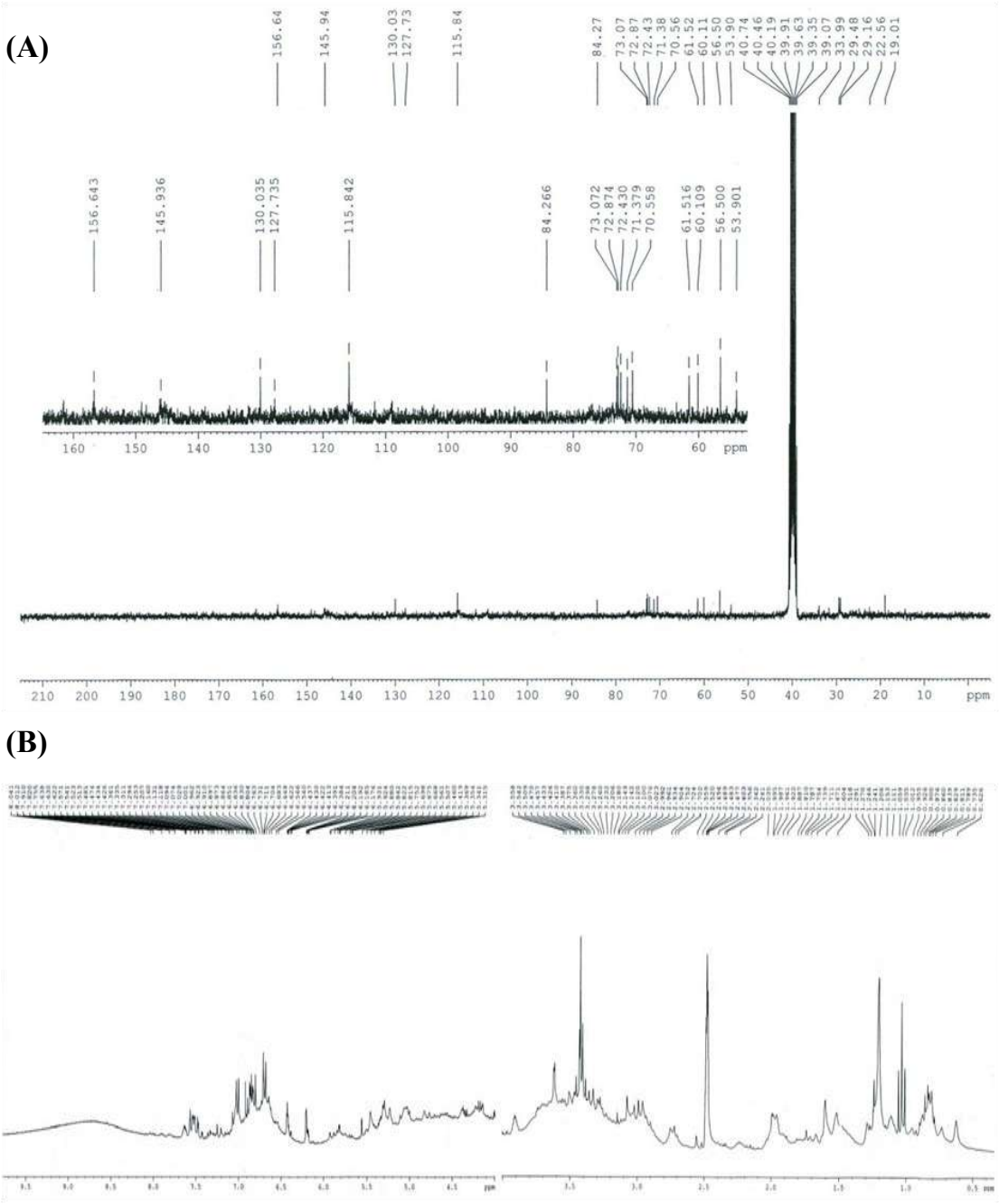

Fig. 4.21. ^{13}C NMR spectra **(A)** and ^{1}H NMR spectra **(B)** of ACL extract.

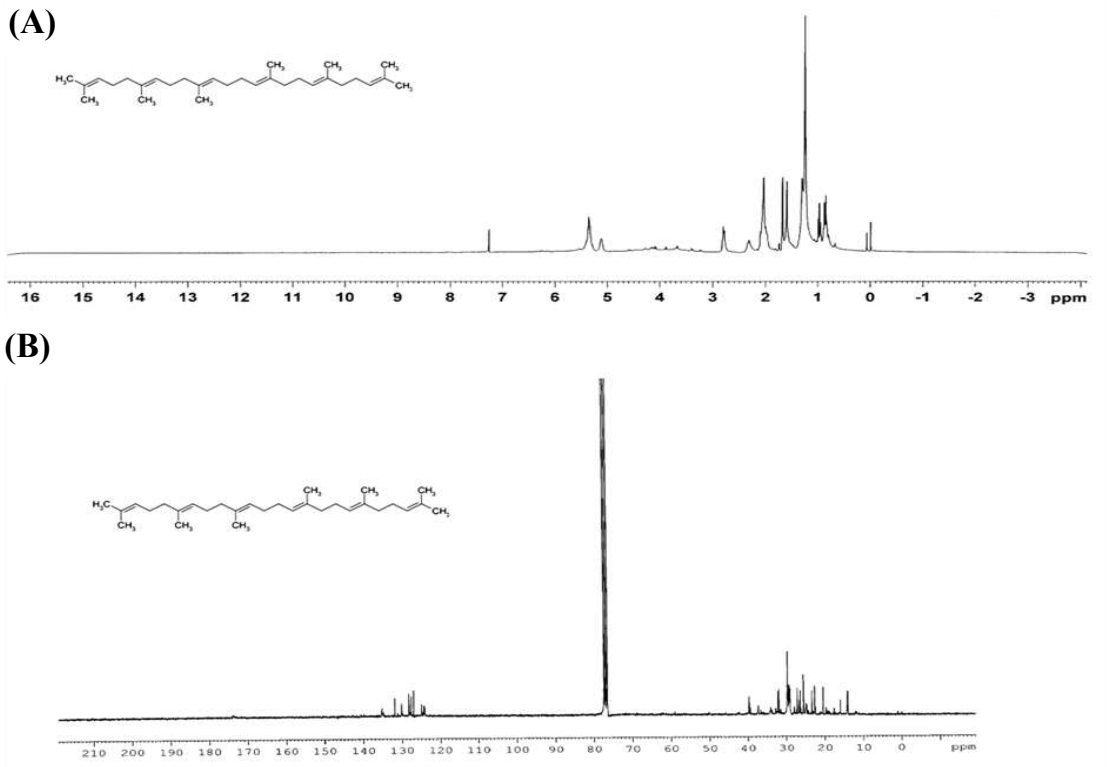

Fig. 4.22. ^{1}H NMR spectra **(A)** and ^{13}C NMR spectra **(B)** of MPD extract representing the structure of squalene.

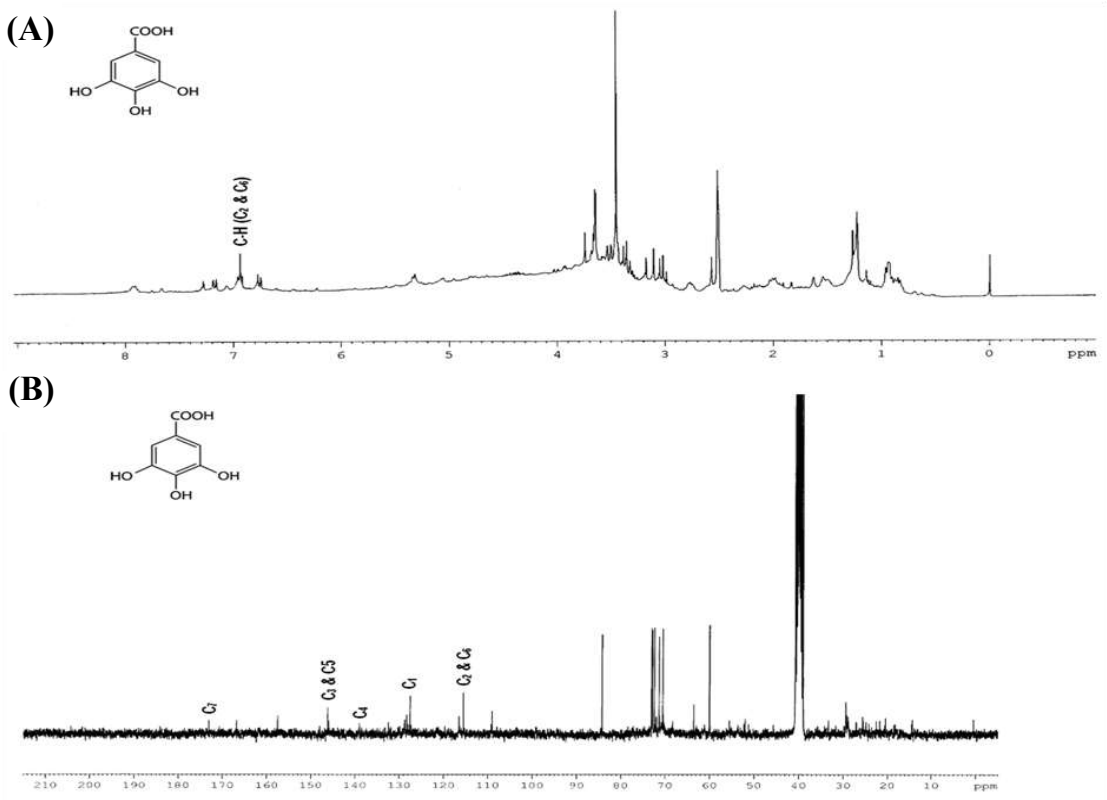

Fig. 4.23. ^{1}H NMR spectra **(A)** and ^{13}C NMR spectra **(B)** of MIN extract representing the structure of gallic acid.

have already been identified in the MPD and MIN extracts (please refer section 4.7.) exerting antioxidative properties. In fact, these metabolites are the best known antioxidants against different free radicals including hydroxyl radical ($OH^{\bullet-}$), singlet oxygen ($^1O_2^{\bullet-}$), superoxide radical ($O_2^{\bullet-}$), H_2O_2, nitric, oxide (NO), peroxynitrite ion ($ONOO^-$) etc., as well as they may be act as suppressors of free radical generating proteins. Hence, a first initiative step was undertaken to gain an insight into the underlying mechanisms between the above mentioned proteins and the active metabolites through *in-silico* computational approach.

In essence, FasL, a type II membrane protein belonging to the tumor necrosis factor (TNF) family, facilitates signaling of cell apoptosis (Lee *et al.*, 1999) which involves caspase 8 activation and a subsequent cascade of events via Fas-associated death domain (FADD/Mort1) adaptor protein leading to DNA fragmentation and cell death (Fuchs *et al.*, 1997). Besides, FasL activation has also been reported to be associated with ROS generation causing necrotic cell death (Medan *et al.*, 2005; Vercammen *et al.*, 1998). The NADPH oxidase, a membrane bound enzyme complex, transfers an electron of the complex to the oxygen molecule in the phagosome or in the cytosol, giving rise to different ROS including superoxide anion ($O_2^{\bullet-}$), hydrogen peroxide, hydroxyl radical ($OH^{\bullet}$), peroxynitrite ($ONOO^-$), hypochlorous acid (HOCl) etc (Han *et al.*, 1998; Pham-Huy *et al.*, 2008). What's more, toll like Receptors (TLR), the significant intra- and extra- cellular ligand-recognition receptors, can also induce the ROS production (Marcato *et al.*, 2008). Therefore, suppressing the activity of these proteins via ligands could stop the generation of ROS damaging the cells. In this context, probable function of some identified antioxidative metabolites (e.g. stigmasterol, β-sitosterol and campesterol; found in MPD and MIN extracts) was investigated in suppressing the ROS generation by means of *in-silico* approach. Result revealed that stigmasterol effectively binds (Fig. 4.24.A-C) with FasL protein, NADPH Oxidase and TLR protein with an affinity of -5.2 kcal/mol, -5.8 kcal/mol and -6.8 kcal/mol respectively (Table 4.15). Interestingly, in the plant extracts like MPD and MIN with its bioactive compounds had already been found to be efficient free radical scavenger in different *in-vitro* antioxidant analysis (please refer 4.2 section). Hence, it could be presumed that stigmasterol probably made the protein inactive, thereby blocked the generation of ROS. Subsequently, β-sitosterol (Fig. 4.25.A-C) and campesterol (4.25.D-F) also exhibited noteworthy binding affinities (Table 4.15) indicating their potent role to suppress the production of ROS. Therefore, MPD and MIN extracts might be treated as ROS-

Table 4.15. Binding affinities between the ligands and proteins.

Ligands	Binding Affinities (kcal/mol)		
	FasL (4MSV)	NADPH (1OEY)	TLR (5AWA)
Stigmasterol	-5.2	-5.8	-6.8
β-Sitosterol	-5.0	-5.8	-6.1
Campesterol	-5.6	-6.6	-5.9

suppressor materials enlightening an innovative idea towards new drug discovery against free radicals.

4.8.2. In-silico drugability prediction and neurodegeneration

Despite of having immense antioxidant and anti-neurodegenerative properties found in selected plant extracts (MPD and MIN) due to presence of several active metabolites including gallic acid, β-sitosterol, stigmasterol and campesterol etc., these were considered as the potential drug target ligands against neurodegenerative disorders (NDs). As a part of drug target establishment, molecular docking was first performed to explore the binding pattern of the above mentioned target compounds with human brain membrane protein (dopamine receptor D3 protein; ID- 3PBL). The D3 protein, localized to the limbic areas of the brain, was selected due to its prominent role in cognition, emotional and endocrine functions and hence, it might be the chief target of antipsychotic therapy involving dopamine antagonists (Nakajima *et al.*, 2013). Results obtained from docking

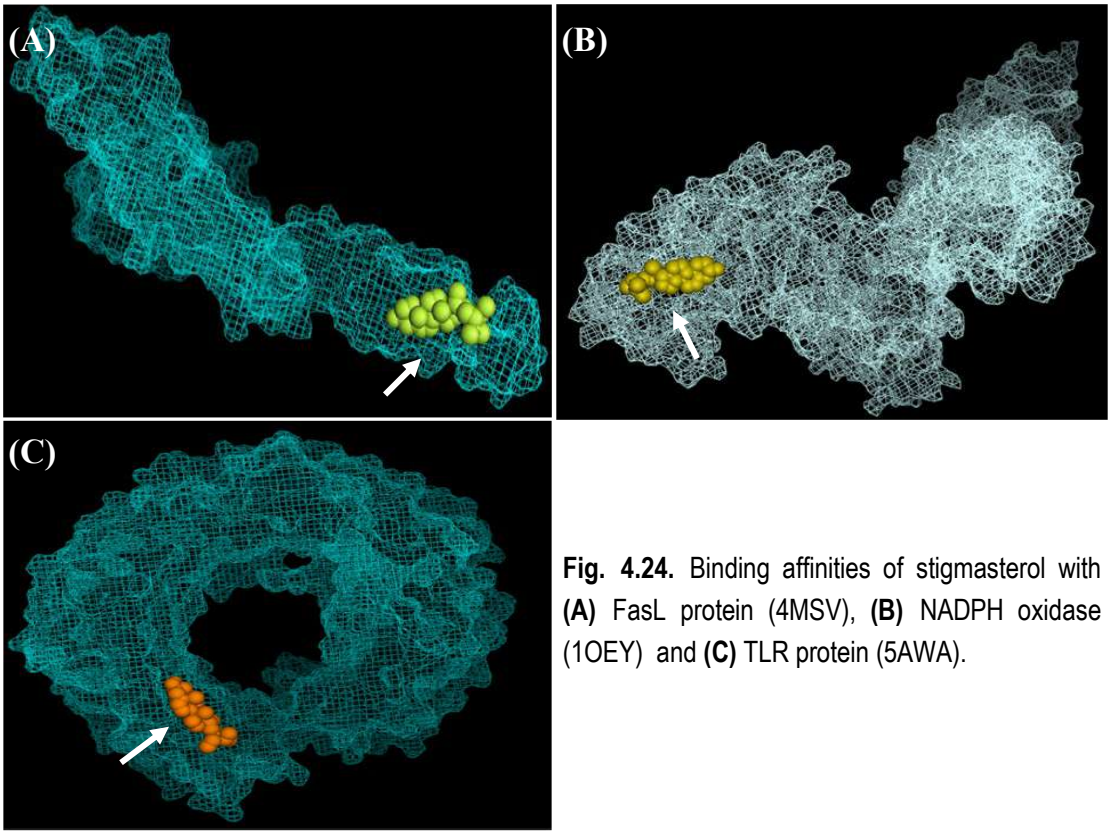

Fig. 4.24. Binding affinities of stigmasterol with **(A)** FasL protein (4MSV), **(B)** NADPH oxidase (1OEY) and **(C)** TLR protein (5AWA).

revealed different binding sites with different affinities. Only the most suitable binding sites with highest affinities were considered. Out of 5 selected ligands, gallic acid (-5.5 kcal/mol) and squalene (-5.3 kcal/mol) displayed comparatively poor binding pattern and affinity towards dopamine D3 protein than the rest of ligands, thereby discarded them. However, other selected ligand compounds i.e., β-sitosterol, stigmasterol and campesterol exhibited higher binding affinities; for instance, campesterol was found to display an affinity of -7.4 kcal/mol of affinity, β-sitosterol revealed -7.7 kcal/mol and stigmasterol displayed -8.4 kcal/mol of

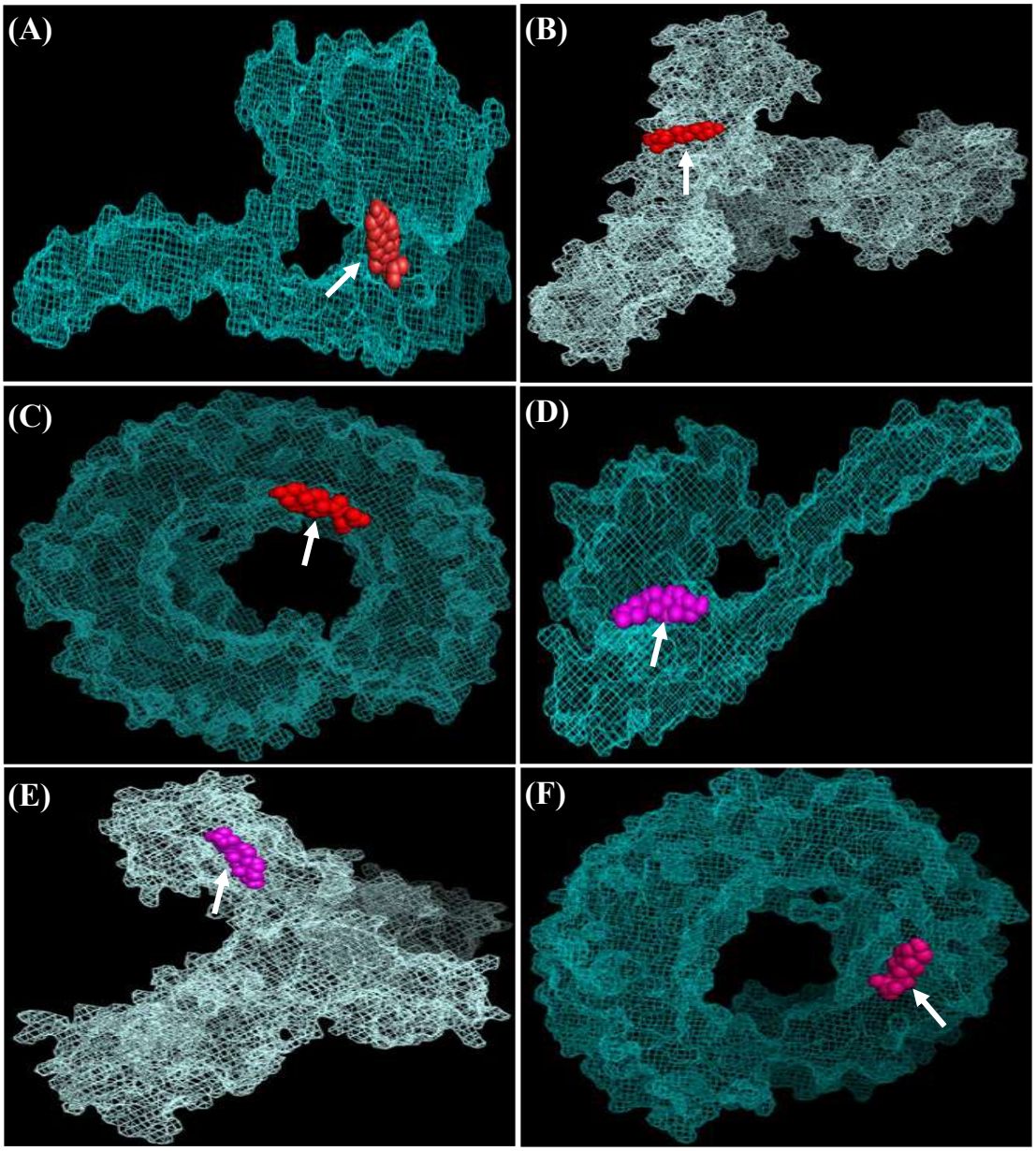

Fig. 4.25. Binding affinities of FasL protein (4MSV), NADPH oxidase (1OEY) and TLR protein (5AWA) with β-sitosterol **(A-C)** and affinities of campesterol with same proteins **(D-F)** respectively.

affinity (Fig. 4.26). Strong binding pattern of these ligand compounds with dopamine receptor D3 protein signified their possible role in the treatment of neurodegeneration.

Since remarkable binding pattern of target compounds was obtained from molecular docking, it was intended to perceive whether those compounds assure to be novel drugs in treating NDs. Screenings of 'Lipinski's rule of five' as well as 'ADMET' (Absorption, Distribution, Metabolism, Excretion and Toxicity) property of a compound are the foremost approaches to establish a compound as an effective drug. In fact, the probability of success of a compound in becoming a realistic CNS (central nervous system) drug depends on some factors that include penetration ability of molecule to cross blood brain barrier (BBB), optimum pharmacokinetic profiling and the effect of the components on brain. Hence, we followed 'Lipinski's Rule of Five' to screen the physiochemical properties of the selected ligand compounds using mechanistic *in-silico* tools, such as, ALOGPS and Chemicalize. The properties were: (1) molecular weight (≤ 500 Da), (2) lipophilicity or logP value (≤ 5), (3) H-bond donor (≤5), and (4) H-bond acceptor (≤ 10) (Table 4.16). Pharmacokinetic (PK) properties of target drugs were further assessed by means of BBB predictor analysis (using fingerprints of MACCS, Openbabel (FP2), Molprint 2D and PubChem) and BioZyne.

It was revealed from Table 4.16 that three out of four rules of Lipinski were

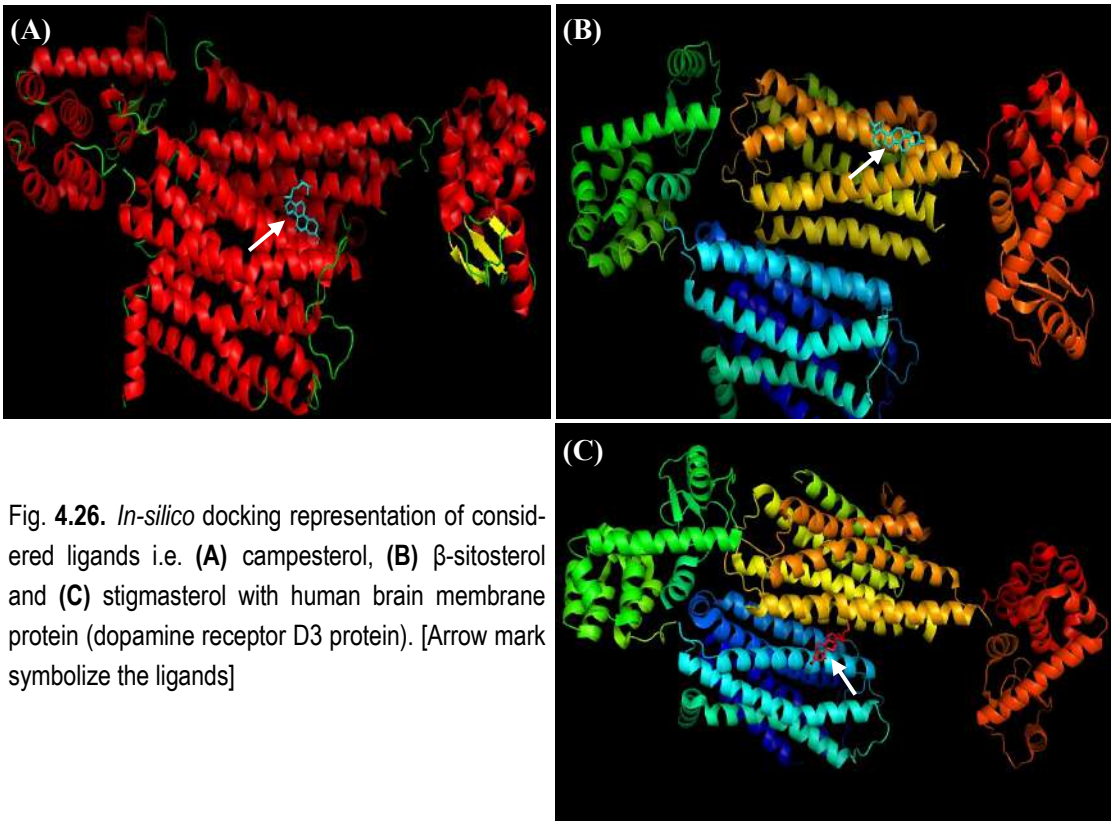

Fig. **4.26.** *In-silico* docking representation of considered ligands i.e. **(A)** campesterol, **(B)** β-sitosterol and **(C)** stigmasterol with human brain membrane protein (dopamine receptor D3 protein). [Arrow mark symbolize the ligands]

Table 4.16. Physiochemical properties of selected ligands as per Lipinski's rule.

Properties	Stigmasterol	β-sitosterol	Campesterol	Lipinski's rule (Present study response)
H-donor	1	1	1	P
H-acceptor	1	1	1	P
Molecular weight (Da)	412.69	414.70	400.68	P
logP	9.43	7.84	7.40	×

religiously obeyed by the selected ligand compounds. However, the logP values in all the cases were found to be way above the prescribe value of Lipinski's rule of Five. Hence, pharmacokinetic properties (i.e., ADMET) of the target ligands were investigated. The analysis involving 'BBB permeability', which is one of the mandatory factors for effectiveness of CNS drug, confirmed that these compounds were BBB+ i.e., they can cross the BBB effectively (Fig. 4.27).

Concurrently, several junctional-proteins like, P-glycoprotein (P-gp) that lies in BBB, block the diffusion of polar solutes from blood to CNS (Alavijeh *et al.*, 2005). In fact, P-gp restricts the entry of most of the free molecules from blood to brain except, some selected small and lipophilic compounds (Miller *et al.*, 2008).

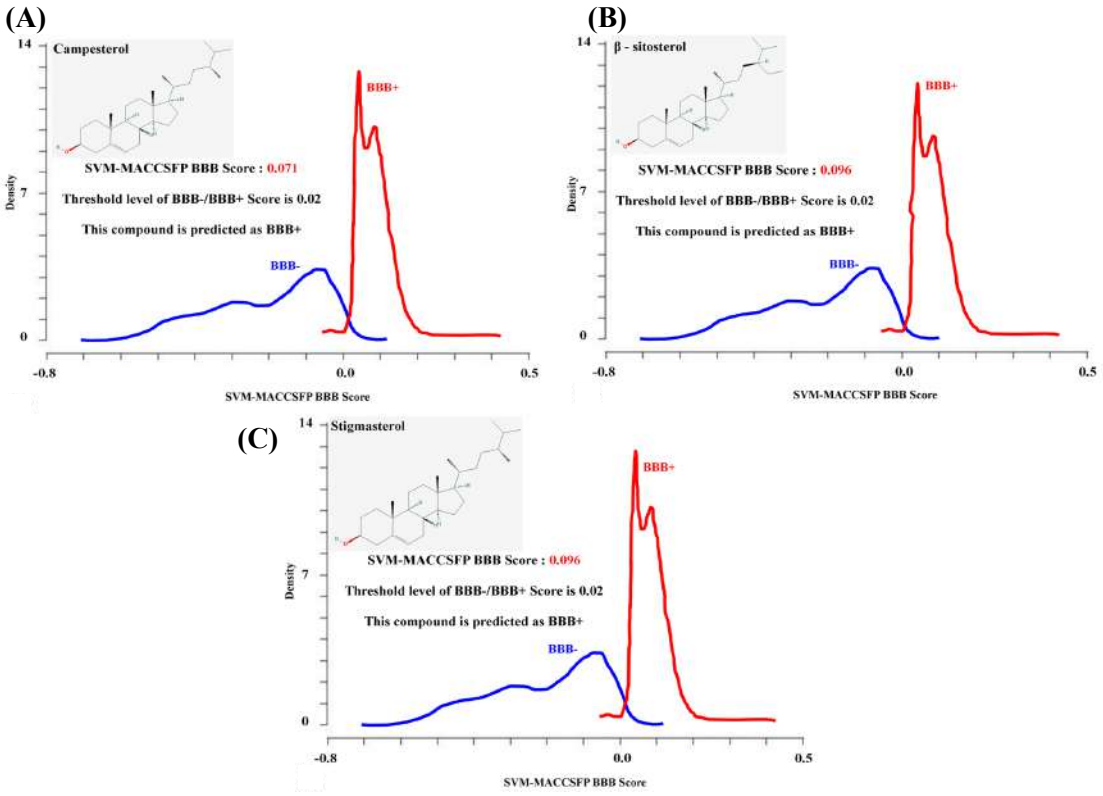

Fig. 4.27. Blood brain barrier (BBB) permeability of ligands i.e. **(A)** campesterol, **(B)** β-sitosterol and **(C)** stigmasterol; where, BBB score of each compound is more than threshold level (0.02) indicating the BBB permeability of selected ligands.

Regarding central nervous system (CNS) treatment, the penetration of drug through the lipid bilayer of BBB and BSB (blood spinal-cord barrier) plays a key role and it is directly dependent on the logP value (lipophilic character) of that molecule (Alavijeh *et al*., 2005). It has been suggested that higher lipophilicity of a drug enhances its permeability through lipid membrane and also paves way for a better distribution and improved metabolic clearance (Riley *et al.*, 2001). Therefore, higher logP value may actually be a blessing in disguise in this case.

The efficacy of an anti-ND agent not only depends on its permeability through BBB but also relies largely on its capability to remain in the brain until its desired action is aptly achieved. In this regard, the intention was to find out whether the target ligands act as P-glycoprotein (P-gp) substrates (Alavijeh *et al*., 2005). The analysis with BioZyne tool proved that the selected ligands were indeed P-gp substrates (Fig. 4.28) that allow successful transport through BBB, thus establishing PS as effective drugs against CNS disorders or NDs. Thus, high logP values and P-gp substrate nature of selected ligands (i.e., PS) indicated a better absorption through CNS (Wils *et al.*, 1994).

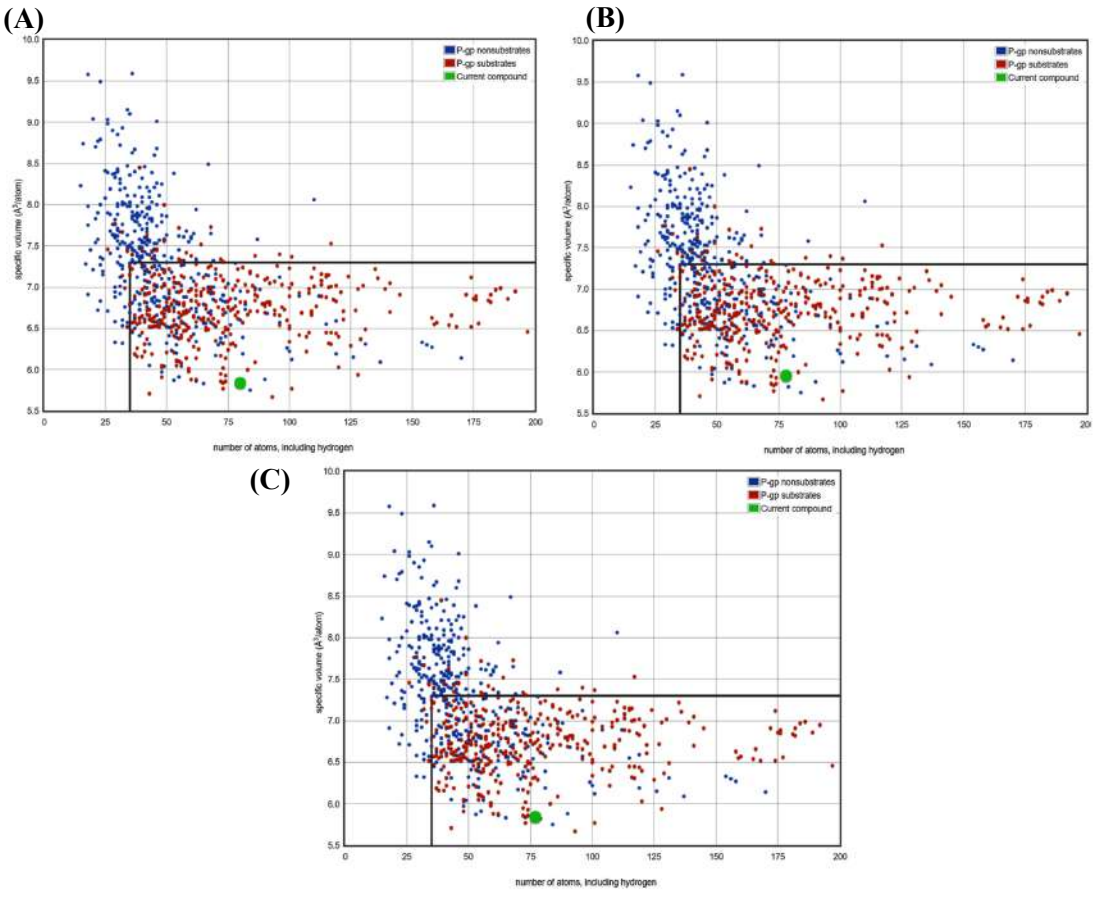

Fig. 4.28. Phospho-glycoprotein (P-gp) substrate property of selected ligands; where, considered ligands (green colored) β-sitosterol **(A)**, stigmasterol **(B)** and campesterol **(C)** clustered with P-gp substrates (red colored).

While considering a phytochemical as a novel CNS drug, lipophilic property of that bioactive compound plays a pivotal role having direct effect on the distribution and metabolism prototype of that compound (Alavijeh *et al*., 2005). It has been observed that the molecules with higher lipophilic nature tend to bind with target proteins more strongly enhancing their "distribution rate" as well as "affinity" towards metabolic enzymes (Alavijeh *et al*., 2005). Thus, higher lipophicity of the target phytocompounds might suggest smooth absorption, effortless distribution and appropriate metabolism in CNS. Besides, smooth transportation (in both directions) of these lipophilic ligands through BBB and BSB ensure their satisfied excretion from CNS making the treatment therapy against NDs more promising. Thus, it might be well justified that the target ligands i.e., phytocompounds namely, stigmasterol, β-sitosterol and campesterol being highly lipophilic, displaying decent P-gp substrate nature, may be rightfully considered as CNS drugs for treating NDs like AD and PD.

4.8.3. In-silico drugability prediction and diabetes

Amongst several phytochemicals identified in *A. nilotica* (ANL), γ-tocopherol, α-tocopherol, β-sitosterol and stigmasterol were found to have effectual anti-diabetic chattels (Jamaluddin *et al*., 1994; Gupta *et al*., 2011). In essence, Majority of the antioxidant enzymes remains under the transcription control of Nrf2 (Ma, 2013) and known to protect against the onset of diabetes (Uruno *et al.*, 2013) and diabetes-related progressive fatty liver diseases (Bataille and Manautou, 2012). Therefore, binding patterns of selected phytochemicals with Nrf2 protein (5FNQ) could be a rational way to investigate anti-diabetic activities of the extracts using molecular docking studies. It has been well-exposed that being inactivated Nrf2 remain seized in cytosol binding with kelch-like ECH-associated protein-1 (Keap1) causing ubiquitination and proteasomal degradation of Nrf2 under physiological condition. During oxidative stress, Nrf2 dissociates form Keap1 by means of Nrf2 phosphorylation or Keap1 modification, thereby activation of Nrf2 take place (Bryan *et al.*, 2013; Klaassen and Reisman, 2010). Once Nrf2 activates, it cannot be ubiquitinilated and translocates into the nucleus interacting with antioxidant response element (ARE) forms a heterodimer with Maf protein which promote the expression of cytoprotective target genes including antioxidant enzymes such as, catalase, SOD and phase II detoxifying enzymes (Zhang *et al.*, 2013). Enhanced activation of Nrf2 by pharmacologic molecules such as BHA, oleanolic acid, ursolic acid and CDDO-Im has been reported to show hepatoprotection against oxidative stress-

Table 4.17. Configurations employed in docking technique for anti-diabetic drugability prediction.

Ligand(s)	X-dimension	Y-dimension	Z-dimension	X-center	Y-center	Z-center
Alpha-tocopherol	120	120	120	15.833	25.778	2.496
Gamma-Tocopherol	120	120	120	12.522	24.23	2.69
β-sitosterol	120	120	120	13.325	25.326	2.36
Catechol	120	120	120	15.268	26.358	5.369

mediated liver damage (Klaassen and Reisman, 2010). Based on this view, a selective identified phytocompounds (catechol, β-sitosterol, α-tocopherol and γ-tocopherol) were docked with 5FNQ protein (Table 4.17) to obtain a clear picture of their underlying mechanism.

Result revealed found α-tocopherol (-7.2 kj/mol) and γ- tocopherol (-7.1 kj/mol) to be the most favored lead molecule (Table 4.18) to bind with 5FNQ at its active site determined by active site prediction server (http://www.scfbio-iitd.res.in/dock/ActiveSite.jsp). In addition to tocopherols, β-sitosterol and catechol were also accounted to be the potent candidates against diabetes (Fig. 4.29) and ROS damage (Gupta *et al*., 2011).

The docking showed that both α- and γ-tocopherols bind at "cavity 1" with amino acid sequence "RHFPTQGSYDLNMAVCI", whereas beta-sitosterol bind (-6.3 kj/mol) with "cavity 3" and cathechol bind (-5.2 kj/mol) with "cavity 6". Henceforth, it may postulate that stiff binding of these selected lead molecules with their active sites or cavities stimulates Nrf2 claiming an effectual protein-ligand interaction (Niture *et al.*, 2014). This result was well-justified by the findings of Niture *et al.* (2014) and Huang *et al.* (2012) who showed that α-tocopherol and γ-tocopherol may act as antagonist to Keap1-Nrf2 interaction resulting dissociation of Nrf2, thereby activate Nrf2 and neutralize the oxidative stress. Therefore, it could be assumed that due to presence of these phytochemicals, ANL could activate Nrf2 facilitating anti-oxidative functions (Fig. 4.30) which ultimately counteract liver injury or diabetic complications and eventually, *A. nilotica* could be treated as future anti-diabetic candidate.

Table 4.18. Chemical properties of selected ligands chosen to be docked with 5FNQ protein.

Docked Protein	Ligand(s)	Molecular weight	Hydrogen bond donor	Hydrogen bond acceptor count	XLogP3-AA
5FNQ	α-tocopherol	430.717 g/mol	1	2	10.7
	γ-Tocopherol	416.69 g/mol	1	2	10.3
	β-sitosterol	414.718 g/mol	1	1	9.3
	Catechol	110.112 g/mol	2	2	0.9

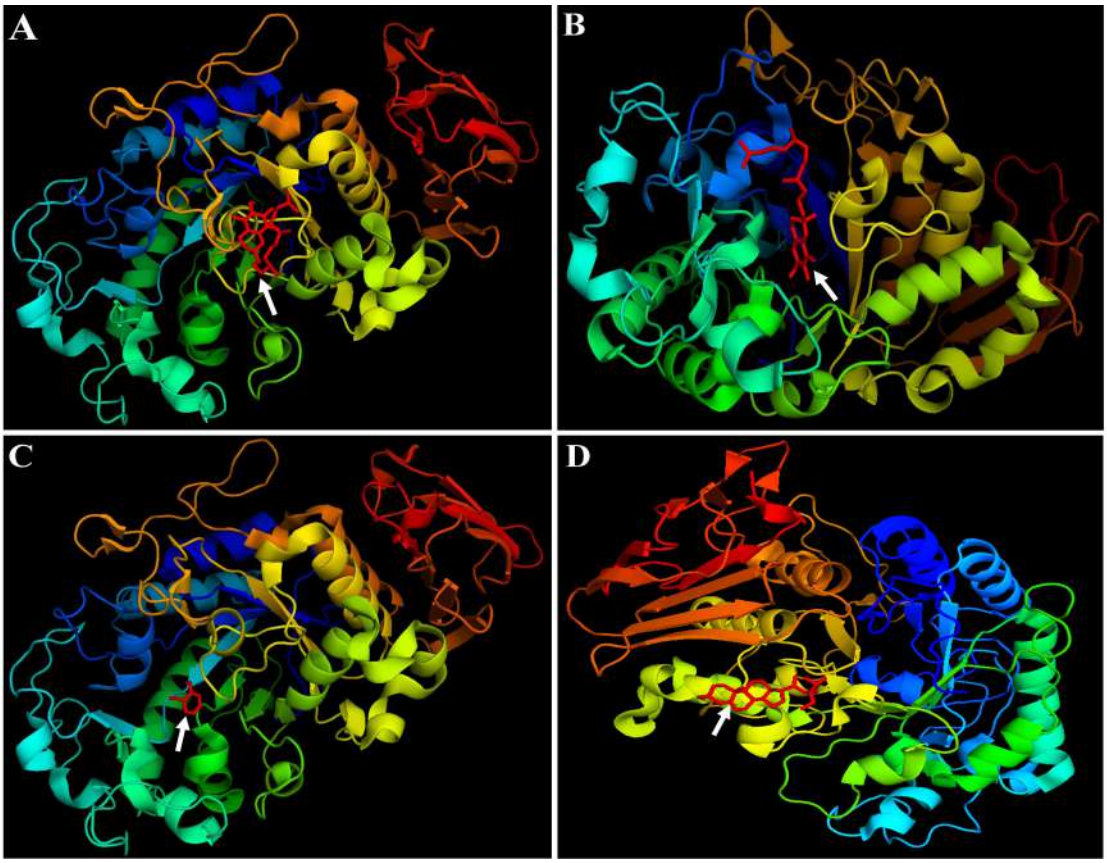

Fig. 4.29. *In-silico* docking representation of ligands such as α-tocopherol **(A)**, γ- tocopherol **(B)**, β-sitosterol **(C)** and catechol **(D)** with Nrf2 transcriptor protein (5FNQ).

4.9. Molecular diversity of different Mimosoids

4.9.1 DNA extraction, purification and quantification

The DNA from 9 Mimosoids was isolated using the standard protocol of Doyle and Doyle (1987) with minor modifications. The DNA-CTAB complex provided a network of whitish precipitate of nucleic acids after proper removal of impurities and further used for downstream processing. Agarose gel analysis of those DNA thus obtained exhibited distinct and

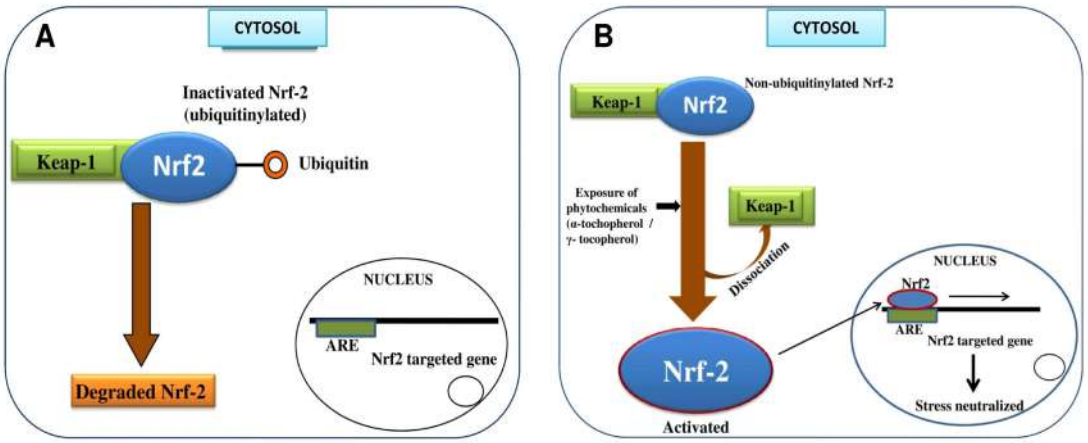

Fig. 4.30. Probable diagrammatic representation of Nrf2 action in the management of diabetes. **(A)** Inactivated Nrf2 and **(B)** Activated Nrf2.

clear bands.

Crude DNA is basically mixed with many contaminants including RNA, protein, polysaccharides etc. which lead to enzymatic reaction with DNA. Therefore, DNA purification is prerequisite step before performing downstream analysis like PCR amplification, DNA restriction and gene cloning. Inclusion of CTAB method in DNA extraction process helps to eliminate polysaccharides from DNA precipitations to a large extent. Subsequently, extraction with phenol:chloroform:isoamyl alcohol indicates the removal of protein impurities from the DNA samples. Further, RNAase enzyme is used to remove RNAs from samples.

In the present study, 2 different types of quantification methods were followed to analyze the quality of DNA. First one is spectrophotometric method and the other one is agarose gel electrophoresis. In spectrophotometric method, the DNAs were quantified in a UV spectrophotometer with 260 nm and 280 nm filters. The results were calculated as the ratio of A_{260}/A_{280} after performing of six replicates and the samples considered only showing a ratio of around 1.8 (Table 4.19).

In gel electrophoresis, the intactness of the DNA was determined with the help of 0.8% Agarose gel electrophoresis using λ DNA/*Eco*RI/*Hind*III double digest indicating molecular weight of the sample DNA (Fig. 4.31). The samples with relatively larger bands were chosen for further downstream process.

Hence, the combination of the above mentioned three steps i.e. extraction, purification and quantification allowed sufficient amount of pure DNA from the leaves of different Mimosoids for PCR amplification.

Table 4.19. List of samples showing their purity

Sample ID	A_{260}/A_{280} ratio for purity
M1	1.75
M2	1.77
M3	1.84
M4	1.78
M5	1.81
M6	1.85
M7	1.72
M8	1.81
M9	1.72

4.9.2 Random Amplified Polymorphic DNA (RAPD) analysis

RAPD is routinely used technique to evaluate the genetic relationship among species, varieties and cultivars. Initially, 45 different decamer primers have been used to study the genetic diversity (RAPD analysis) of 9 species under Mimosoideae (Raj *et al.*, 2011). Out of the 45 primers screened, 23 resulted distinct and scorable bands ranging from 190 bp to 1763 bp (Table 4.20).

A total of 330 bands were generated of which all are polymorphic bands. Interestingly, the percentage of polymorphism was found to be 100% and the number of polymorphic bands (Table 4.20) generated by each decamer primers ranged in between 2 (OPB13) and 20 (OPA01). The RAPD profile of the 9 accessions of Mimosoideae generated using primers OPA 01, OPA 16, OPB 13 and OPN 05 are represented in Fig. 4.32.A -D. A similarity matrix was further drawn using Dice coefficient of similarity (Nei and Li, 1979) ranging from 0.528 to 0.867 (Table 4.21).

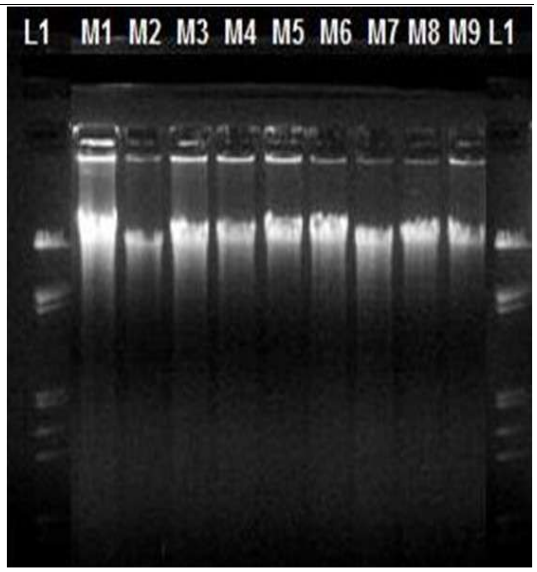

Fig. 4.31. Crude DNA of different Mimosoid samples (Lane M1-M9: different samples of Mimosoids under study (Refer **Table 3.2** for the name of species); L1: λ DNA/*Eco*RI/*Hind*III double digest DNA ladder.

Table 4.20. Total number and size of amplified bands, number of monomorphic and polymorphic bands generated and percentage of polymorphism generated by the RAPD primers.

Primer ID	Sequence (5'-3')	Total bands amplified	Monomorphic bands	Polymorphic bands	Percentage of polymorphism	Band size (bp)
OPA01	CAGGCCCTTC	**20**	0	20	100%	1327-269
OPA02	TGCCGAGCTG	18	0	18	100%	1445-247
OPA03	AGTCAGCCAC	13	0	13	100%	1486-336
OPA04	AATCGGGCTG	12	0	12	100%	1429-455
OPA07	GAAACGGGTG	18	0	18	100%	1600-279
OPA10	GTGATCGCAG	14	0	14	100%	1471-274
OPA11	CAATCGCCGT	11	0	11	100%	1314-214
OPA12	TCGGCGATAG	10	0	10	100%	1422-421
OPA13	CAGCACCCAC	15	0	15	100%	1244-205
OPA16	AGCCAGCGAA	11	0	11	100%	1500-315
OPA17	GACCGCTTGT	16	0	16	100%	1613-232
OPA18	AGGTGACCGT	16	0	16	100%	1450-285
OPA19	CAAACGTCGG	8	0	8	100%	1500-225
OPA20	GTTGCGATCC	19	0	19	100%	1638-196
OPB01	GTTTCGCTCC	14	0	14	100%	1422-413
OPB11	GTAGACCCGT	10	0	10	100%	1485-320
OPB12	CCTTGACGCA	5	0	5	100%	1125-**190**
OPB13	TTCCCCCGCT	**2**	0	2	100%	1085-250
OPF09	CCAAGCTTCC	15	0	15	100%	1500-248
OPG19	GTCAGGGCAA	15	0	15	100%	1525-210
OPN05	ACTGAACGCC	12	0	12	100%	1571-266
OPN13	AGCGTCACTC	18	0	18	100%	1725-317
OPN19	GTCCGTACTG	8	0	8	100%	**1763**-524
	Total	**330**	**0**	**330**	**100%**	

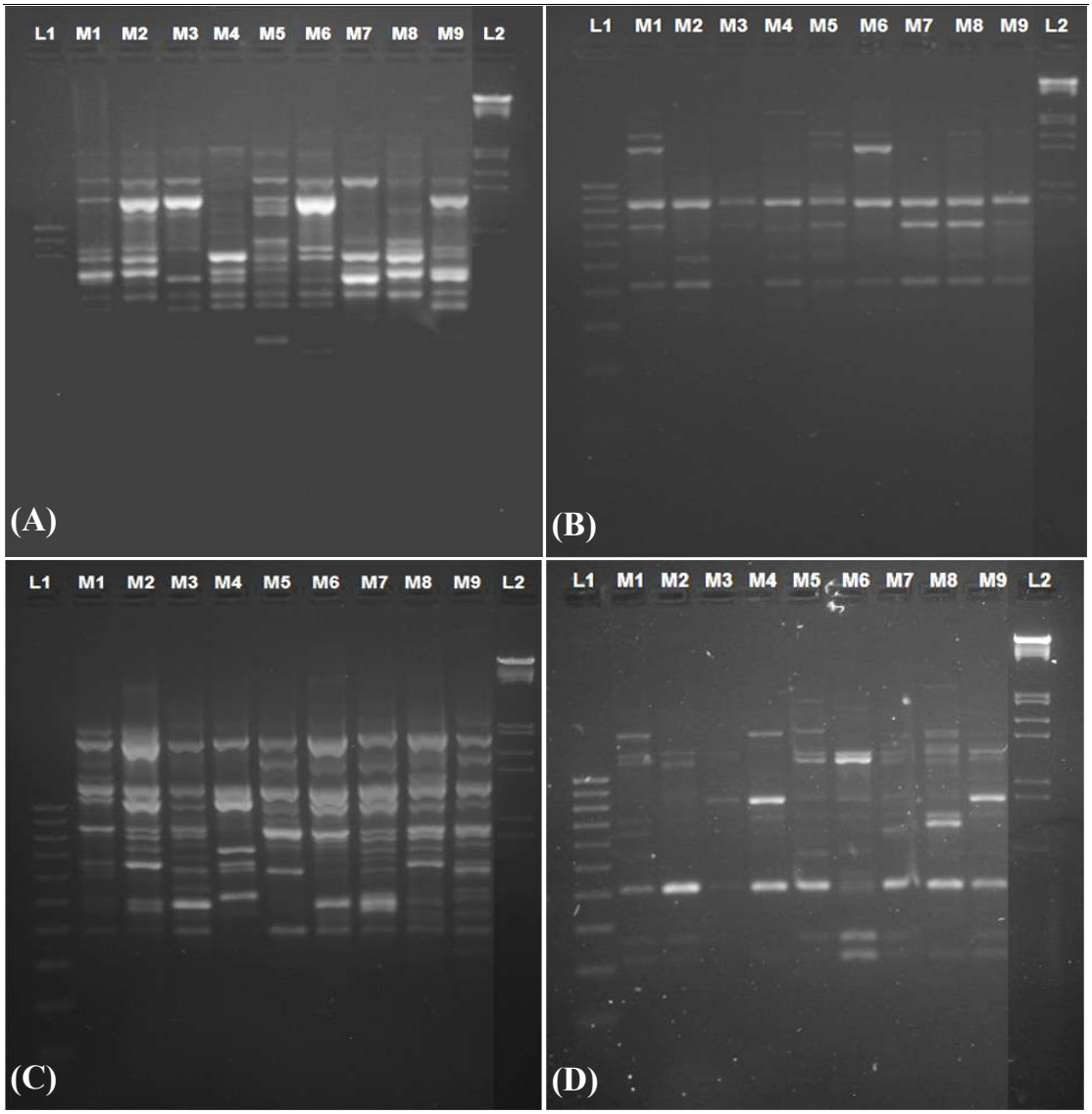

Fig. 4.32. Representatives of RAPD profiling of 9 accessions of Mimosoids amplified with **(A)** OPA01, **(B)** OPA 16, **(C)** OPB 13 and **(D)** OPN 05 primers. Lane L1: 100 bp molecular marker; Lane M1-M9 different accessions of Mimosoids under study (refer table 3.2); Lane L2: λ DNA/EcoRI/HindIII double digest DNA ladder.

The lowest similarity was observed between *Mimosa pudica* and *Albizia lebbeck*, while the highest value was recorded between *Acacia catechu* (*Senegalia catechu*) and *A. nilotica*. A dendrogram was constructed on the basis of the data obtained from RAPD analysis using NTSYSpc (Fig. 4.33).

In fact, RAPD markers are the most suitable ones to analyze the genetic variation of both intra and inter-population (Li *et al.*, 2008). The dendrogram prepared from RAPD analysis revealed that the members of *Mimosa*, *Acacia*, *Albizia* and *Samanea* formed a group in which members of *Acacia* were found to be form a loose sub-group. *Acacia nilotica* and *A. catechu* shared a node at 86.7% whereas *A. concinna* exhibited a cluster with *A. nilotica* and *A. catechu* sharing a node at 84.9% and 85.8% respectively. In addition, *Albizia lebbeck* appeared as a distinct

Table 4.21. The similarity matrix obtained using Dice coefficient of similarity among the 9 species of Mimosoideae based on RAPD profiling.

	M1	M2	M3	M4	M5	M6	M7	M8	M9
M1	1								
M2	0.616	1							
M3	0.622	0.651	1						
M4	0.584	0.654	0.684	1					
M5	0.648	0.643	**0.867**	0.687	1				
M6	0.589	0.613	0.849	0.634	0.858	1			
M7	**0.528**	0.545	0.587	0.595	0.613	0.572	1		
M8	0.625	0.631	0.66	0.634	0.663	0.628	0.648	1	
M9	0.631	0.648	0.672	0.669	0.699	0.657	0.637	0.7	1

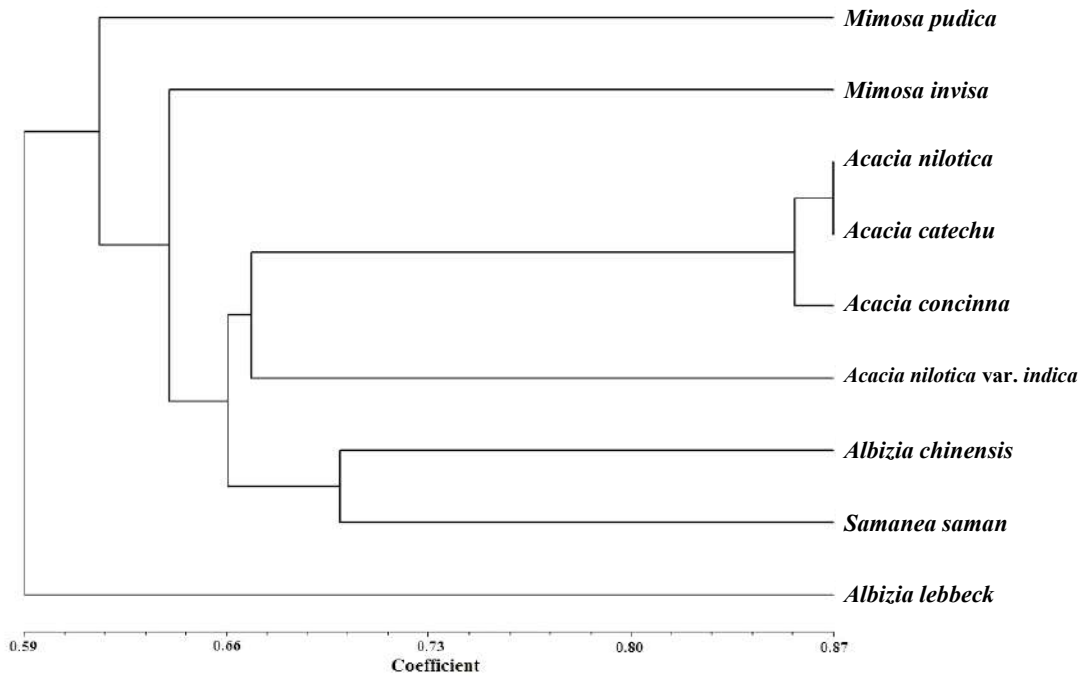

Fig. 4.33. Dendrogram obtained from UPGMA cluster analysis of RAPD markers illustrating the genetic relationships among the 9 accessions of Mimosoids.

outgroup in the dendrogram. The correspondence analysis of both 2D (Fig. 4.34) and 3D (Fig. 4.35) plotting and corroborated the cluster analysis result.

Hence, it might be inferred that RAPD markers are praiseworthy for analyzing genetic variations among the species and could be utilized as molecular taxonomic characters to analyze the genetic relationships among the species of Mimosoideae. Similar results were also documented by Sulain *et al*. (2013) using RAPD analysis where *M. pudica* was found to be closely related to *M. pigra* and *M. invisa*. Nanda *et al*. (2004) also reported the genetic relationships of six Acacia species using RAPD in which *A. farnesiana* and *A. catechu* were the closest

member sharing with 30% similarity whereas *A. auriculiformis* and *A. concinna* shared about 28% and 18% similarity, respectively, with the cluster formed by *A. farnesiana* and *A. catechu*. Hence, the RAPD markers exhibited the potentiality to conserve the identified clones as well as

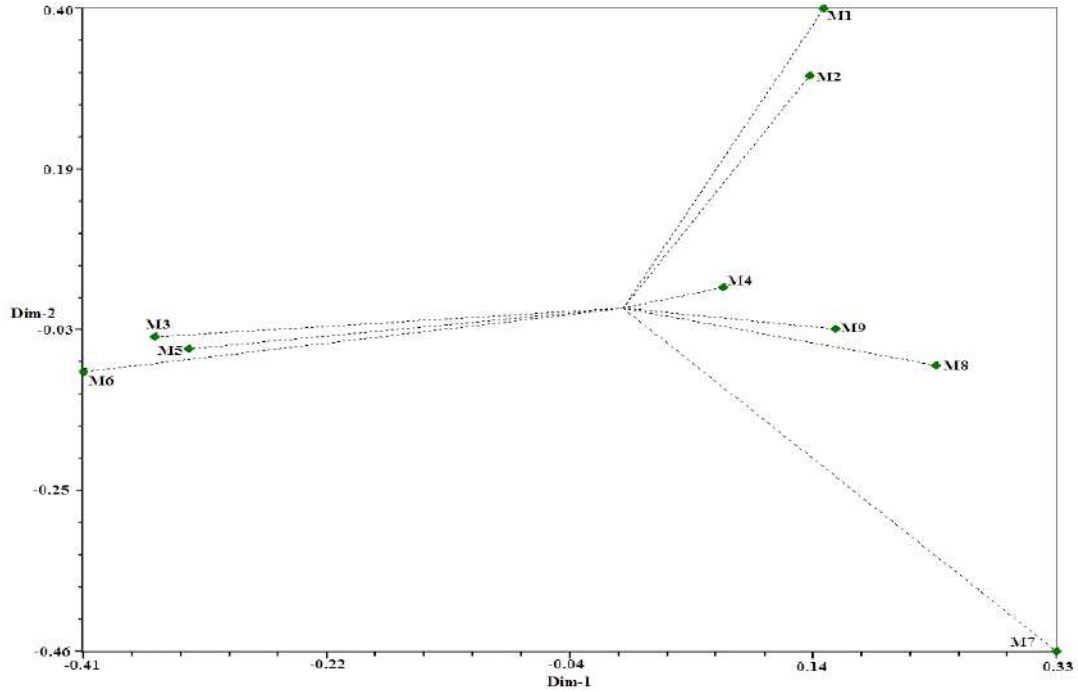

Fig. 4.34. Principal co-ordinate analysis of 9 species of Mimosoids based on RAPD analysis data representing 2-dimensional plot.

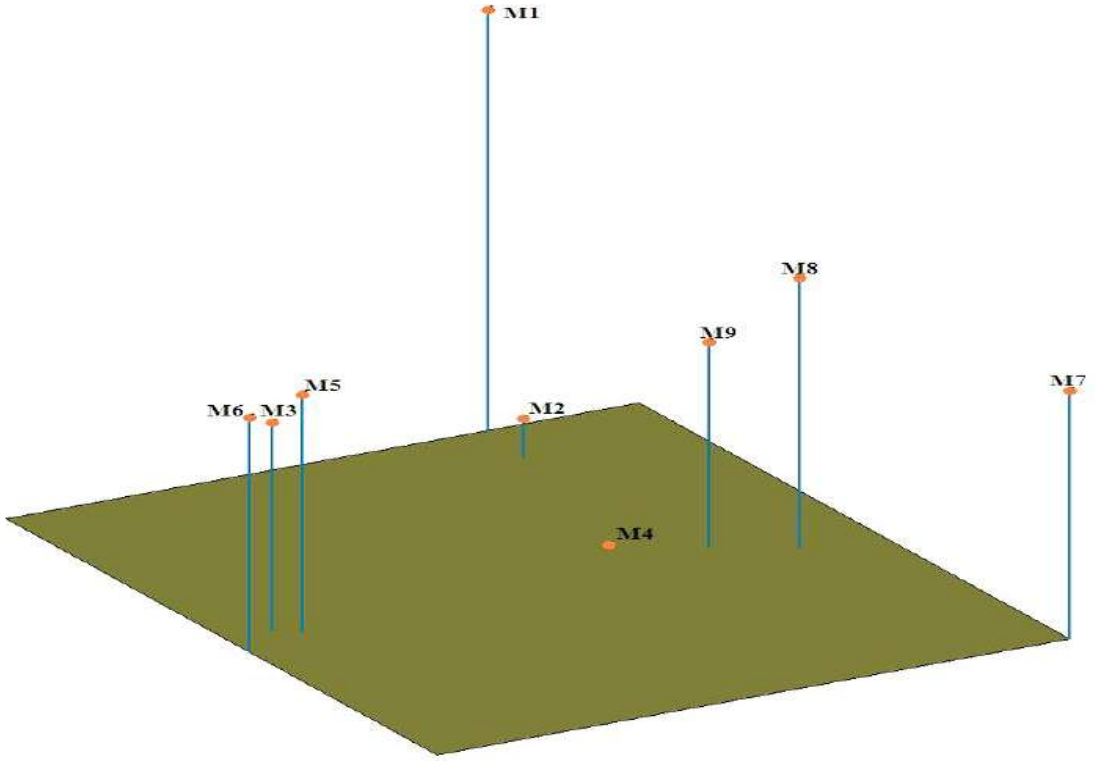

Fig. 4.35. Principal co-ordinate analysis of 9 species of Mimosoids based on RAPD analysis data representing 3-dimensional plot.

to characterize the genetic relatedness among the species of Mimosoids.

4.9.3. PCR-RFLP analysis of the trnL-trnF region of Mimosoids chloroplast genome

PCR-RFLP is a simple and cheap method playing a vital role in accessing the genetic diversity of different plant species. Therefore, it is applied to study the fingerprinting of selected species under the subfamily Mimosoideae found in Northern provinces of Bengal.

4.9.3.1. PCR amplification

In the present study, 9 species from the subfamily Mimosoideae were employed to PCR amplification with locus specific primer pair Tab c 5′-CGAAATCGGTAGACGCTACG-3′and Tab f 5′-ATTTGAACTGGTGACACGAG -3′ developed based on the Tab c-f in "Taberlet" (TrnL-TrnF) region of the chloroplast genome of different Mimosoids for which the nucleotide information was available with respect to other plant species in the public domain. The primer pair effectively amplified the Tab c-f in "Taberlet" (TrnL-TrnF) region of the Inter-Generic Spacer (IGS) region of the species of Mimosoideae. The amplified product is shown in Fig. 4.36.

4.9.3.2. PCR product restriction digestion and agarose gel analysis

The PCR product obtained from the prime pair Tab c-f were subjected to restriction digestion using 5 different restriction enzymes like *Eco*RI, *Taq*I, *Hinf*I, *Hae*III and *Hpa*I to short out the degree of genetic variation among different species under Mimosoideae. Amongst 8 enzymes studied, 3 restriction enzymes (*Alu*I, *Mbo*I and *Msp*I) were found to be unsuccessful to digest the PCR products while the other five restriction enzymes produced a total of 20 polymorphic bands (Table 4.22).

Digestion with *Eco*RI resulted in producing three bands except *Albizia lebbeck* and *Samanea saman* where only one band was generated. The total percentage of polymorphism was found to be 86.96%. Among the five restriction enzymes, *Hae*III, *Hpa*I and *Hinf*I produced four bands whereas *Taq*I and *EcoR*I reproduced six and two bands respectively. The percentage of polymorphism was found to be 100% in case of *Hae*III, *Hpa*I and *Taq*I while *Hinf*I and *Eco*RI showed 66.66% polymorphism (Fig. 4.37.A-D).

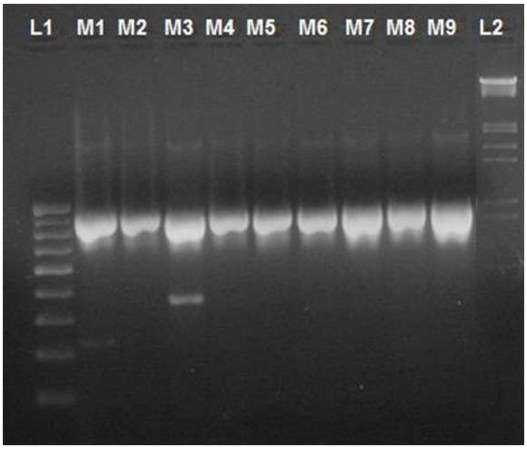

Fig. 4.36. Amplification of 9 species of Mimosoids with primer Tab c-f (TrnL-TrnF). Lane L1: 100bp DNA ladder; Lane M1-M9: Different species of Mimosoids as listed in **Table 3.2** and L2: λ DNA/ EcoRI/HindIII double digest DNA ladder.

Table 4.22. Total fragments, number of polymorphic bands generated by using different restriction enzymes.

Restriction enzyme	Optimum temperature	No. of cuts	No. of polymorphic bands	Percentage of polymorphism
Eco RI	37ºC	3	2	66.66%
Hin fI	37ºC	6	4	66.66%
Hae III	37ºC	4	4	100%
Hpa I	37ºC	4	4	100%
Taq I	65ºC	6	6	100%
		23	**20**	**86.96%**

4.9.3.3. PCR-RFLP data analysis

A total of 23 scorable bands were produced by the various restriction digestion enzymes. Of the 23 cuts 20 were polymorphic. The number of polymorphic bands ranged from two in *Eco*RI and six in *Taq*I. These clear and distinct bands were scored and used for further analysis (Table 4.22).

A dendrogram was prepared (Fig. 4.38) on the basis of similarity estimates using the unweighted pair group method with arithmetic average (UPGMA) using NTSYSpc version (2.0) (Rohlf, 1998b).

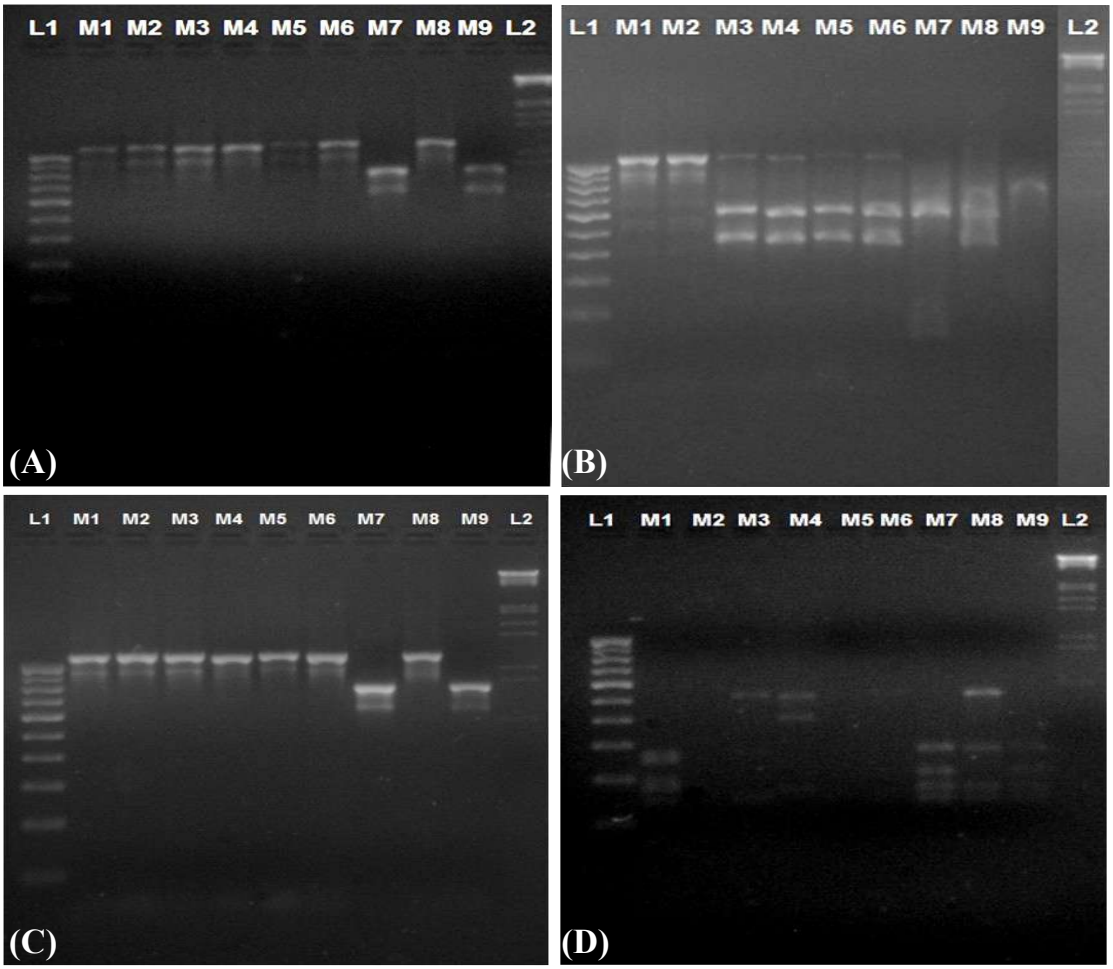

Fig. 4.37. Restriction digestion products of TrnL-TrnF region of chloroplast genome by **(A)** *Eco*RI , **(B)** *Hae*III , **(C)** *Hinf* I and **(D)** *Taq*I. Lane L1: 100 bp molecular marker; Lane M1-M9 different accessions of Mimosoids under study (refer table 3.2); Lane L2: λ DNA/EcoRI/HindIII double digest DNA ladder.

The dendrogram revealed two clusters; one of which consisted of 7 species sub-dividing into two groups. The first group comprises with 3 species (*Mimosa pudica*, *M. invisa* and *Albizia chinensis*) with a high level of genetic similarity (77%) between *M. pudica* and *M. invisa* (Table 4.23). The second group consisted of 4 species (*Acacia nilotica*, *Acacia nilotica var indica*, *Acacia catechu*, *Acacia concinna*). Interestingly, similar type of closeness among the four species of *Acacia* was also observed in the RAPD-dendrogram.

The second cluster is made up of two species i.e. *Albizia lebbeck* and *Samanea saman* with a genetic similarity of 100%. Both the 2D and 3D plot (Fig. 4.39.A-B) of the correspondence analysis of the RFLP data corroborated the dendrogram. Henceforth, from the above analysis it could be inferred that in the present study notable polymorphism (86.96%) has been found among the selected species due to their polyphyletic nature of the different genera under Mimosoideae.

4.9.4 DNA barcoding analysis

DNA barcoding is a novel and innovative technique which can be used to explore the evolution, identification and genetic relatedness of unknown plants and animal species by using a short stretch of DNA sequence (Hebert and Gregory, 2005). Chloroplast and mitochondrial genes are being recently used to study the sequence variation at generic and species level. The chloroplast genes such as matK and TrnL-F have been utilized by various workers to study the plant evolutionary pattern as well as to resolve various anomalies in the taxonomic levels.

4.9.4.1. Sequencing of PCR-product and Submission to GenBank

Since sequencing of matK and TrnL-F region of *Acacia catechu*, *A. nilotica*, *A. nilotica* var *indica*, *Albizia lebbeck* and *Samanea saman* were found in gene bank, PCR amplification of only 4 species were

Table 4.23. The similarity matrix obtained using Dice coefficient of similarity among the 9 species of Mimosoideae based on PCR-RFLP profiling.

	M1	M2	M3	M4	M5	M6	M7	M8	M9
M1	1.00								
M2	0.77	1.00							
M3	0.59	0.66	1.00						
M4	0.59	0.66	0.92	1.00					
M5	0.59	0.81	0.85	0.85	1.00				
M6	0.59	0.81	0.85	0.85	1.00	1.00			
M7	0.48	0.25	0.37	0.37	0.37	0.37	1.00		
M8	0.77	0.55	0.74	0.66	0.59	0.59	0.48	1.00	
M9	0.48	0.25	0.37	0.37	0.37	0.37	1.00	0.48	1.00

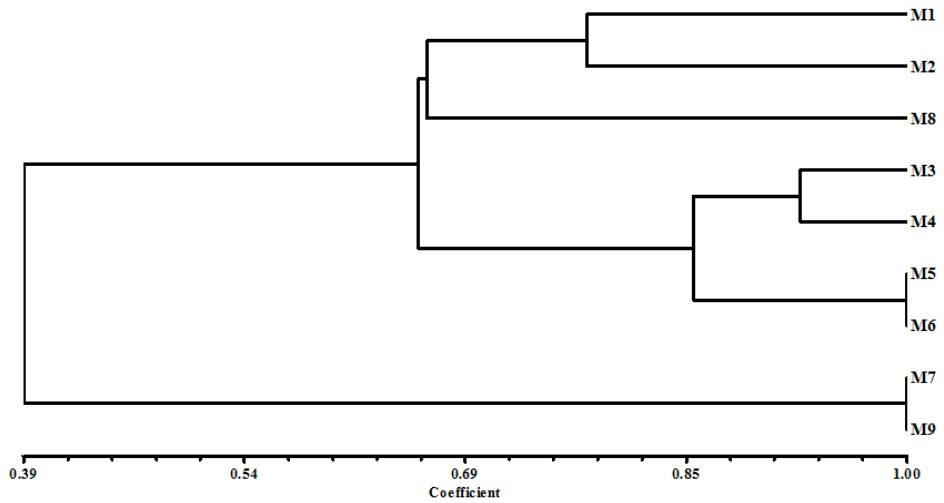

Fig. 4.38. A dendrogram based on the restriction digestion products data of the TrnL-TrnF region of 9 species under Mimosoideae.

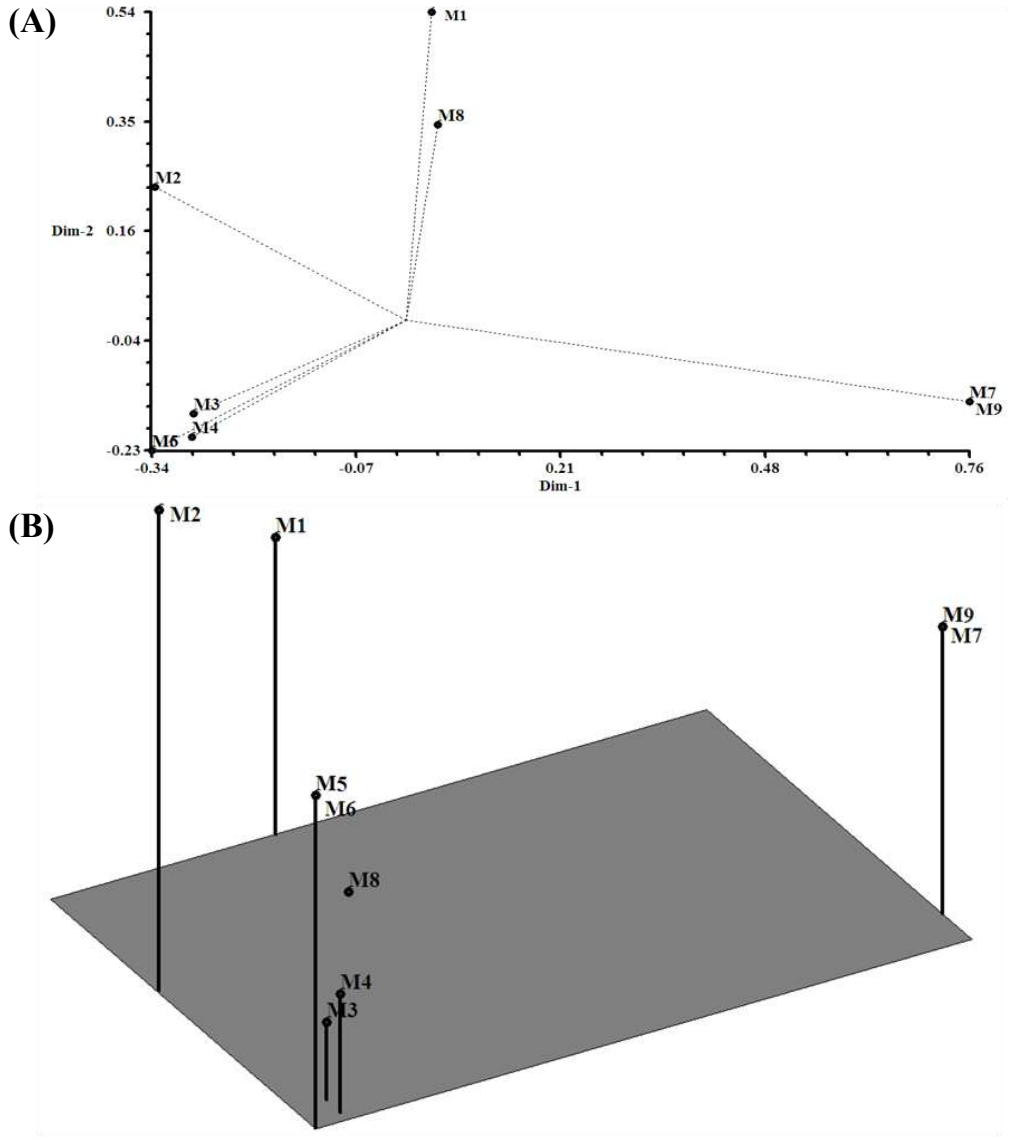

Fig. 4.39. Principal coordinates analysis of 9 species of Fabaceae based on restriction digestion products of TrnL-TrnF region of chloroplast genome. **(A)** 2-dimensional plot and **(B)** 3-dimensional plot.

performed including *Mimosa pudica*, *M. invisa*, *Acacia concinna* and *Albizia chinensis* (Table 4.24). A total of 6 samples (3 matK and 3 TrnL-F) of above mentioned species were sequenced from Chromous Biotech Pvt. Ltd, Bangalore for both the forward and reverse primers individually. The sequence analysis resulted in an average of 790 bp for each reaction. Nucleotide BLAST was further performed for each of the obtained sequence to find out the homology with the sequences already present in the GenBank. The nucleotide BLAST showed 95-100% identity with the *Mimosa, Acacia* and *Albizia* sequences already available in the GenBank. After authentication of the sequences, they were submitted to the GenBank (Fig. 4.40.A-B). The list of different species of Mimosoids along with their GenBank accession number is given in Table 4.24.

4.9.5. Data analysis

Apart from RAPD analysis, DNA barcoding is another kind of taxonomic method that has become a rational approach for identifying million species of animals and plants, based on the analysis of short, standardized and universal DNA regions. Molecular documentation of different taxa and their validated systematic position in the respective family of plant kingdom had always been a challenging task. Chloroplast gene like matK and IGS region like TrnL-F could be pivotal to resolve this problem. In the present study, a few selected species under family Fabaceae (please refer Table 3.6) were employed to explore inter-generic and intra-generic differences using matK and TrnL-F locus. The phylogenetic analysis (Fig. 4.41.A-B) of the matK and TrnL-F region region revealed a close relationship among the selected taxa. Interestingly, Fig. 4.41.A discloses that *M. pudica* and *M. invisa* share 99% similarity while *Senegalia catechu* (Syn: *Acacia catechu*) and *Acacia concinna* share 96% similarity reflecting their close genetic relatedness as found in traditional classification (Cronquist, 1981).

Result also exhibited that a total of 2 major clades were formed; one of which consisted of Mimosoideae and Caesalpinioideae while other single one is Papilionoideae. Therefore, it can be attributed to the fact that the all the selected taxa under the subfamily Mimosoideae and Caesalpinioideae were clubbed together and shared more similarities with each other (94%) than the subfamily Papilionoideae (Fig. 4.41.A). What's more a similar trend was also observed in Fig. 4.41.B that the seven species from Mimosoideae and one species from Caesalpinioideae grouped together forming the first clade whereas the remaining six genera of Papilionoideae clubbed together to make the second clade demonstrating their different place within the family. The present genetical approach through matK and TrnL-F clearly reflected

Table 4.24. List of species with the submitted GenBank accession numbers for TrnL-TrnF and matK.

Sl. No.	Taxa	matK accession number	TrnL-F accession number
1.	*Mimosa invisa*	LM643807	LM643811
2.	*Mimosa pudica*	----	LM643810
3.	*Acacia concinna*	LM643808	----
4.	*Albizia chinensis*	LM643809	LM643812

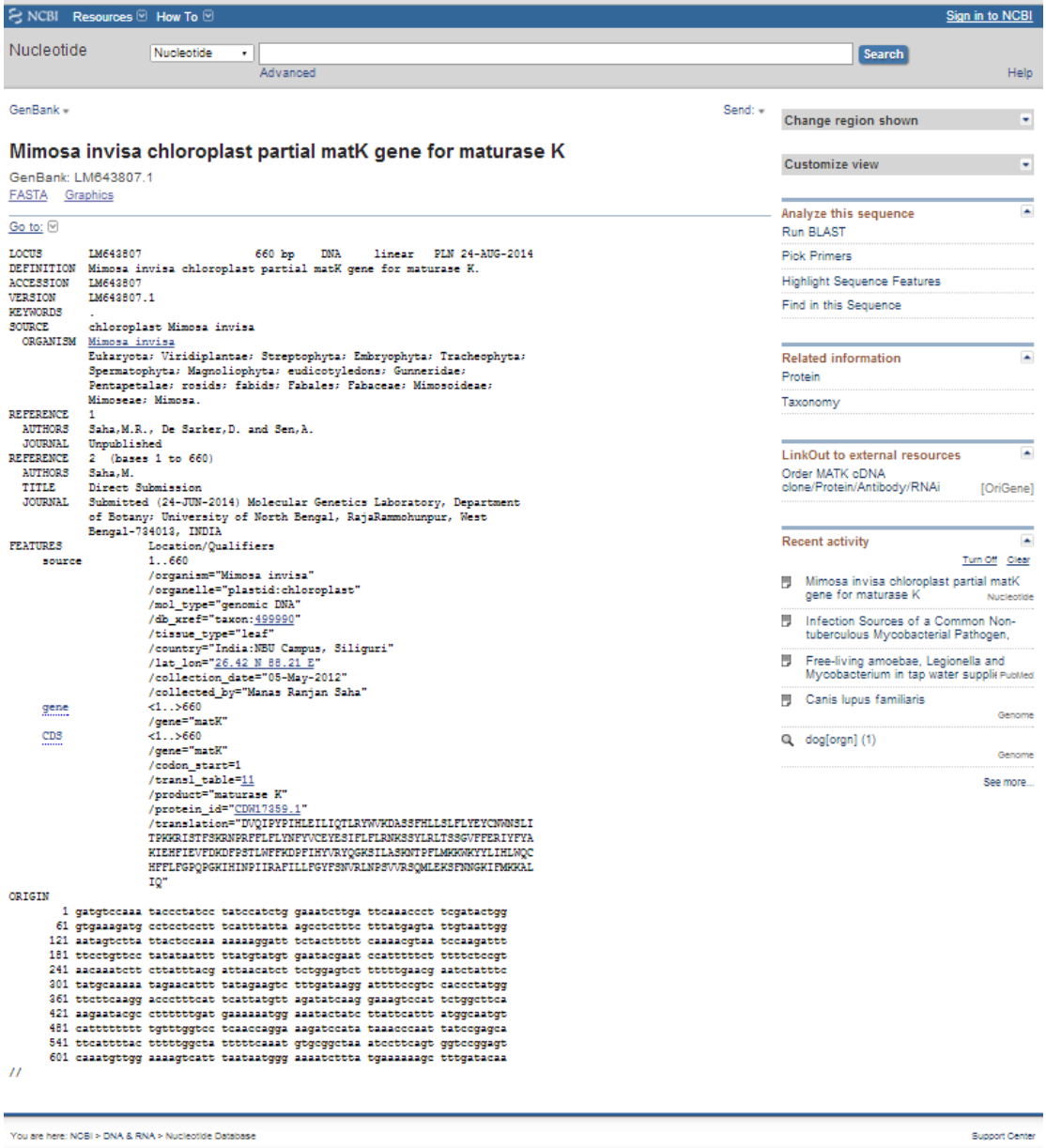

Fig. 4.40.A. Snapshot of partial matK gene sequence of *Mimosa invisa* submitted to GenBank (NCBI).

that the members of Mimosoideae and Caesalpinioideae are closer than the members from Papilionoideae validating the traditional classification (Cronquist, 1981). Hence, from the above illustration, it may conclude that DNA barcode serve a reliable genetical approach to place the morphologically similar or dissimilar or

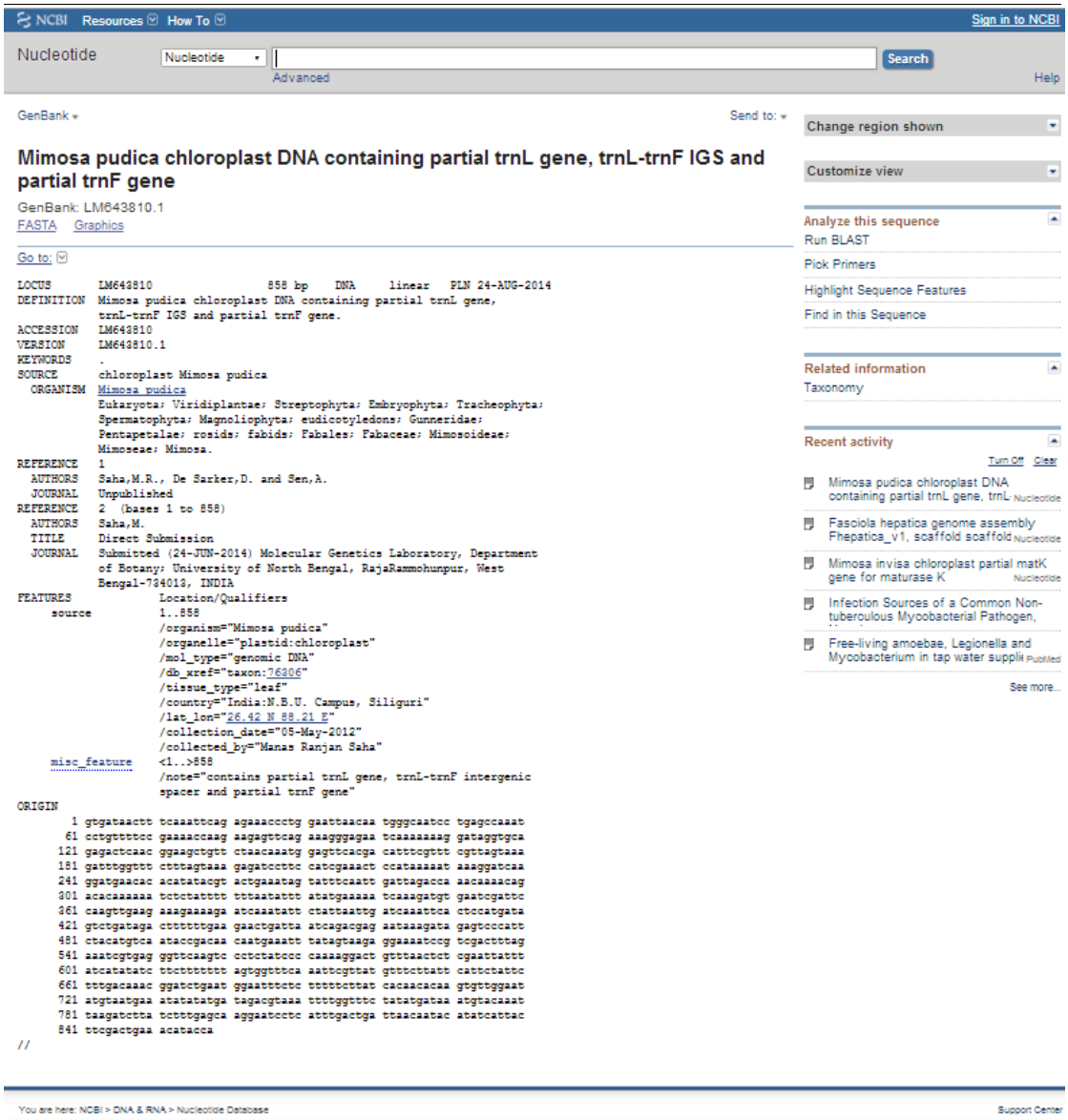

Fig. 4.40.B. Snapshot of partial trnL-trnF Intergenic Spacer (IGS) sequence of *Mimosa pudica* submitted to GenBank (NCBI).

disputed taxa into its appropriate systematic position.

In summary, the present study of DNA profiling in selected Mimosoideae clearly showed that it was possible to analyze the RAPD patterns for correlating their similarity and distance between species by which one could predict the origin of the species to a great extent. Further, the application of DNA barcode like matK and TrnL-F became more practical for defining the uniqueness as well as helpful in validation of systematic position of species and taxa identification (Schaferhoff *et al.*, 2010; Selvaraj *et al.*, 2008).

4.10. Exploration of medicinal and diversity of microsymbionts

4.10.1. Medicinal aspect

4.10.1.1. In-vitro antioxidative assay

In-vitro free radical scavenging activity between root and root-nodule collected

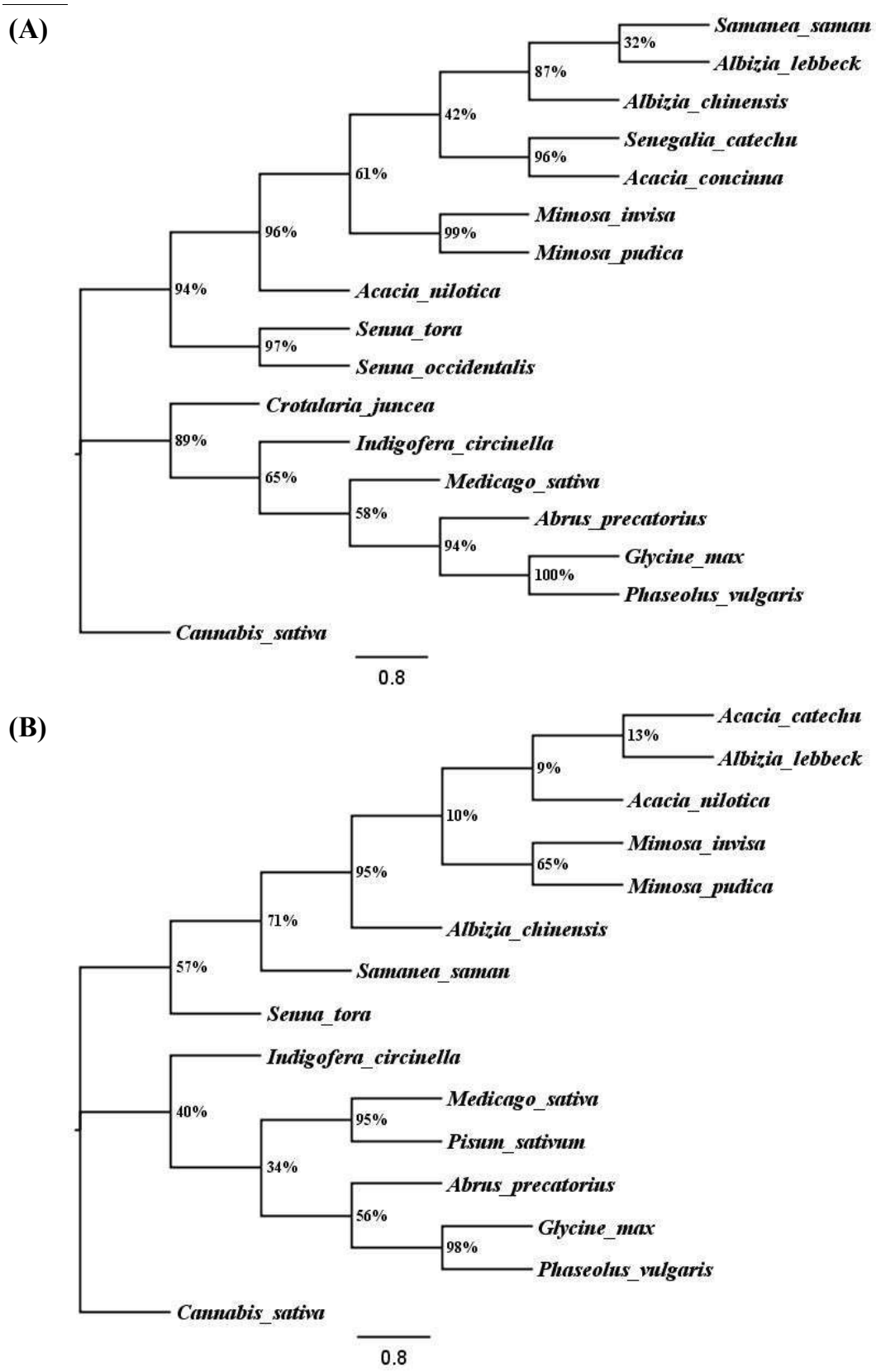

Fig. 4.41. Most parsimonious tree (neighbour joining method) showing the relationship of matK region of 16 different taxa **(A)** and TrnL-F region of 15 different taxa **(B)** belonging from subfamilies, Mimosoideae, Papilionoideae and Caesalpinioideae within the family Fabaceae and one outgroup taxa from Cannabaceae. The tree indicates the phylogenetic evolution of different subfamilies Mimosoideae; Papilionoideae; Caesalpinioideae. Numbers at nodes indicate the bootstrap values.

from *M. pudica*, *M. invisa* and *A. nilotica* were evaluated separately through DPPH, hydroxyl radical and nitric oxide scavenging assay. Result revealed lower percentage of inhibitory activity in all cases (< 30% at 200µg/ml) in comparison with leaf extract. Between root and root-nodule extract, we found hardly a little difference (Table 4.25) suggesting that the presence of *Rhizobium* in the root-nodule failed to change the antioxidant properties of the plant part. Therefore, no further initiative was carried out.

4.10.2. Molecular documentation

Since no difference was obtained in antioxidative profiling of roots and root nodules, it was further perceived whether there is any genetical variation among micro-symbionts. Therefore, root nodules of *M. pudica*, *M. invisa* and *A. nilotica* were collected from two different geographical locations of Bengal; one is from Malda and another one from Sibmandir and subsequently *Rhizobium* was collected from pure culture. Afterward, isolation of genomic DNA was subjected.

4.10.2.1. DNA isolation, purification and quantification

4.10.2.1.1. DNA isolation

Rhizobium genomic DNA was isolated using the standard protocol of William and Feil (2012) with minor modifications. Prior to isolation, an efficient lysis is a prerequisite for good yield of nucleic acid for further downstream processing. The agarose gel analysis of the DNA thus obtained showed distinct and clear bands.

4.10.2.1.2. DNA purification

Crude DNA is basically mixed with many contaminants including RNA, protein, polysaccharides etc. which lead to enzymatic reaction with DNA. Therefore, DNA purification is prerequisite step before performing downstream analysis like PCR amplification, DNA restriction and gene cloning. Inclusion of CTAB method in DNA extraction process helps to eliminate polysaccharides from DNA precipitations to a large extent. Subsequently, extraction with phenol:chloroform:isoamyl alcohol (25:24:1) indicates the removal of protein impurities from the DNA samples. Further, RNAase enzyme is used to remove RNAs from samples.

4.10.2.1.3. DNA quantification

In the present study, 2 different types of quantification methods were followed to analyze the quality of DNA. First one is spectrophotometric method and the other one is agarose gel electrophoresis (Fig. 4.42). In spectrophotometric method, the DNAs were quantified in a UV spectrophotometer with 260 nm and 280 nm filters. The results were calculated as the ratio of A_{260}/A_{280} after performing of six replicates and the samples considered only showing a ratio of around 1.8 (Table 26).

Table 4.25. Antioxidant activities of root and root-nodule collected from different host.

Host	Root			Root-nodule		
	DPPH#	Hydroxyl#	NO#	DPPH#	Hydroxyl#	NO#
M. pudica	22.17±0.35	19.04±0.60	24.52±0.93	21.05±1.51	19.27±1.25	22.31±0.93
M. invisa	24.74±1.35	18.37±0.34	23.87±1.43	23.87±0.46	20.85±2.46	24.40±1.78
A. nilotica	21.57±2.62	20.26±0.84	23.21±0.89	22.81±0.67	21.46±0.78	22.98±1.34

inhibition percentage at 200µg/ml.

4.10.2.2. RAPD analysis

RAPD fingerprinting was used for studying the genetic diversity among indigenous *Rhizobium* population isolated from two distinct regions from northern parts of Bengal province in India (Please refer Table 3.7). In RAPD analysis, 12 different primers each of 10-mers in length have been used for the six isolated strains.

Table 4.26. List of *Rhizobium* samples showing their purity.

Sample ID	A_{260}/A_{280} ratio for purity
I	1.77
II	1.79
III	1.74
IV	1.76
V	1.81
VI	1.83

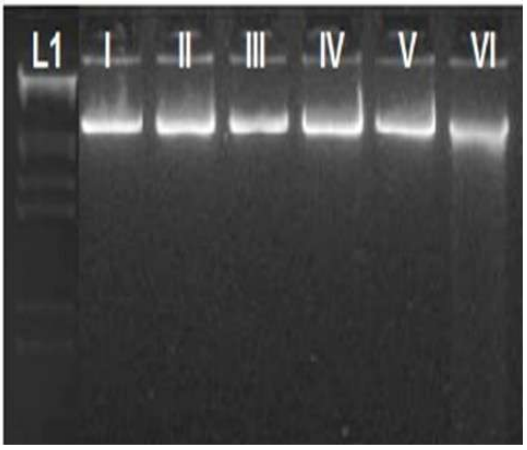

Fig. 4.42. Crude DNA of *Rhizobium*. Lane L1: λ DNA/ EcoRI/ Hind III double digest DNA ladder; Lane I-VI: different *Rhizobium* strains under study (please refer **Table 3.7** for the strain's name).

Out of the 12 primers screened, 7 revealed distinct and scorable bands of various intensities and the size of the bands was ranged from 134 bp to 2175 bp (Table 4.27).

The amplification patterns revealed 97.39% polymorphism and the number of polymorphic bands generated by each decamer primers ranged in between 12 (OPD-03) and 21 (OPQ-01). After analysis of the sequences of the primers, it was found that all the primers which failed to amplify were of AT-rich. It sounds reasonable now since the *Rhizobium* is largely a GC rich genus. A representative of RAPD profile of the 6 *Rhizobium* strains generated using OPA 18 and OPY 04 has been showed in Fig. 4.43.A-B.

A similarity matrix was further drawn using Dice coefficient of similarity (Nei and Li, 1979) ranging from 0.59 to 1.00 (Table 4.28). The lowest similarity was observed between isolate-I and isolate-III while the highest value was recorded between isolate-V and isolate-VI. A dendrogram was constructed on the basis of the data obtained from RAPD analysis using NTSYSpc (Fig. 4.44).

Herein, the dendrogram was divided into

Table 4.27. Total number and size of amplified bands, number of monomorphic and polymorphic bands generated and percentage of polymorphism generated by the RAPD primers.

Primer ID	Sequence (5'-3')	Band No	MB	PB	Pol %	Band size (bp)
OPA 02	TGCCGAGCTG	19	0	19	100%	385-**2175**
OPQ 01	GGGACGATGG	**21**	0	21	100%	165-1137
OPA18	AGGTGACCGT	17	0	17	100%	145-1875
CRL 7	GCCCGCCGCC	14	2	12	85.71%	230-1900
OPY 04	AAGGCTCGAC	20	0	20	100%	275-1813
DAF 9	CCGACGCGGC	12	0	12	100%	**134**-1024
OPD 03	GTCGCCGTCA	**12**	1	11	91.66%	338-1800
Total		115	3	112	97.39%	

MB= Monomorphic bands; PB= Polymorphic bands; Pol %= Polymorphism %

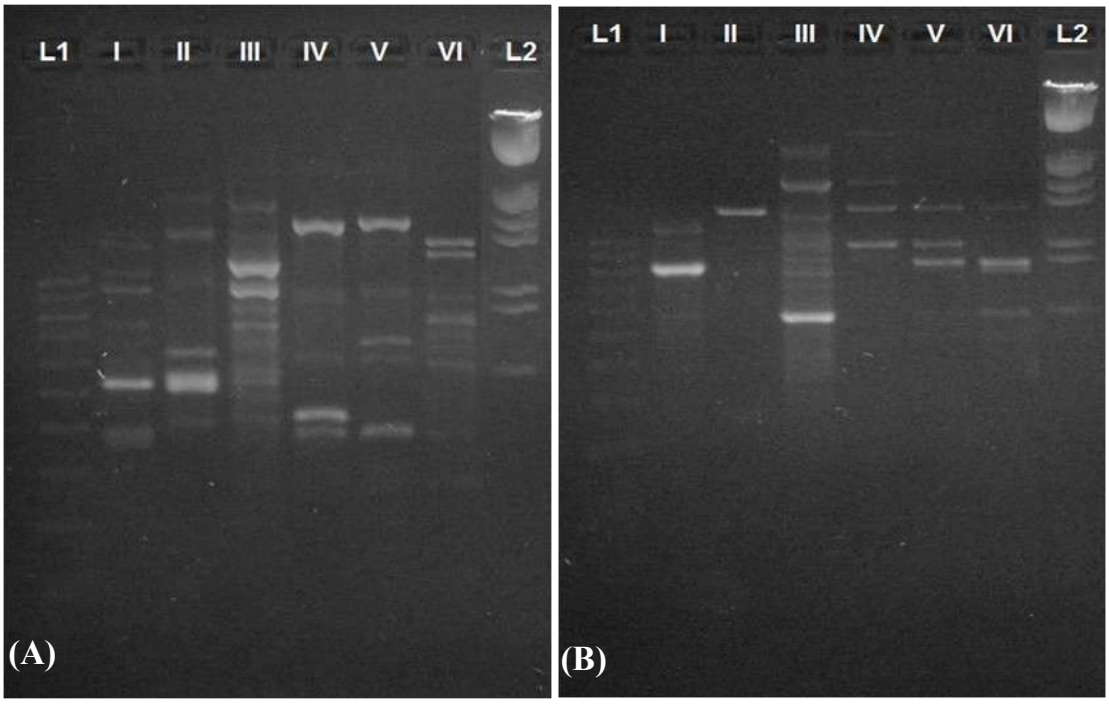

Fig. 4.43. DNA Gel showing the DNA bands of six *Rhizobium* strains amplified by the RAPD primers **(A)** OPA 18 and **(B)** OPY 04. Lane L1: 100 bp DNA ladder; Lane I-VI: different *Rhizobium* strains under study (**Please refer Table 3.7** for the strain's name); Lane L2: λ DNA/*Eco*RI/*Hind*III double digest DNA ladder.

Table 4.28. The similarity matrix obtained using Dice coefficient of similarity among the 6 isolates of *Rhizobium* from 2 regions of northern parts of Bengal province in India based on RAPD profiling.

	I	II	III	IV	V	VI
I	1.00					
II	0.76	1.00				
III	**0.59**	0.68	1.00			
IV	0.59	0.68	0.92	1.00		
V	0.59	0.82	0.85	0.85	1.00	
VI	0.59	0.82	0.85	0.85	**1.00**	1.00

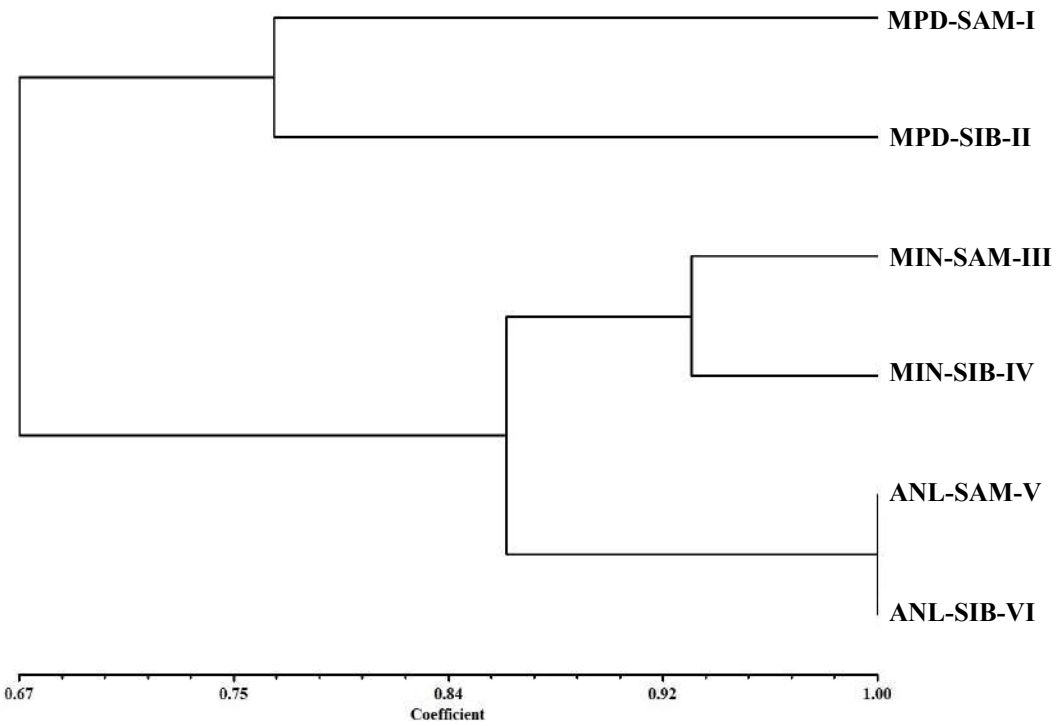

Fig. 4.44. Dendrogram derived from UPGMA cluster analysis of RAPD markers illustrating the genetic relationships among the 9 *Rhizobium* strains.

three clusters, the first cluster contained isolate-I and isolate-II share a node at 76%, whereas, the second cluster revealed high level of genetic similarity (92%) i.e. within isolate-II and isolate-III and 100% of genetic similarity was observed in case of isolate-V and VI comprising the third clade. The only variation found is from host species to host species.

Hence, it can be inferred that there is a major difference present between the micro-symbionts of various species; for instances, three major clades were observed in the phylogenetic tree which were separated as per their host specificity. This resut once again reiterated the host specificity of *Rhizobium*.